N.M.R. INVESTIGATION OF NUCLEAR SPIN ISOMERISM IN THE AMMONIUM IONS

N.M.R. INVESTIGATION OF NUCLEAR SPIN ISOMERISM IN THE AMMONION IONS

By

ARTHUR WATTON, B. Sc.

A Thesis

Submitted to the Faculty of Graduate Studies

in Partial Fulfilment of the Requirements

for the Degree

Doctor of Philosophy

McMaster University

May 1971

DOCTOR OF PHILOSOPHY (1970) McMASTER UNIVERSITY
(Physics) Hamilton, Ontario.

TITLE: N.M.R. Investigation of Nuclear Spin Isomerism in the Ammonium Ions

AUTHOR: Arthur Watton, B.Sc. (Imperial College, London)

SUPERVISOR: Professor H. E. Petch

NUMBER OF PAGES: ix, 135

SCOPE AND CONTENTS:

The possibility of isomeric nuclear spin states existing among the ammonium ions at low temperatures has been investigated for some twenty ammonium salts. Measurements have been made of the proton absorption signals at 4.2°K, and the temperature dependences, where previously unavailable, of the spin-lattice relaxation time.

Some of the salts exhibit the normal rigid lattice spectra and second moments characteristic of distinguishable protons, but most exhibit some degree of line narrowing at 4.2°K. The data shows that thermally activated reorientations are effectively frozen out at this temperature and cannot be responsible for such narrowing.

It is concluded that the narrow spectra, although indicative of indistinguishability among the protons, are not attributable solely to spin isomerism, but are being modified by a further mechanism, probably tunneling of the ammonium ion through the crystal field barrier.

ACKNOWLEDGEMENTS

I would like to thank Dr. H. E. Petch for his support and advice both during the course of this work and the preparation of this thesis.

I am greatly indebted to Dr. M. M. Pintar for initially suggesting this topic and for his constructive interest in its development.

My thanks are especially extended to Stane Vrscaj for designing and maintaining much of the equipment used, and to Allan Sharp for his assistance in gathering much of the relevant data. Also, I would like to express my appreciation to Beth for her patience and encouragement.

This research was made possible by grants-in-aid to Dr. Petch from the National Research Council of Canada, and the Defence Research Board of Canada.

TABLE OF CONTENTS

LIST OF FIGURES

LIST OF TABLES

CHAPTER I

INTRODUCTION

Bersohn and Gutowsky (1954) performed proton magnetic resonance absorption measurements on a single crystal of ammonium chloride (NH_4Cl) at 77°K and deduced that the spectra obtained were those of a system of four interacting, but distinguishable protons, located on the corners of a rigidly oriented tetrahedron (the ammonium group). Such a system will be referred to as a "4-spin 1/2" system, the second moment* for which will be referred to as the "rigid lattice" value. This is the value one would expect for a lattice of stationary, distinguishable nuclei arranged in groups of four ($\sim 50\ G^2$ in the ammonium salts). Proton absorption measurements from 20°K to room temperature for a number of ammonium salts have since been reported by Richards and Schaefer (1961). Apart from the lineshapes they also presented the temperature dependence of the linewidth, defined as the separation in gauss of the absorption derivative maxima, and of the second moment. Among these salts a number (e.g. ammonium tellurate, -sulphate, -metavanadate, -persulphate, and -dichromate) had second moments at 20°K which were

---

*Defined as the mean square deviation of the absorption lineshape from the Larmor field.

considerably less than the usual "rigid lattice" value.

There are a number of possible mechanisms which could narrow the absorption line and reduce the second moment:

a) Thermally Activated Motional Narrowing

To first order, the second moment of the complete absorption spectrum is independent of thermal motions. However, the frequency components associated with the random correlations of these processes can shift parts of the spectrum into the wings producing satellites of weaker intensity. If the thermal motion is fast enough, i.e. when its correlation frequency ν_c (defined as $1/2\pi\tau_c$, where τ_c is its correlation time), is much higher than a characteristic frequency of the linewidth, then these satellites are pushed so far out and, hence, become so weak that they are lost in the noise. The second moment of the remaining spectrum, which is what is observed, is thus reduced. As the temperature is lowered, thermal activations become less frequent, τ_c increases and ν_c decreases until eventually ν_c is much less than the linewidth. All components are then observed and the second moment normally attains its "rigid lattice" value.

b) Quantum Mechanical Tunneling

Quantum mechanical tunneling of the ammonium ion from one orientation to another, through the hindering barrier of the crystal field, may shift some parts of the spectrum by an amount comparable to the associated tunneling frequency.

Again, if this frequency is high enough, these components would become lost in the wings and not observed, thus reducing the second moment of the remaining part of the spectrum. It should be emphasized that, unlike the random processes involved in thermal motion, tunneling is a coherent process which, not being thermally activated, can be effective at the lowest temperatures.

This interpretation of line narrowing has been applied to the tunneling of a methyl group by Allen (1968).

c) Spin Isomerism

The requirement that the total wave function of the ammonium group be anti-symmetric under exchange of any two protons necessitates the existence of nuclear spin states of certain permutation symmetries (spin isomers) only with certain spatial symmetry states. If the spatial states of different symmetries are well separated in energy by the crystal field then transitions between different spin isomer states, involving, as they would, simultaneous changes in spatial states (and energies), would not be observed in first order, again narrowing the observed line shape. Because this mechanism is not thermally activated it can also be effective at low temperatures, the spectrum of methane below 2°K being interpreted on this basis by Tomita (1953).

For the ammonium salts with low second moments mentioned previously, Richards and Schaefer concluded that some degree of motional disorder still exists at 20°K, implying the thermal motion interpretation of line narrowing, mechanism a). Similar conclusions had been arrived at for the sulphate and tetrafluoroberyllate salts by Blinc and Levstek (1960).

The difficulties of this interpretation can be exemplified for the case of ammonium sulphate: In order to obtain quantitative agreements with the experimentally observed low temperature second moment of 33.3 ± 1.1 G^2, Richards and Schaefer had to assume that 2/3 of the ammonium ions were "rigid", while 1/3 were rapidly reorienting (a "semi rigid lattice") at this temperature. This assumption is inconsistent with the known crystal structure, in which there are equal numbers of each of two inequivalent ammonium ions. If the interpretation of a "semi rigid lattice" were correct, 1/2 of the ammonium ions would have to be "rigid" and 1/2 reorienting, which would not give quantitative agreement with the observation.

These results on the sulphate indicated that, in at least some ammonium salts, the low temperature line narrowing observed was unlikely to be the result of thermally activated molecular reorientation. At the same time, the evidence found by Tomita for the existence of isomeric spin states in methane at low temperatures suggested that this mechanism may also be effective among the ammonium ions, which

are structurally similar to the methane molecules. The present work was therefore undertaken in order to investigate fully this possibility of spin isomerism among the ammonium group protons at low temperatures. With this objective, line shape studies have been made of some twenty ammonium salts at 4.2°K, together with measurements, where possible, of the temperature dependence of the spin-lattice relaxation time, T_1. The activation energies and correlation times obtained from the latter have been used to test the assertion that reorientation cannot be responsible for line narrowing at very low temperatures.

CHAPTER II

THEORY

II.1 INTRODUCTION

The fundamental theory of Nuclear Magnetic Resonance is well established and can be found in many standard text books (see, for example, Abragam (1961), Slichter (1963)). For this reason no basic theory will be given in this work. Attention will be focussed instead on the problem of spin isomerism and its manifestation in N.M.R.

II.2 SPIN ISOMERISM - PRELIMINARIES

The N.M.R. absorption line shape of a tetrahedrally co-ordinated four proton system exhibiting spin isomerism has been derived theoretically and applied to the case of solid methane (CH_4) by Tomita (1953). Tomita's treatment is tractable because the carbon-proton contribution to the dipolar interaction is negligibly small compared to the proton-proton contribution. This is because the only carbon isotope with a non-negligible magnetic dipole moment is C^{13} which occurs with a natural abundance of only 1%. In the case of the ammonium salts however, the nitrogen isotope N^{14}, whose natural abundance is greater than 99%, possesses a dipole moment which, though small, is not negligible. This, in conjunction with the small nitrogen-proton separa-

tion in the ammonium group (less than the proton-proton separation) leads to a significant contribution from the nitrogen nucleus to the dipolar interaction energy. This complication renders a general analytical solution for the absorption line shape intractable. We therefore adopt the procedure of first developing Tomita's theory without the nitrogen contribution and then estimating qualitatively and quantitatively how the inclusion of this effect will incorporate itself into the result.

II.3 HAMILTONIAN

The Hamiltonian for a number of interacting nuclear spins in a strong external magnetic field H_o is;

$$H = H_z + H_d$$

where H_z is the Zeeman part expressing the interaction of the spins with H_o, while H_d is the dipolar part expressing the dipolar interactions of the spins with each other. Considering contributions only from the protons we have;

$$H_z = -\gamma\hbar H_o \sum_i I_{iz}$$

and the inter-proton dipolar interaction H_{dp} is

$$H_{dp} = \sum_{i>j} A_{ij}[I_{iz}I_{jz} - \tfrac{1}{4}(I_i^+I_j^- + I_i^-I_j^+)]$$

where i, j label the protons, $\underline{I}_i$ represents the spin operator of proton i, and $\underline{H}_o$ defines the z direction of the co-ordinate system. The quantities A_{ij} are defined by;

$$A_{ij} = \frac{\gamma^2\hbar^2}{r_{ij}^3}(1 - 3\cos^2\theta_{ij})$$

where θ_{ij} is the angle the inter-proton vector $\underline{r}_{ij}$ makes with $\underline{H}_o$.

As is usual, in the expression for $\mathcal{H}_{dp}$ only the adiabatic part of the dipolar Hamiltonian has been taken since this is the only part which contributes to the splitting of the degenerate spin levels in first order (e.g. Abragam ch. IV). To calculate this dipolar splitting in first order, $\mathcal{H}_{dp}$ is treated as a perturbation on $\mathcal{H}_z$ (which is perfectly justified since the local dipolar field is typically 10 G or less while the applied field, H_o, is of the order of 10^4 G). Furthermore, $\mathcal{H}_{dp}$ can be regarded as being composed of contributions from protons in the same ammonium group (intra-ionic) and on different groups (inter-ionic). Of these two, since the ammonium groups themselves are well separated from one another compared with the dimensions of a group itself, the inter-ionic contribution can be regarded as a perturbation on the intra-ionic one. Thus, in first order, we need consider only the splitting caused by the dipolar interaction among the four tetrahedrally co-ordinated protons in a single ammonium group.

II.4 SYMMETRY ADAPTED STATES

The eigenstates of $\mathcal{H}_z$ form a basis for the perturbation calculation of the dipolar splitting. For the four proton

system we are considering, these eigenstates are labelled by $|m_1 m_2 m_3 m_4\rangle$, where m_i is the eigenvalue of I_{iz}. Since protons have spin $I_i = 1/2$, the m_i's can assume the two values $\pm 1/2$. Thus there are 16 of these basis states. However, it is more convenient to use as a basis a set of spin functions which is reduced with respect to the substitution group of four identical nuclei (isomorphous to the tetrahedral group of real rotations). The 16 spin states reduce to the irreducible members $5A + E + 3T^*$, to each of which there corresponds a definite eigenvalue of the total nuclear spin operator, $\underline{I}(= \underline{I}_1 + \underline{I}_2 + \underline{I}_3 + \underline{I}_4)$, of the proton group. This reduction is shown in matrix form in Table I, in which ${}_M\phi_i^R$ represents the basis state belonging to the i'th row of the R'th irreducible representation, and M is the eigenvalue of I_z.

The harmonic oscillator spatial ground state of an ammonium ion sitting in an infinite potential well is twelve fold degenerate (there being twelve equivalent orientations corresponding to even permutations of protons). These reduce, with respect to the tetrahedral symmetry group of the ion, to the irreducible members A+E+3T. In a finite crystal field the degeneracy of the different members is, in general, removed, but if the crystal field has itself tetrahedral symme-

---

*A, E, and T label the bases of the irreducible representations of the tetrahedral group of dimensionality one, two and three respectively.

TABLE I

Symmetry adapted spin states. In right hand column (+) represents spin up and (-) represents spin down.

$$
\begin{pmatrix}
{}^{2}\phi_1^{A} \\
{}^{2}_{1}\phi_1^{A} \\
2\sqrt{3}\ {}^{1}\phi_1^{T} \\
\sqrt{6}\ {}^{1}\phi_2^{T} \\
\sqrt{2}\ {}^{1}\phi_3^{T} \\
\sqrt{6}\ {}^{0}\phi_1^{A} \\
2\sqrt{3}\ {}^{0}\phi_1^{E} \\
2\ {}^{0}\phi_2^{E} \\
\sqrt{6}\ {}^{0}\phi_1^{T} \\
2\sqrt{3}\ {}^{0}\phi_2^{T} \\
2\ {}^{0}\phi_3^{T}
\end{pmatrix}
=
\begin{pmatrix}
1 & & & & & & & & & & & & & & & \\
 & 1 & 1 & 1 & 1 & & & & & & & & & & & \\
 & 1 & 1 & 1 & -3 & & & & & & & & & & & \\
 & 1 & 1 & -2 & 0 & & & & & & & & & & & \\
 & 1 & -1 & 0 & 0 & & & & & & & & & & & \\
 & & & & & 1 & 1 & 1 & 1 & 1 & 1 & & & & & \\
 & & & & & 2 & -1 & -1 & -1 & -1 & 2 & & & & & \\
 & & & & & 0 & 1 & -1 & 1 & -1 & 0 & & & & & \\
 & & & & & 1 & 1 & 1 & -1 & -1 & -1 & & & & & \\
 & & & & & 2 & -1 & -1 & 1 & 1 & -2 & & & & & \\
 & & & & & 0 & -1 & 1 & 1 & -1 & 0 & & & & &
\end{pmatrix}
\begin{pmatrix}
++++ \\
-+++ \\
+-++ \\
++-+ \\
+++- \\
--++ \\
+--+ \\
-+-+ \\
-++- \\
+-+- \\
++--
\end{pmatrix}
$$

try the three different T members remain degenerate. A schematic representation of the spatial level scheme is as follows:

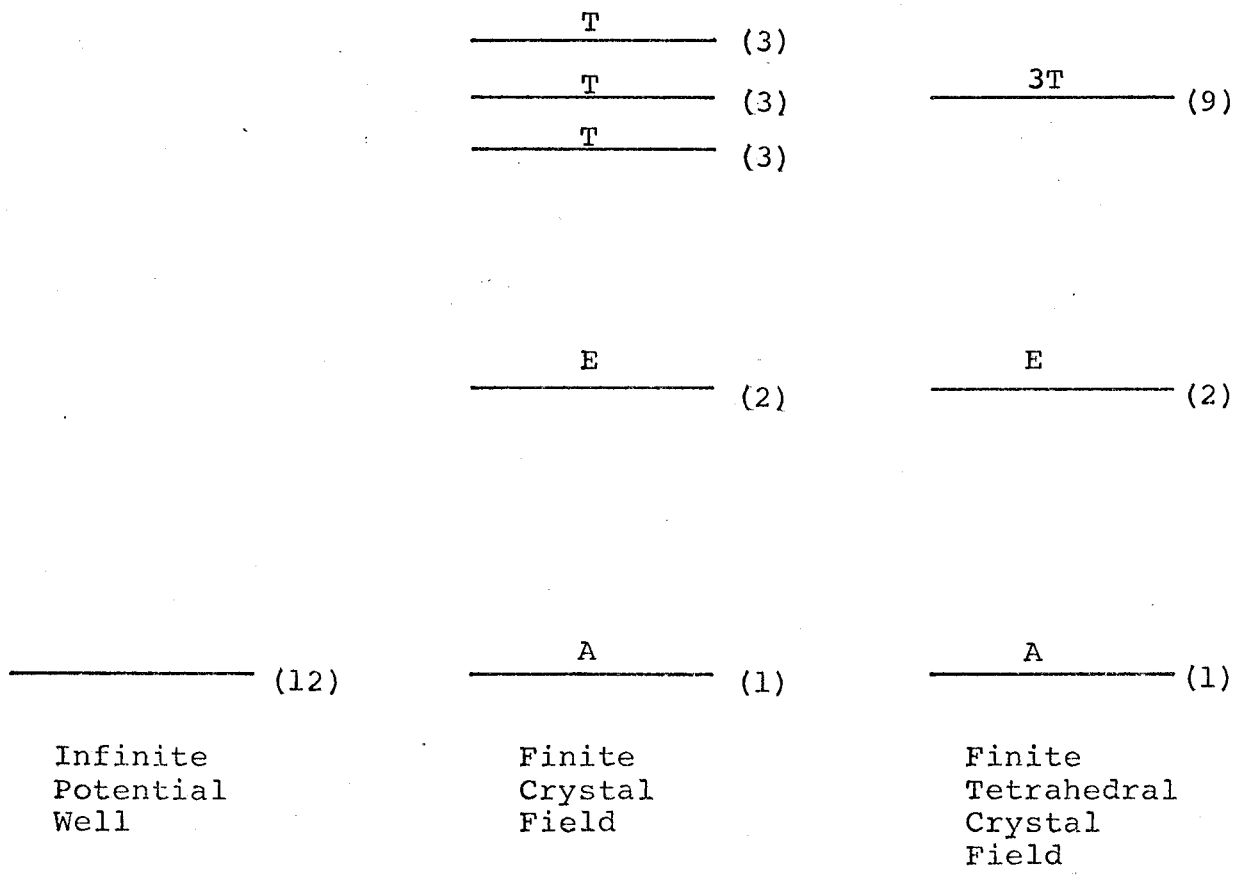

The numbers in parantheses with each level show the degeneracy of that level.

The matrix elements of H_{dp} between the members of the reduced basis spin states can now be calculated (see Appendix A), and are shown in Tables II and III. In the absence of any symmetry considerations, diagonalization of this representation of H_{dp} would give the perturbed eigenvalues. However, the total wave function Ψ, in the absence

TABLE II

Matrix elements of H_{dp} ——— (a)

$2\phi_1^A$	a_2								
$1\phi_1^A$		a_1	b_1	c_1	d_1				
$1\phi_1^T$		b_1	e	f	g				
$1\phi_2^T$		c_1	f	h	k				
$1\phi_3^T$		d_1	g	k	ℓ				
$0\phi_1^A$						a_0	b_0	c_0	O	O	O
$0\phi_1^E$						b_0	O	O	O	O	O
$0\phi_2^E$						c_0	O	O	O	O	O
$0\phi_1^T$						O	O	O	-2e	-2f	-2g
$0\phi_2^T$						O	O	O	-2f	-2h	-2k
$0\phi_3^T$						O	O	O	-2g	-2k	-2ℓ

TABLE III

Matrix elements of H_{dp} ——— (b)
Elements of Table II in terms of A_{ij}

$$\begin{pmatrix} -4a_2 \\ -8a_1 \\ -8b_1/\sqrt{3} \\ -16c_1/\sqrt{6} \\ -16d/\sqrt{2} \\ -24e \\ -48f/\sqrt{2} \\ -48g/\sqrt{6} \\ -12h \\ -12k/\sqrt{3} \\ -4\ell \\ -4a_o \\ -8b_o/\sqrt{2} \\ -8c_o/\sqrt{6} \end{pmatrix} = \begin{pmatrix} 1 & 1 & 1 & 1 & 1 & 1 \\ 1 & 1 & 1 & 1 & 1 & 1 \\ 1 & 1 & 1 & -1 & -1 & -1 \\ 2 & -1 & -1 & 1 & 1 & -2 \\ 0 & -3 & 3 & 3 & -3 & 0 \\ -3 & -3 & -3 & 1 & 1 & 1 \\ 6 & -3 & -3 & -1 & -1 & 2 \\ 0 & -3 & 3 & -1 & 1 & 0 \\ 0 & 0 & 0 & -2 & -2 & 1 \\ 0 & 0 & 0 & 1 & -1 & 0 \\ 0 & 0 & 0 & 0 & 0 & -1 \\ 1 & 1 & 1 & 1 & 1 & 1 \\ -2 & 1 & 1 & 1 & 1 & -2 \\ 0 & -1 & 1 & -1 & 1 & 0 \end{pmatrix} \begin{pmatrix} A_{12} \\ A_{23} \\ A_{13} \\ A_{14} \\ A_{24} \\ A_{34} \end{pmatrix}$$

of any spin-rotational interaction, can be written as a product of space and spin co-ordinate dependent parts i.e.;

$$\Psi = \phi_{space} \cdot \psi_{spin}$$

if all other co-ordinate states, such as vibrational and electronic, are in their symmetric ground state. Now, protons are fermions and so Ψ must be antisymmetric under exchange of any pair, or, equivalently, symmetric under any real rotation, since this is equivalent to the interchange of two pairs. Thus, for Ψ to belong to the totally symmetric representation, physically real states occur only in the combinations $\phi(A)\psi(A)$, $\phi(E)\psi(E)$, $\phi(T)\psi(T)$, corresponding to meta-, para-, and ortho-groups respectively. If the spatial states are well separated in energy ($\sim$ 15°K for a free rotor, although less for an oscillator) only spin transitions are observed which conserve the symmetry type (A, E, or T). Only the matrices of these irreducible representations need to be diagonalized.

We will define a cartesian co-ordinate system fixed with respect to the ammonium group as shown in Figure 1, with origin at the nitrogen nucleus. In this reference frame $\underline{H}_o$ has spherical angular co-ordinates (θ,ϕ) as shown, in terms of which (see Appendix B) the A_{ij}'s are given by;

FIGURE 1

NH_4 co-ordinate system. $\underline{H}_o$ has spherical angular co-ordinates (θ,ϕ).

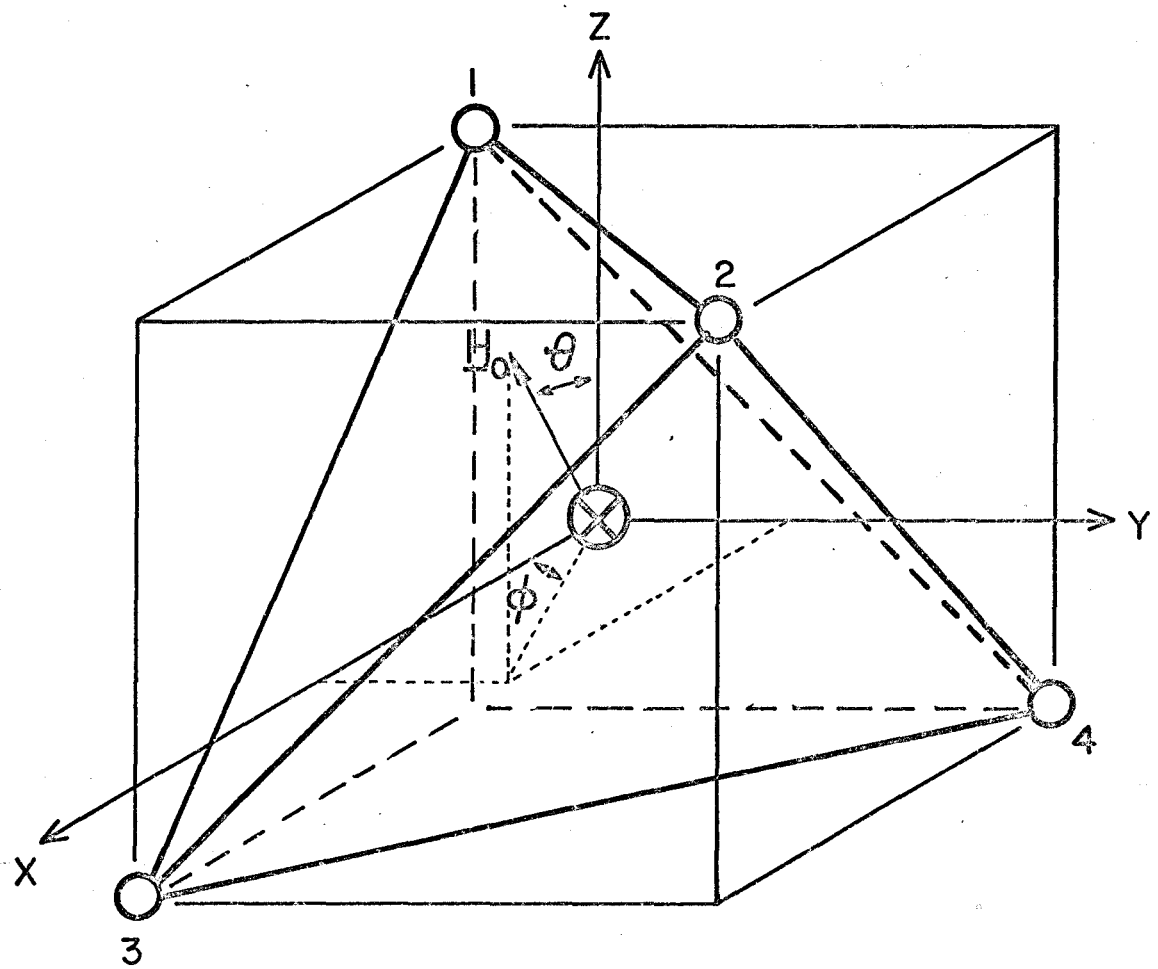

PROTONS

NITROGEN

$$\left.\begin{aligned}
A_{12} &= A[1 - \tfrac{3}{2}\sin^2\theta(\cos\phi + \sin\phi)^2] \\
A_{23} &= A[1 - \tfrac{3}{2}(\sin\theta\sin\phi + \cos\theta)^2] \\
A_{13} &= A[1 - \tfrac{3}{2}(\sin\theta\cos\phi - \cos\theta)^2] \\
A_{14} &= A[1 - \tfrac{3}{2}(\sin\theta\sin\phi - \cos\theta)^2] \\
A_{24} &= A[1 - \tfrac{3}{2}(\sin\theta\cos\phi + \cos\theta)^2] \\
A_{34} &= A[1 - \tfrac{3}{2}\sin^2\theta(\sin\phi - \cos\phi)^2]
\end{aligned}\right\} \qquad (2.1)$$

where $A = \dfrac{\gamma^2\hbar^2}{r^3}$

r being the proton-proton separation.

II.5 META TRANSITIONS (A STATES)

The matrix elements of these states are symmetric combinations of the A_{ij}'s and so;

$$a_2 = a_1 = a_0.$$

This can be seen directly by summing the elements given by equation (2.1). This means that diagonalization of the one dimensional A type representation gives zero for the first order change in energy of these states. The spectrum of transitions among these states thus consists of a delta-function at H_o.

The transition probability can be calculated for the transition $M \rightarrow M'$ by;

$$P_A(M\rightarrow M') = |\langle {}_M\phi_1^A | I_x | {}_{M'}\phi_1^A \rangle|^2 \qquad (2.2)$$

since the r.f. field which induces transitions does so through its interaction with the x-component of the nuclear spin (see Abragam etc). Using this expression and the states given in Table I, the transition probabilities are calculated to be (Appendix C);

$$P_A(\pm 1 \rightleftarrows 0) = \frac{3}{2} \text{ for two transitions.}$$

$$P_A(\pm 2 \rightleftarrows \pm 1) = 1 \text{ for two transitions.}$$

The total transition probability for all A type transitions is then;

$$P_A(\text{total}) = 5 \qquad (2.3)$$

II.6 PARA TRANSITIONS (E STATES)

Proton groups of this symmetry type are associated only with I = 0 (no resultant magnetic moment) so no transitions are observed and we need not consider them further.

II.7 ORTHO TRANSITIONS (T STATES)

We need to diagonalize the 3×3 sub-matrices in Table II defined among the states ${}_M\phi_i^T$. The trace of the M = 1 sub-matrix is given by;

$$Tr = e + h + \ell$$

which, by substitution from Table III, is a symmetric combination of the A_{ij}'s and therefore zero. By manipulation of the matrices, the secular equations may be written in

standard forms. For the case M = 1, the normalized eigenvalue equation becomes,

$$x^3 - \frac{3}{16} x + \frac{1}{32} \cos \Psi(\theta,\phi) = 0 \qquad (2.4)$$

where the eigenvalue $= \frac{\gamma^2 \hbar^2}{r^3} x$

and

$$\cos\Psi(\theta,\phi) = 1 - \frac{27}{2} \sin^2 2\phi \cos^2\theta \sin^4\theta \qquad (2.5)$$

Equation (2.4) can be solved by the standard technique for a cubic equation (see Appendix D), to give three real solutions;

$$\left.\begin{aligned} x_1 &= -\frac{1}{2} \cos \frac{\Psi}{3} \\ x_2 &= \frac{1}{2} \cos \left(\frac{\pi - \Psi}{3}\right) \\ x_3 &= \frac{1}{2} \cos \left(\frac{\pi + \Psi}{3}\right) \end{aligned}\right\} \qquad (2.6)$$

The matrix for M = 0 is twice the negative of the matrix for M = 1. The eigenfunctions are therefore the same while the eigenvalues x_i' are twice the negative of those for M = 1. i.e.;

$$x_i' = -2x_i \ .$$

The transition probabilities between the two sets of states is given by the equivalent T state expressions to equation (2.2). However, we can now make use of the fact that

I_x, being a symmetric combination of the I_{ix} is invariant under all permutations of spins, and thus belongs to an A type representation. Therefore, the function $I_x|_M\phi_i^T>$ still belongs to the i'th row of the T'th irreducible representation. From group theory it is known that the scalar product of two functions is zero unless they belong to the same row of the same irreducible representation (e.g. Hamermesh (1962), ch. 6). Therefore, the matrix element $<_M,\phi_j^T|I_x|_M\phi_i^T>$ is zero unless i = j, and then is independent of i. This can also be seen directly by evaluating the matrix elements using the states given in Table I (Appendix C). This means that of the nine possible T type transitions from M = 1 to M = 0, only three are allowed here - those from x_i to x_i'. Hence, three lines occur, shifted from H_o by $3x_i$, i = 1,2,3. The results for M = -1 are identical except for a change in sign, so that finally there are six ortho lines at $\pm 3x_i$, i = 1,2,3. Using the equivalent expression to equation (2.2) the ortho transition probabilities are calculated to be (Appendix C);

$$P^T(\pm 1 \rightleftarrows 0) = \frac{1}{2} \quad \text{for six transitions,}$$

so that the total transition probability for all orth-transitions is;

$$P^T(\text{total}) = 3 \ . \qquad (2.7)$$

II.8 POWDER SPECTRA

The foregoing has been concerned with the absorption spectrum from a single crystal. In a powder sample consisting of many small, randomly oriented crystallites, all orientations are present. The observed spectrum is then the result of taking a polycrystalline average over all orientations of $\underline{H}_o$.

A single crystal line occurs at;

$$3x_1 = \frac{3}{2}\cos\frac{\Psi}{3} = \frac{3}{2}\eta \qquad (2.8)$$

where η is defined so that $-1 \leq \eta \leq 1$. Then the probability of finding an absorption line between η and $\eta + \Delta\eta$ in a powder sample is;

$$w(\eta)\Delta\eta = \frac{1}{4\pi}\iint_R \sin\theta d\theta d\phi$$

the integration being performed over the region R where $\eta \leq \eta(\theta,\phi) \leq \eta + \Delta\eta$. Inverting the solution for $\eta(\theta,\phi)$ to give $\phi = \phi(\theta,\eta)$, This integration reduces to;

$$w(\eta) = \frac{1}{4\pi}\int_R \frac{\partial\phi}{\partial\eta}(\theta,\eta)d(\cos\theta) \qquad (2.9)$$

Expanding cos Ψ gives;

$$\cos\Psi = 4\cos^3\frac{\Psi}{3} - 3\cos\frac{\Psi}{3}$$

$$= 4\eta^3 - 3\eta$$

From equation (2.5) we define a function $f(\eta)$ such that;

$$f(\eta) = \frac{2}{27}(1 + 3\eta - 4\eta^3) = \Theta(\theta)\sin^2 2\phi \qquad (2.10)$$

where

$$\Theta(\theta) = \cos^2\theta\sin^4\theta$$

from which it can be seen that f must lie in the region $4/27 \geq f \geq 0$.

Now $$\frac{\partial\phi}{\partial\eta} = \frac{\partial f}{\partial\eta} \Big/ \frac{\partial f}{\partial\phi}$$

and from equation (2.10);

$$\frac{\partial f}{\partial\phi} = 4[f(\Theta - f)]^{\frac{1}{2}}$$

and

$$\frac{\partial f}{\partial\eta} = \frac{2}{9}(1 - 4\eta^2) = f'. \qquad (2.11)$$

Clearly then, R is the region for which $\Theta \geq f \geq 0$.

Defining a new variable ξ, as;

$$\xi = \cos^2\theta$$

we can write;

$$\Theta = \xi(1 - \xi)^2 .$$

Then if the roots of the equation;

$$\Theta = f$$

are α_1, α_2, α_3 $(\alpha_1 \geq \alpha_2 \geq \alpha_3)$, we can write;

$$\Theta - f = (\xi - \alpha_1)(\xi - \alpha_2)(\xi - \alpha_3)$$

and so;

$$w(\eta) = \frac{|f'|}{24\pi f^{\frac{1}{2}}} \int_{\alpha_3}^{\alpha_2} \frac{d\xi}{[\xi(\xi-\alpha_1)(\xi-\alpha_2)(\xi-\alpha_3)]^{\frac{1}{2}}} \qquad (2.12)$$

the region of integration being α_3 to α_2 because outside this region the integrand is complex. A schematic representation of the function $\Theta(\xi)$ and the solution of $\Theta = f$ is shown in Figure 2.

As can be seen, since $0 \leq \xi \leq 1$, the only real region where $\Theta \geq f$ is where $\alpha_2 \geq \xi \geq \alpha_3$.

From the standard forms of elliptic integrals, equation (2.12) can be reduced (e.g. Bowman, 1961) to the form;

$$w(\eta) = \frac{2}{4\pi} \frac{|f'|}{f^{\frac{1}{2}}} \frac{K(k^2)}{[\alpha_2(\alpha_1-\alpha_3)]^{\frac{1}{2}}} \tag{2.13}$$

where

$$k^2 = \frac{\alpha_1(\alpha_2-\alpha_3)}{\alpha_2(\alpha_1-\alpha_3)} \tag{2.14}$$

and $K(k^2)$ is a complete elliptic integral of the 1st kind.

For another absorption line at;

$$\eta = \cos\left(\frac{\pi - \Psi}{3}\right),$$

if we substitute $\Psi' = \pi - \Psi$ we have;

$$\eta = \cos\frac{\Psi'}{3},$$

and $$\cos\Psi = -\cos\Psi'$$

so that;

$$f_2(\eta) = \frac{2}{27}(1 - 3\eta + 4\eta^3)$$

which is the same as equation (2.10) if η is replaced by $-\eta$. So exactly the same spectrum results except for it being inverted through $\eta = 0$ (H_o). The transitions for negative

FIGURE 2

Schematic representation of $\Theta(\xi)$. α_1, α_2, α_3 are the roots of the equation $\Theta(\xi) = f$

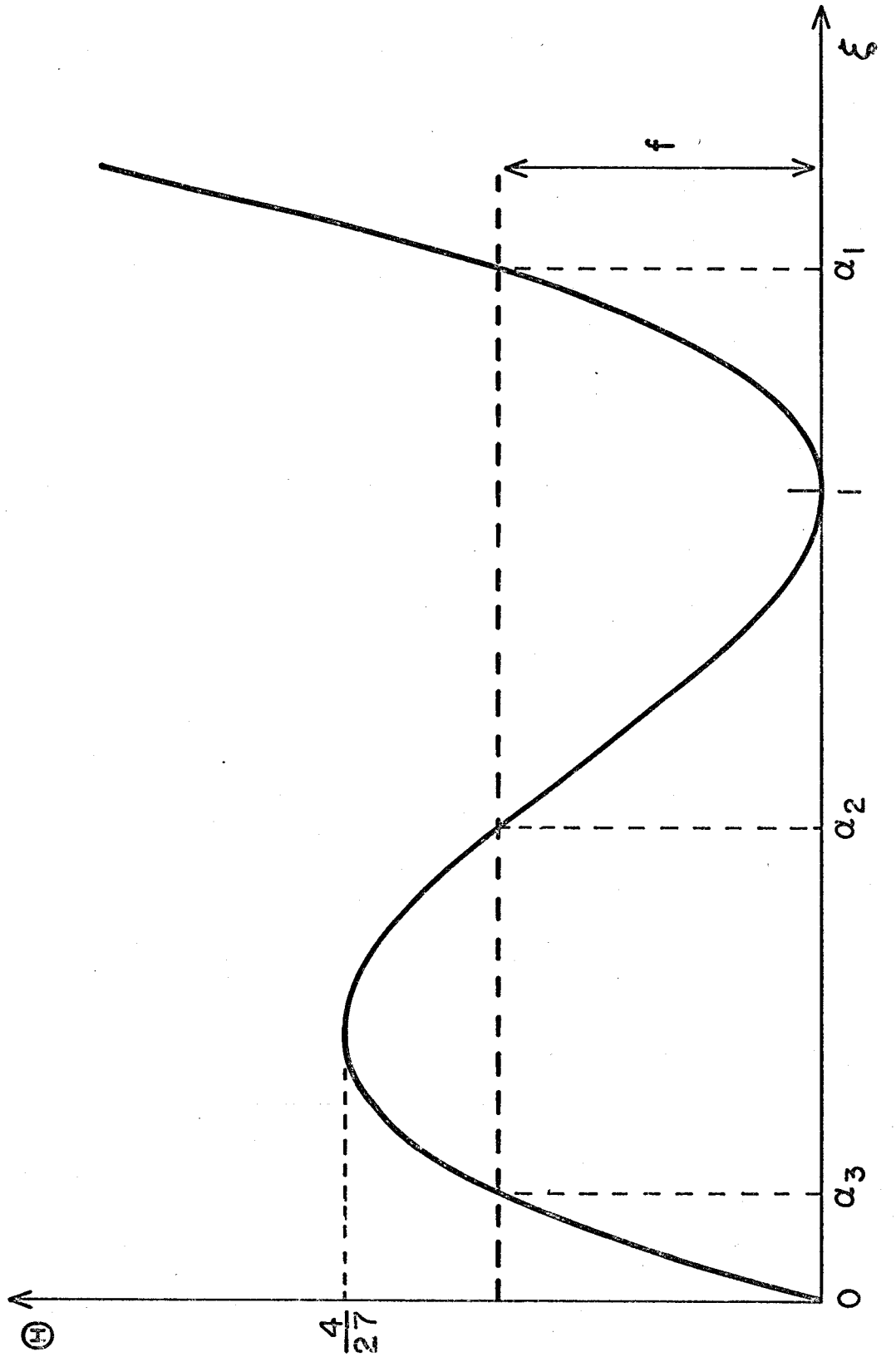
ξ
f
α1
1
α2
α3
0
4/27
Φ

M values will, in the same sense, be the inverse of those for positive M. The total spectrum will thus be given by solving equation (2.13) for $w(\eta)$ and symmetrizing about $\eta = 0$.

II.9 NEIGHBOURING IONS

The effect of the neighbouring ions on the lineshape may be considered to be a broadening of each skeletal component line into a gaussian function of the form;

$$\frac{1}{(\langle \Delta H^2 \rangle)^{\frac{1}{2}}} \exp\left\{ \frac{-(H-H_o)^2}{2\langle \Delta H^2 \rangle} \right\} \qquad (2.15)$$

where $\langle \Delta H^2 \rangle$ is the inter-ionic contribution to the second moment. The net lineshape is then obtained by convoluting both the meta and ortho lineshapes calculated previously with a gaussian function of the above form, and summing their contributions weighted appropriately. Because of the statistical correlations (Bright Wilson, Jr., 1935), the mixing ratio of the different symmetry types of ion is proportional to the spin weight only. The appropriate weighting ratio of meta: ortho is thus given by equations (2.3) and (2.7) as 5:3.

II.10 THE FORM OF $w(\eta)$

The roots of the equation

$$\theta = \xi(1 - \xi)^2 = f$$

are found, by the standard technique for solving cubic equations (Appendix D), to be;

FIGURE 3

Unbroadened ortho component $W(\eta)$ for $\eta \geq 0$. For negative η, $W(-\eta) = W(\eta)$. Scale unit for η is $\frac{3}{2}\frac{\gamma\hbar}{r^3}$.

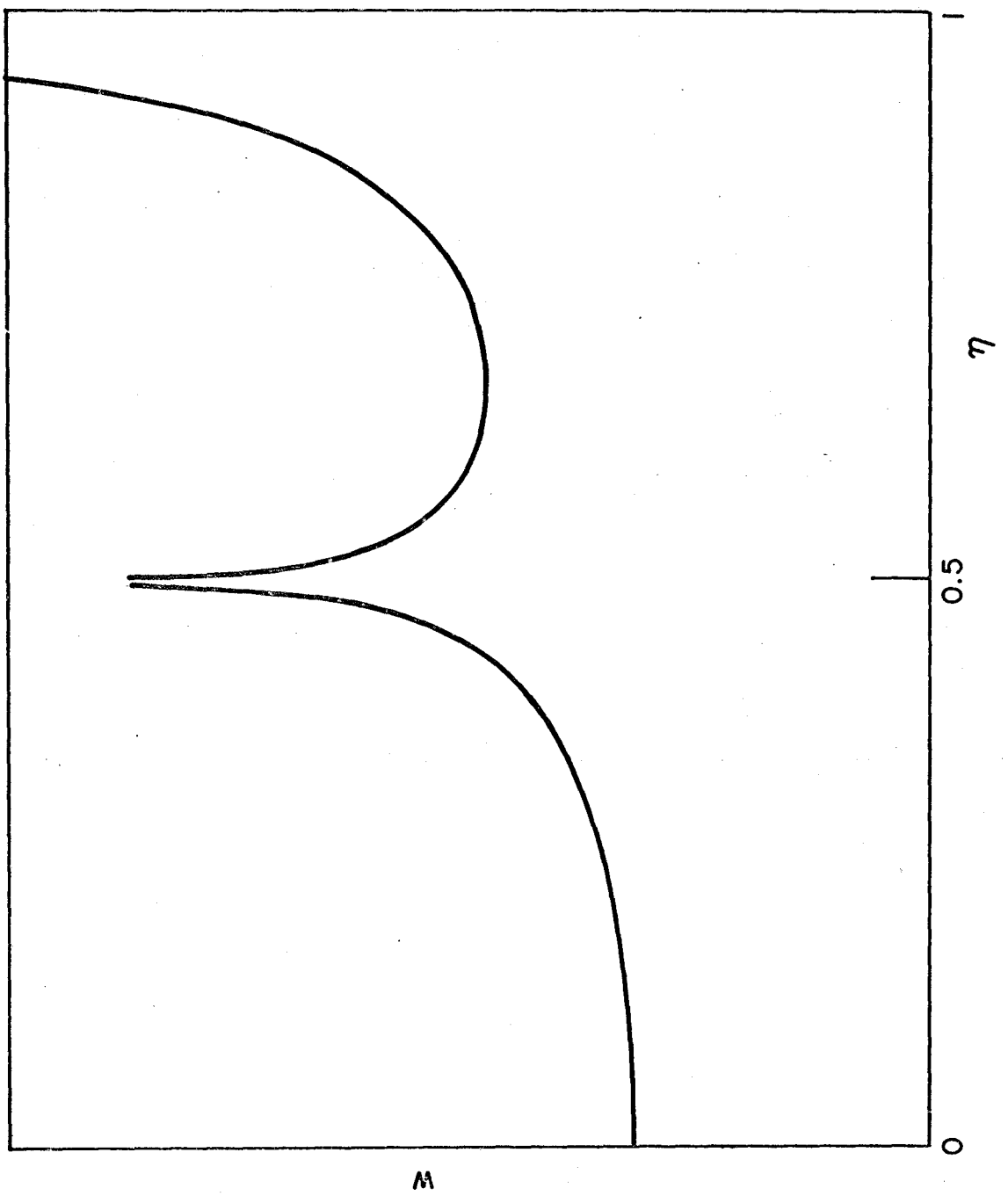
1
η
0.5
0
M

$$\left.\begin{aligned} \xi &= \frac{2}{3}(1 - \cos\chi) \\ \text{where} \quad \sin 3\chi &= \frac{\sqrt{27f(4-27f)}}{2} \\ \text{and} \quad \cos 3\chi &= \frac{2-27f}{2} \end{aligned}\right\} \qquad (2.16)$$

The solutions ξ, in descending order of magnitude, give α_1, α_2, α_3.

According to equation (2.13) $w(\eta)$ becomes infinite when either;

$$f = 0, \text{ or } k^2 = 1, \qquad (2.17)$$

the latter because $K(1) = \infty$.

From equation (2.14), $k^2 = 1$ when $\alpha_1 = \alpha_2$, which, by solving equations (2.16), or, more obviously, by inspection of Figure 2, occurs when $f = 0$. i.e. the conditions in equations (2.17) are identical.

From equation (2.10), $f = 0$ when;

$$\eta = 1 \text{ or } -\frac{1}{2}$$

$W(\eta)$, the symmetrized form of $w(\eta)$ defined as;

$$W(\eta) = w(\eta) + w(-\eta) \qquad (2.18)$$

and derived by the use of equations (2.10), (2.16), (2.14) and (2.13) is shown in Figure 3. The convolution of this function with a gaussian will require special treatment in the region of the anomalous infinities, i.e. where $\eta = \pm\frac{1}{2}$ and ± 1.

Near $\eta = 1$ we define the small variable δ_1 such that;

$$\eta = 1 - \delta_1$$

which, by substitution into (2.10), (2.16) and (2.14), gives (Appendix E);

$$k^2 = 1 - \frac{4\sqrt{6}}{9} \delta_1^{3/2} \qquad (2.19)$$

Near $\eta = -1/2$ we define the small variable δ_2 in the same way;

$$\eta = -\frac{1}{2} \pm \delta_2 .$$

The same series of substitutions leads (Appendix E) to;

$$k^2 = 1 - \frac{16}{27} \delta_2^3 . \qquad (2.20)$$

Letting $k^2 = 1 - \varepsilon^2$, where ε is a small quantity, it can be shown (Appendix F) that;

$$K(1 - \varepsilon^2) = 2 \ln 2 - \ln \varepsilon \qquad (2.21)$$

if ε is of the second order of smallness. i.e. ε must be small compared with a quantity β (defined in Appendix F) which is of the first order of smallness, so that;

$$\varepsilon^2 << \beta^2 << 1 . \qquad (2.22)$$

From equation (2.19), near $\eta = 1$;

$$\varepsilon_1^2 = \frac{4\sqrt{6}}{9} \delta_1^{3/2}$$

and from equation (2.20), near $\eta = -1/2$;

$$\varepsilon_2^2 = \frac{16}{27} \delta_2^3$$

so that substituting these values in equation (2.21) and using equations (2.10), (2.11) and (2.13) we find;

$$\left.\begin{aligned} w(1 - \delta_1) &= \frac{2}{4\pi} \times \frac{\sqrt{6}}{4} \delta_1^{-1/2} \ (\ell n\ 6 - \ell n\ \delta_1) \\ w(-\tfrac{1}{2} \pm \delta_2) &= \frac{2}{4\pi} \times 2 \ (\ell n\ 3 - \ell n\ \delta_2) \end{aligned}\right\} \qquad (2.23)$$

II.11 INTER-IONIC BROADENING

The spectral broadening effect of the neighbouring molecules can now be incorporated by convoluting $W(\eta)$ with the gaussian function $g(\eta)$ defined by;

$$g(\eta) = \frac{1}{a\sqrt{\pi}} \exp\{-\frac{\eta^2}{a^2}\}$$

where a^2 is the $\langle \Delta H^2 \rangle$ defined in equation (2.15), but normalized to the units of η. The broadened lineshape for the ortho-transitions $I^T(x)$ is then;

$$I^T(x) = \int_{-\infty}^{\infty} W(\eta) g(x-\eta) d\eta$$

$$= \frac{1}{a\sqrt{\pi}} \int_{-1}^{1} W(\eta) \exp[-\frac{(x-\eta)^2}{a^2}] d\eta$$

since $W(\eta) = 0 \quad$ for $|\eta| > 1$.

Integrating analytically over the anomalous regions, $I^T(x)$ can be written (Appendix G) as;

$$I^T(x) = I_1(x) + I_2(x) + I_3(x) + I_4(x) \qquad (2.24)$$

where;

$$I_1(x) + I_3(x) = \frac{1}{a\sqrt{\pi}} \left\{ \int_0^{\frac{1}{2}-\Delta_1} W(\eta) \left[\exp\left\{ - \frac{(x-\eta)^2}{a^2} \right\} + \exp\left\{ -\frac{(x+\eta)^2}{a^2} \right\} \right] d\eta + \int_{\frac{1}{2}+\Delta_1}^{1-\Delta_2} W(\eta) \left[\exp\left\{ - \frac{(x-\eta)^2}{a^2} \right\} + \exp\left\{ -\frac{(x+\eta)^2}{a^2} \right\} \right] d\eta + \frac{3}{4} \Delta_2 \left[\exp\left\{ - \frac{(x-1)^2}{a^2} \right\} + \exp\left\{ - \frac{(x+1)^2}{a^2} \right\} \right] \right\} \qquad (2.24a)$$

which can be evaluated numerically, and;

$$I_2(x) = \frac{1}{a\sqrt{\pi}} \left\{ \frac{2}{\pi} \Delta_1 (1 + \ell n\ 3 - \ell n\ \Delta_1) \left[\exp\left\{ - \frac{(x+\frac{1}{2})^2}{a^2} \right\} + \exp\left\{ -\frac{(x-\frac{1}{2})^2}{a^2} \right\} \right] \right\} \qquad (2.24b)$$

and;

$$I_4(x) = \frac{1}{a\sqrt{\pi}} \frac{\sqrt{6}}{4\pi} \Delta_2^{\frac{1}{2}} (2+\ell n6-\ell n\Delta_2) \left[\exp\left\{ - \frac{(x-1)^2}{a^2} \right\} \exp\left\{ - \frac{(x+1)^2}{a^2} \right\} \right] \qquad (2.24c)$$

Δ_1 and Δ_2 being small enough to satisfy the condition (2.22).

The broadened lineshape, $I^A(x)$, for the meta-transitions is obtained by convoluting the spectrum for an isolated group (a delta function at H_o) with the same gaussian function used for the ortho-broadening;

$$I^A(x) = \frac{1}{a\sqrt{\pi}} \int_{-\infty}^{\infty} \delta(\eta) \exp\{-\frac{(x-\eta)^2}{a^2}\}$$

$$= \frac{1}{a\sqrt{\pi}} \exp\{-\frac{x^2}{a^2}\} \ .$$

The total lineshape can now be obtained by summing $I^A(x)$ and $I^T(x)$ weighted by their transition probabilities in the ratio 5:3. Results of this calculation for $\langle \Delta H^2 \rangle$ of $1G^2$, $2G^2$, $4G^2$ and $6G^2$, and a proton-proton separation of 1.68 Å, (typical values for the ammonium salts) are shown in Figure 4.

II.12 SECOND MOMENT

The second moment (M_2) could be evaluated directly from the above broadened lineshapes, but we can note that;

$$M_2 = M_2' + \langle \Delta H^2 \rangle$$

where M_2' is the intra-ionic contribution to M_2 and is independent of the broadening factor $\langle \Delta H^2 \rangle$. Thus M_2' need only be evaluated once and M_2 then found by adding $\langle \Delta H^2 \rangle$.

The contribution to M_2' from the meta spectrum (a delta function) is zero, and from the ortho spectrum (Appendix H) is;

$$M_2'(\text{ortho}) = \frac{S_1 + A_2/4 + S_3 + A_4}{A_1 + A_2 + A_3 + A_4} \qquad (2.25)$$

FIGURE 4

Theoretical spin isomer absorption spectra with broadening factors, $\langle \Delta H^2 \rangle$, of 1, 2, 4 and 6 G^2, and an inter-proton distance of 1.68 Å.

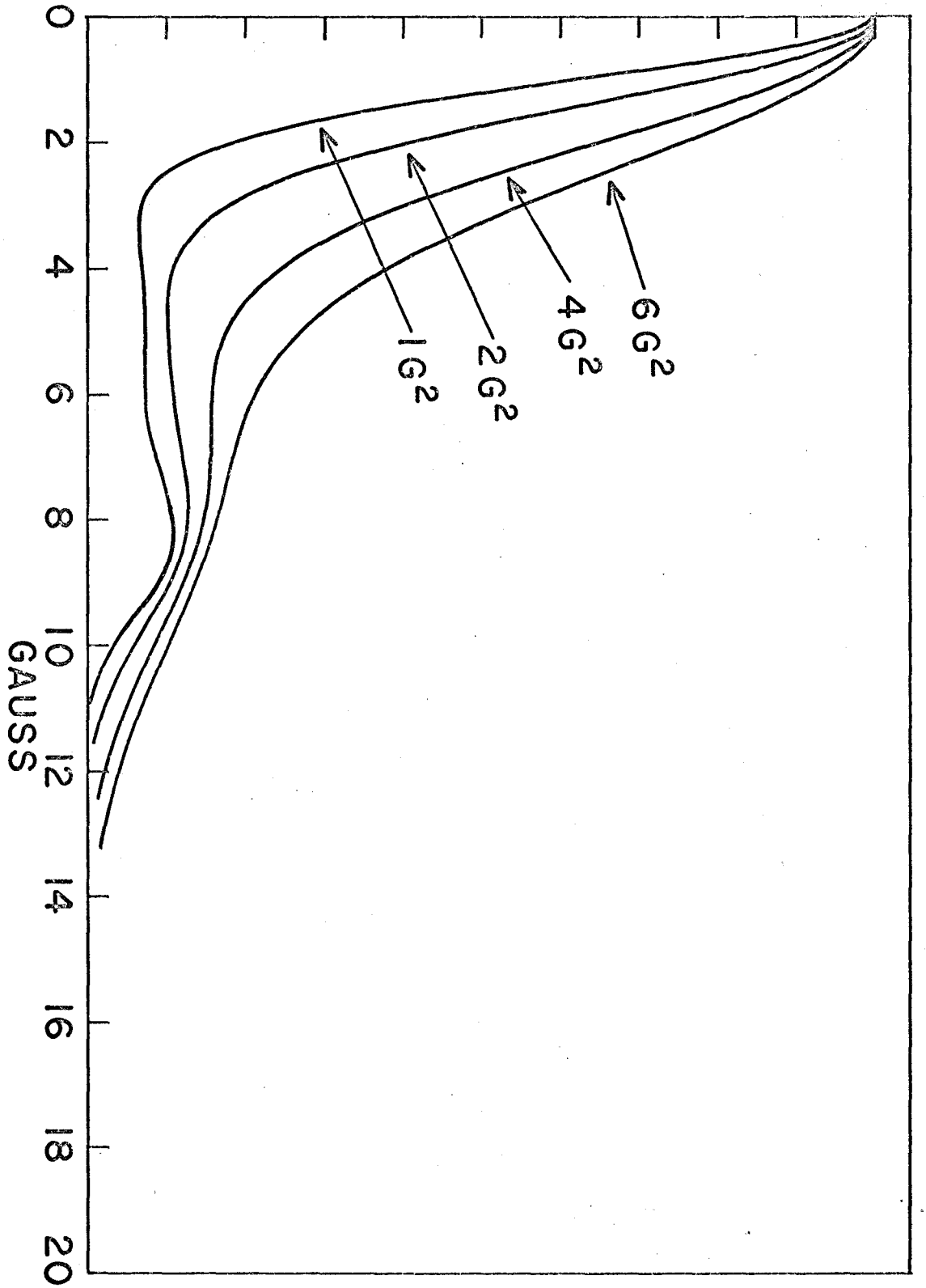
0
2
4
6
8
10
12
14
16
18
20
GAUSS
1 G²
2 G²
4 G²
6 G²

where;

$$S_1 = \int_0^{\frac{1}{2}-\Delta_1} \eta^2 W(\eta)\,d\eta \qquad (2.25a)$$

$$S_3 = \int_{\frac{1}{2}+\Delta_1}^{1-\Delta_2} \eta^2 W(\eta)\,d\eta \qquad (2.25b)$$

$$A_1 = \int_0^{\frac{1}{2}-\Delta_1} W(\eta)\,d\eta \qquad (2.25c)$$

$$A_3 = \int_{\frac{1}{2}+\Delta_1}^{1-\Delta_2} W(\eta)\,d\eta \qquad (2.25d)$$

$$A_2 = \frac{2\Delta_1}{\pi}\,(1 + \ell n\ 3 - \ell n\ \Delta_1) \qquad (2.25e)$$

$$A_4 = \frac{3\Delta_2}{4} + \frac{\sqrt{6}}{4\pi}\,\Delta_2^{\frac{1}{2}}\,(2 + \ell n\ 6 - \ell n\ \Delta_2) \qquad (2.25f)$$

Δ_1 and Δ_2 again satisfying condition (2.22).

Using equations (2.25) with a proton-proton separation of 1.68 Å gives M_2' (ortho) = 39.8 G^2, and since (Appendix H);

$$M_2' = \frac{3}{8}\,M_2' \text{ (ortho)}$$

we find that $M_2' = 14.9\ G^2$. We therefore expect M_2 to be in the range from 16 G^2 to 21 G^2 for $\langle \Delta H^2 \rangle$ from 1 G^2 to 6 G^2.

II.13 NITROGEN CONTRIBUTION

In order to include the nitrogen contribution in the spectrum we must go back to the original expression for

the dipolar Hamiltonian H_d and write

$$H_d = H_{dp} + H_{dn}$$

where H_{dp} is the proton contribution treated previously, and H_{dn} the nitrogen contribution. Since, as was explained before, only the adiabatic part of H_d (i.e. that part which commutes with the total Hamiltonian) contributes to the level splitting in first order, we can write H_{dn} as the truncated part;

$$H_{dn} = \sum_i A_{io} I_{iz} I_{nz}$$

where I_{iz}, I_{nz} are the z-component spin operators for proton i and the nitrogen nucleus respectively, and;

$$A_{i0} = \frac{\gamma \gamma_n \hbar^2}{r_{pn}^3} (1 - 3 \cos^2\theta_{i0})$$

γ, γ_n being the gyromagnetic ratios for the proton and nitrogen nuclei respectively, $\underline{r}_{pn}$ the proton-nitrogen vector and θ_{i0} the angle which $\underline{r}_{pn}$ makes with $\underline{H}_o$. It should be noted that the truncated H_{dn} does not contain the "flip-flop" terms $I_i^+ I_n^-$ analogous to those in H_{dp} because a simultaneous inversion of a proton and a nitrogen spin, having different magnetic moments, does not conserve energy. i.e. the term is non-adiabatic. Also, by the same argument used for the protons, only the intra-ionic contribution to H_{dn} need be considered in first order.

The basic spin states for the isolated ionic group must now be defined by the z-component spin quantum numbers of the protons and the nitrogen nucleus. For simplicity, and also to maintain as close an analogy as possible with the foregoing proton treatment, this latter quantum number (n) will be written as a subscript on the proton states defined previously and given in Table I. i.e. the spin states are now written as $|m_1 m_2 m_3 m_4>_n$ where m_i is $\pm$ 1/2 and, since the abundant isotope of nitrogen (N^{14}) has a spin $I_n = 1$, n can assume any one of the three values 0, $\pm$1.

The presence of the nitrogen nucleus at the centre of the tetrahedral ammonium group makes no difference to the symmetry considerations, so that for each of the three values of n Table I defines the same symmetry adapted set of states. With these as basis states the matrix representation of H_{dn} can be calculated (Appendix A). The relevant diagonal part (between states of the same symmetry) for n = 1 is shown in Tables IV and V. The matrix for n = -1 is the negative of that for n = 1, while the matrix for n = 0 is zero.

In the same reference frame defined by Figure 1 we have (Appendix B);

TABLE IV

Matrix elements of H_{dn} ——— (a).
States labelling rows and columns are ordered as in Table II.

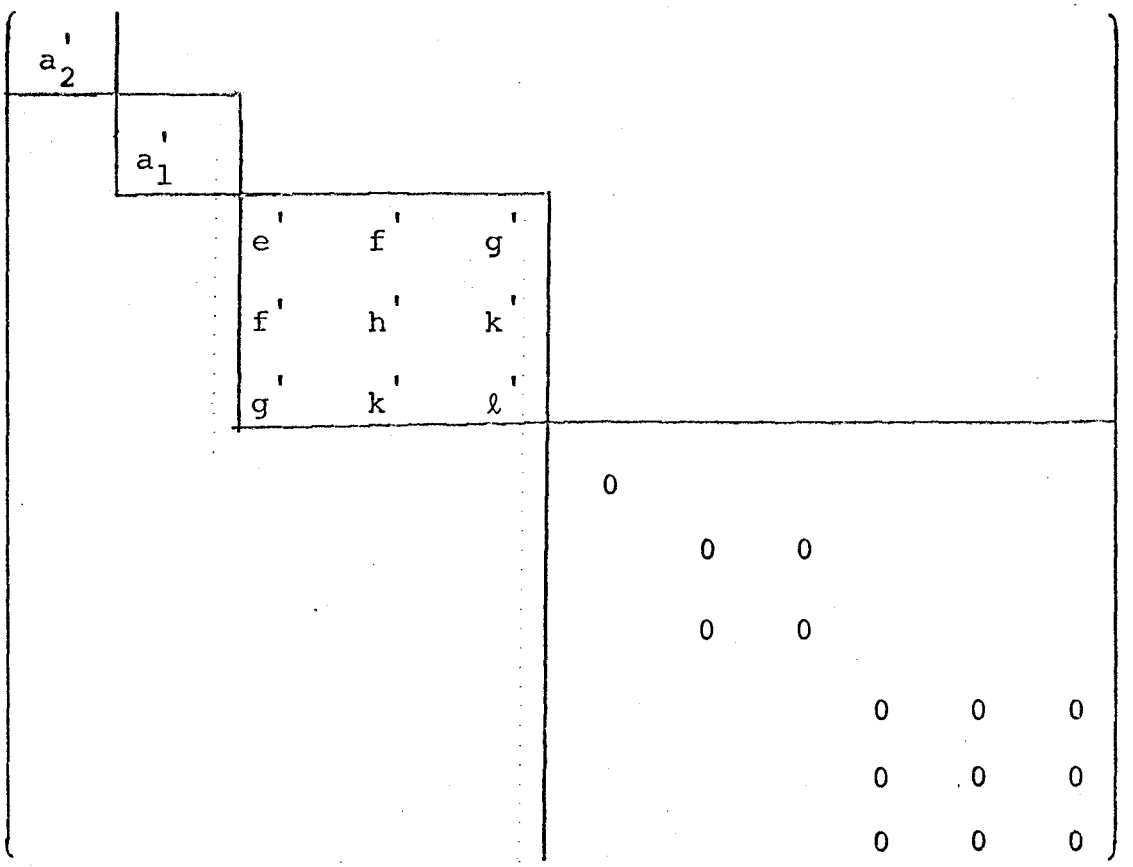

TABLE V

Matrix elements of H_{dn} ——— (b)
Elements of Table IV in terms of
A_{i0}

$$\begin{pmatrix} 2a_2' \\ 4a_1' \\ 12e' \\ 6\sqrt{2}f' \\ 2\sqrt{6}g' \\ 6h' \\ 2\sqrt{3}k' \\ 2\ell' \end{pmatrix} = \begin{pmatrix} 1 & 1 & 1 & 1 \\ 1 & 1 & 1 & 1 \\ 5 & 5 & 5 & -3 \\ -1 & -1 & 2 & 0 \\ -1 & 1 & 0 & 0 \\ 2 & 2 & -1 & 3 \\ -1 & 1 & 0 & 0 \\ 0 & 0 & 1 & 1 \end{pmatrix} \begin{pmatrix} A_{10} \\ A_{20} \\ A_{30} \\ A_{40} \end{pmatrix}$$

$$\left.\begin{aligned} A_{10} &= A_o[-\sin^2\theta\sin2\phi + \sin2\theta(\sin\phi + \cos\phi)] \\ A_{20} &= A_o[-\sin^2\theta\sin2\phi - \sin2\theta(\sin\phi + \cos\phi)] \\ A_{30} &= A_o[\ \sin^2\theta\sin2\phi - \sin2\theta(\sin\phi - \cos\phi)] \\ A_{40} &= A_o[\ \sin^2\theta\sin2\phi + \sin2\theta(\sin\phi - \cos\phi)] \end{aligned}\right\} \qquad (2.26)$$

where $$A_o = \frac{\gamma\gamma_n\hbar^2}{r_{pn}^3}$$

By directly summing these, the symmetric combinations a_2' and a_1' are found to be identically zero. Therefore the A type states are unshifted in first order by the nitrogen contribution and so the meta-spectrum is unaltered, remaining a delta function at H_o. In general however the T type states are shifted by the nitrogen contribution, the matrix elements for M = 0 no longer being simply twice the negative of those for M = 1. This complication makes the analytical solution of the spectrum for an arbitrary crystal orientation intractable. Since the angular dependence of the absorption lines needs to be known in order to take a polycrystalline average, the line shape calculation for a powder sample has not been attempted. However, the absorption spectrum can be readily calculated for any given crystal orientation. In particular, it can be seen from equation (2.26) that for a [1,0,0] field direction where $\theta = \pi/2$ and $\phi = 0$ we have;

$$A_{i0} = 0 \text{ for all } i.$$

The same is true for the equivalent [0,1,0] and [0,0,1] directions. This means that all the matrix elements in Tables IV and V are zero, the nitrogen nucleus making no contribution

to the spectrum for these field directions. i.e. the previous proton derivation applies.

Inserting the appropriate values of θ and ϕ into equation (2.5) gives;

$$\cos\Psi = 1$$

from which $\Psi = 0, 2\pi$ etc, which, by substitution in equations (2.6) and (2.8) yields absorption lines at;

$$\eta_1 = -1$$
$$\eta_{2,3} = \frac{1}{2}$$

plus the equivalent lines on the other side of H_o arising from negative M transitions. With the same dimensions of the ammonium group used before, this means absorption for the [1,0,0] field direction should occur at H_o (for the meta-states) and $H_o \pm 4.5$ G and $H_o \pm 8.89$ G (for the ortho-states), with relative intensities 10:2:1 (to be consistent with total intensities in ratio 5:3). A resulting spectrum broadened by a typical $\langle \Delta H^2 \rangle$ of 2 G^2 is shown in Figure 5.

FIGURE 5

Theoretical spin isomer absorption spectrum for a single crystal with $\underline{H}_o$ along the [1,0,0] direction. The broadening factor, $\langle \Delta H^2 \rangle$, used is 2 G^2 and the inter-proton distance 1.68 Å.

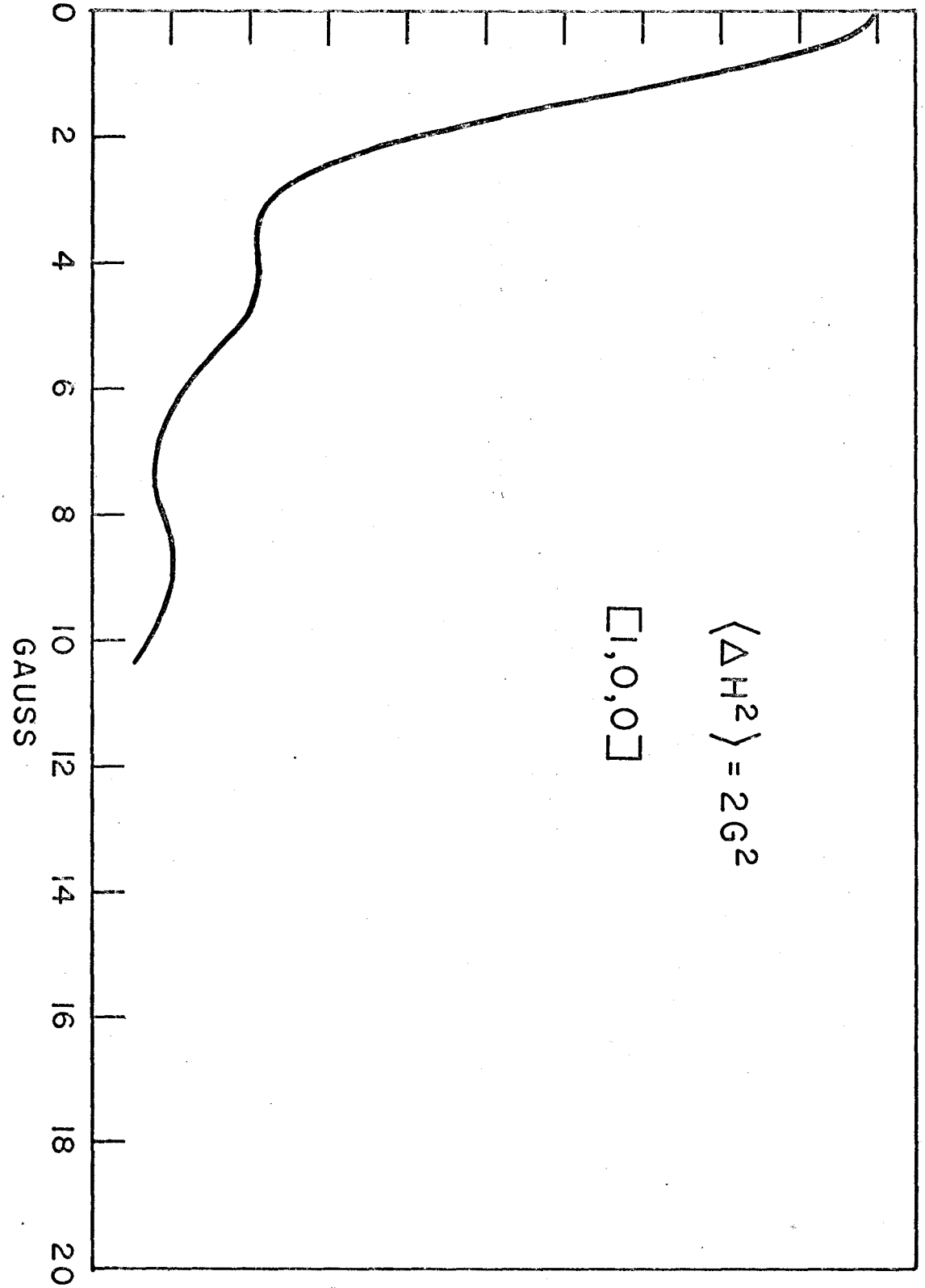
0
2
4
6
8
10
12
14
16
18
20
GAUSS
⟨ΔH²⟩ = 2G²
[1,0,0]

CHAPTER III

APPARATUS AND EXPERIMENTAL PROCEDURE

III.1 ABSORPTION

Magnetic fields of up to 10,000 G in a 3" pole face gap were provided by a 12" Varian electromagnet monitored by a Varian V-FR 2503 Fieldial. The broadening of the signal due to the field inhomogeneity (as checked by the broadening of the proton signal of a paramagnetically contaminated water sample) was of the order of 1 G with the sample sizes used (up to 1.4 cm in diameter by 1 cm in length).

The sample coil, which is attached to the end of a probe and located inside a dewar fixed between the pole faces of the magnet, is part of the resonating circuit of a Pound-Knight-Watkins marginal oscillator operating at a frequency of approximately 40 MHz. An audio frequency generator modulates the applied field, at an amplitude much smaller than the linewidth, through a pair of Helmholz coils mounted on the pole faces. The signal is first r.f. amplified and detected, then fed to a wide band audio frequency amplifier followed by a lock-in amplifier, where it is mixed with the audio frequency signal from the a.f. generator and phase detected. The d.c. output, approximately proportional to the derivative

of the line shape curve, is plotted by a pen recorder as the field is scanned linearly through the resonance by the Fieldial. A block diagram for the system is given in Figure 6a with a circuit diagram of the marginal oscillator in Figure 6b.

The marginal oscillator was operated at sufficiently low r.f. power levels to ensure that distortion effects caused by nuclear spin saturation were negligible. This was checked for in two ways. Firstly, after holding the applied field (H_o) off resonance for some time ($\sim$ 10 min.) to allow the spins to achieve thermal equilibrium with the lattice, H_o would be switched suddenly into resonance (in fact to the maximum of the derivative spectrum). Starting with an arbitrary r.f. power level the signal was observed to decay with time as the nuclear Zeeman levels became saturated. This procedure was repeated with the r.f. power level lowered progressively until a value was reached at which no saturation decay of the signal could be observed after switching H_o into resonance. Care was taken during the collection of data to ensure that the r.f. power level always remained below this value.

Secondly, a direct measurement was made of the exciting r.f. field (H_1). The r.f. voltage induced across a secondary pick-up coil fixed in the vicinity of the sample coil was measured on an oscilloscope. The capacitor of the tank

circuit of the marginal oscillator was then shorted out and an r.f. voltage from a signal generator applied to the sample coil. The amplitude of the signal from the generator was adjusted so that the voltage across the pick-up coil, as measured on the oscilloscope, was the same as that previously induced by the marginal oscillator. The output from the signal generator was simultaneously applied to the oscilloscope and the r.f. voltage applied to the sample coil read directly. This was taken as being equal to the r.f. voltage originally produced across the sample coil by the oscillator. In this way it was determined that voltage levels of less than 10 mV were used across the 1μ Henry coil during the collection of data.

The magnetic induction (B) at the centre of a long cylindrical coil (Reitz and Milford,1960), is:

$$B = 4\pi\left(\frac{N}{L}\right)\frac{I}{10} = H_1$$

where I (amps) is the current through the L(cm) coil of N turns. A voltage of 10 mV across the coil produced a current of 0.04 mA giving, according to the above formula, an H_1 of 0.25 mG. For this field value, a T_1 of 100 sec. and a T_2 of 10 μsec (typical values for these salts at this temperature) the saturation factor ($\gamma^2 H_1^2 T_1 T_2$) is 0.05. Since $\gamma^2 H_1^2 T_1 T_2 << 1$, the saturation was negligible for all measurements.

The above tests demonstrated conclusively that the marginal oscillator was operating in the linear regime and that the experimental signal was proportional to the derivative of the line shape.

FIGURE 6a

Block diagram of the absorption spectrometer.

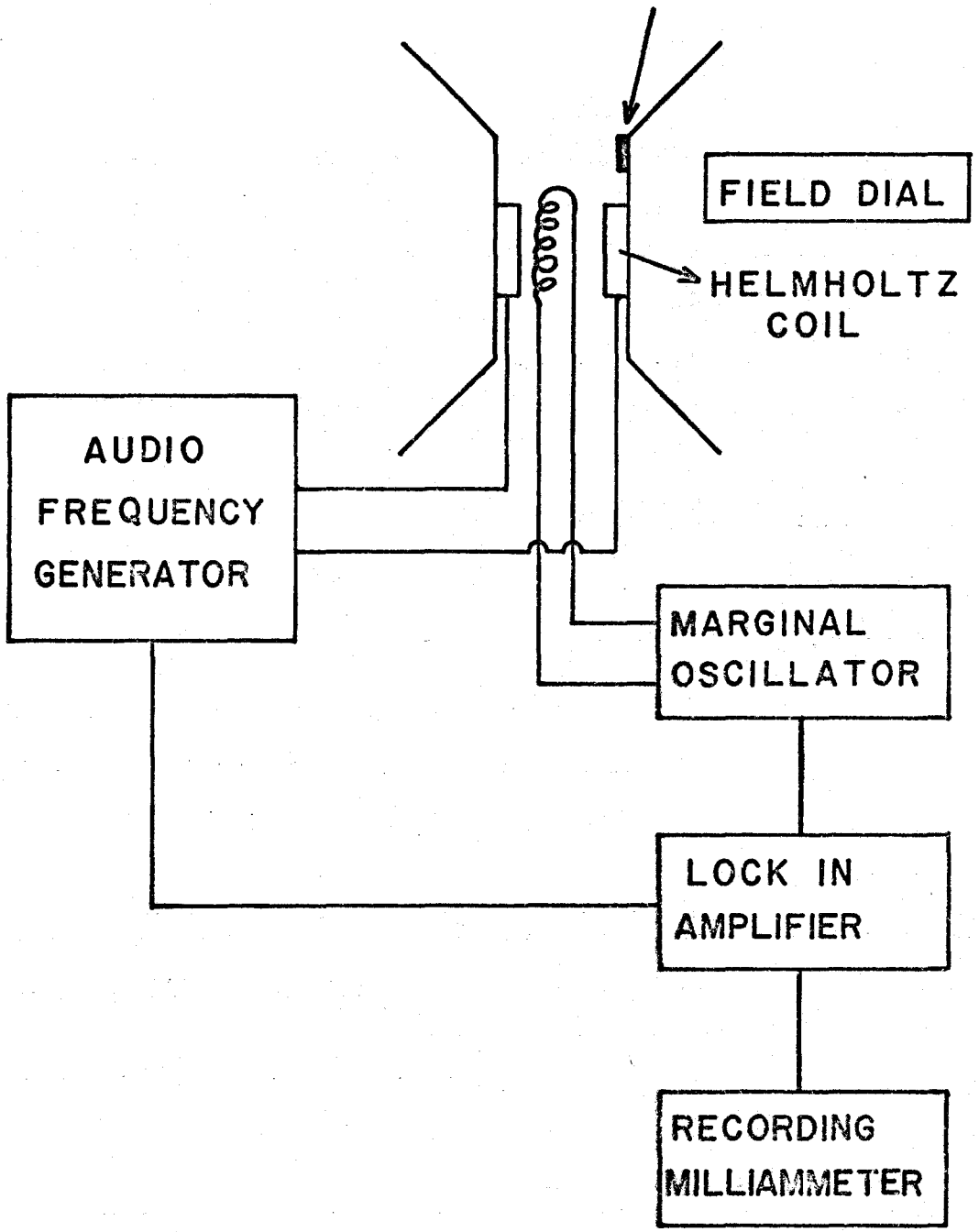
FIELD DIAL
HELMHOLTZ COIL
AUDIO FREQUENCY GENERATOR
MARGINAL OSCILLATOR
LOCK IN AMPLIFIER
RECORDING MILLIAMMETER

Figure 6b

Circuit diagram of marginal oscillator

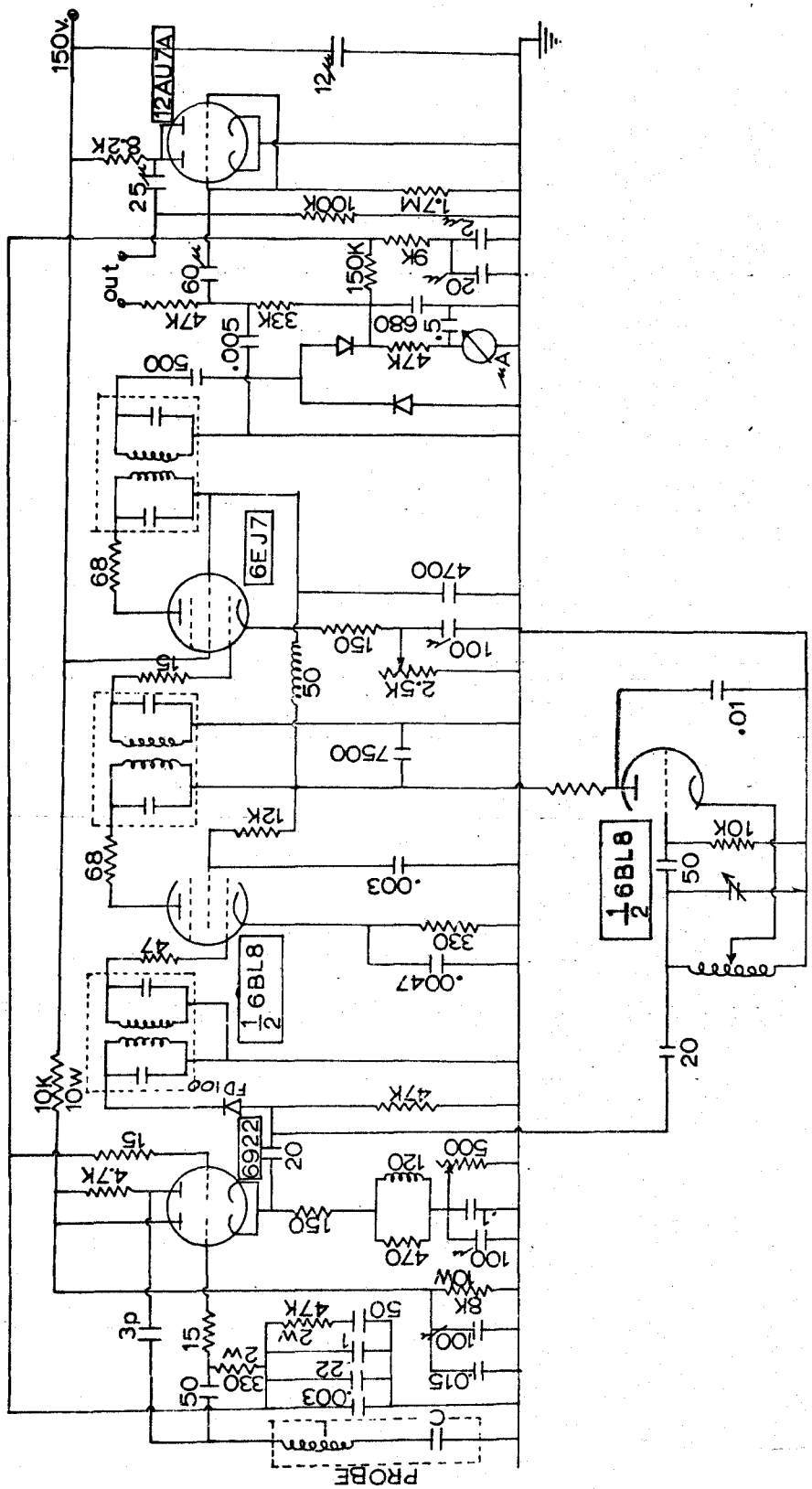
150v
12AU7A
12μ
2.2K
25μ
100K
1.7M
2μ
out
60μ
150K
9K
20
47K
33K
.005
.005
680
μA
47K
500
6EJ7
68
4700
150
100
2.5K
50
15
7500
.01
12K
68
.003
10K
50
6BL8
330
.0047
47
6BL8
20
10K
10w
FD100
47K
6922
20
15
4.7K
500
120
150
100
470
10W
8K
100
.015
3p
15
50
50
4.7K
2W
1
2W
330
22
.003
C
PROBE

III.2 SPIN LATTICE RELAXATION

Under steady state conditions the total nuclear magnetic moment of the sample is directed along the applied field $\underline{H}_o$, which we can designate as the z direction. It is well known that an oscillating magnetic field $2H_1\cos\omega_L t$ applied at the Larmor frequency ω_L of the nuclei being studied changes the orientation of this nuclear moment, and that if applied for a time $t=\pi/2\gamma H_1$, rotates it through 90° into the x-y plane. If the oscillating field is then removed, the spins, initially coherent in the x-y plane, lose coherence in a time T_2 so reducing the magnetic moment in this plane to zero, and relax back along H_o in a time T_1. If an identical 90° pulse is applied after a time τ, much longer than T_2, the nuclear moment recovered along H_o is again rotated into the x-y plane. Detecting this x-y component of the nuclear moment by the voltage it induces in the coil of a tuned tank circuit gives a signal proportional to the magnetization recovered along H_o in time τ. Observing this for various τ's allows T_1 to be calculated.

The experimental arrangement employed is shown schematically in Figure 7. Variable width pulses at repetition times in the range from 10^{-4} to 10^{2} seconds provided from Tektronix series 160 waveform and pulse generator units were amplified and used to gate an r.f. oscillator which then supplied 30G r.f. pulses to a tuned coil surrounding the teflon sample holder. The signal detected in the coil was then amplified and rectified before being displayed on a high frequency oscilloscope equipped with a polaroid camera for recording the free induction decay amplitude. The spectrometers used operated at 5.4, 19, 20.7 and 42 MHz, the

FIGURE 7

Block diagram of the T_1 spectrometer.

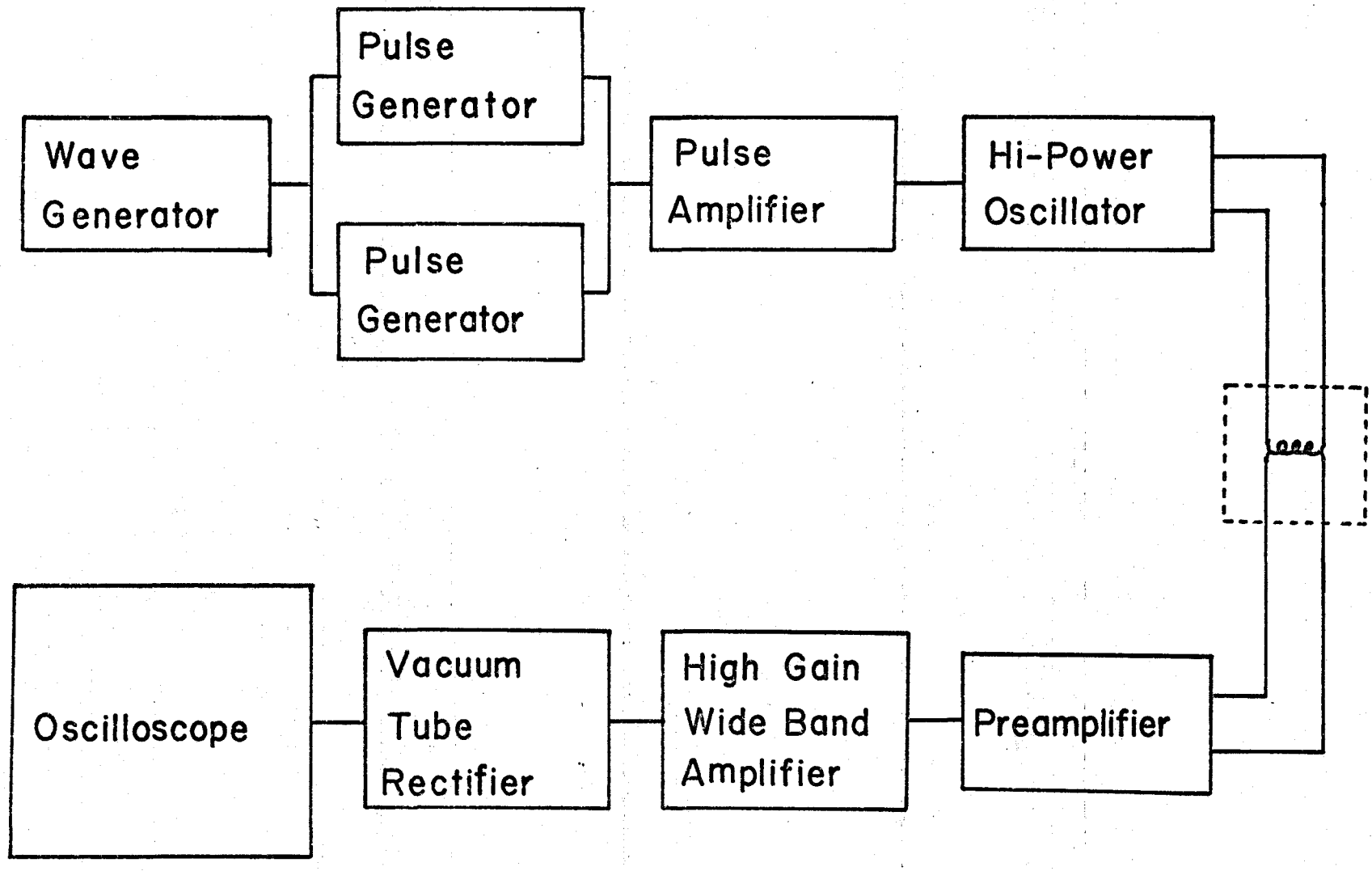
Wave Generator
Pulse Generator
Pulse Generator
Pulse Amplifier
Hi-Power Oscillator
Oscilloscope
Vacuum Tube Rectifier
High Gain Wide Band Amplifier
Preamplifier

r.f. amplifier having the fast recovery (6 μsec dead time) necessary to observe the signal before it decays (in time T_2) after the 90° pulse.

III.3 TEMPERATURE CONTROL

To obtain temperatures down to that of liquid nitrogen the sample, inside its teflon holder and pickup coil, was contained inside a dewar held between the pole faces of the magnet. A controlled heater immersed in a source of liquid nitrogen provided a steady boil off of nitrogen gas which was either passed directly over the sample or preheated by a hot nichrome coil. Adjusting the variacs powering both heaters, temperatures in the approximate range from 80°K to 400°K were obtained, and measured by a copper-constantan thermocouple located close to the sample.

For temperatures below 77°K a helium cooled Andonian cryogenic system was used. A needle valve controlled the flow of helium gas from the pressurized liquid helium storage chamber into the sample chamber. The sample was mounted on a copper block on which was wound a heating coil, and in which was embedded a germanium and a platinum resistance thermometer. By balancing the helium flow with a low heater power, a stable temperature could be maintained over many hours. With this arrangement temperatures down to that of liquid helium (4.2°K) could be attained.

III.4 SINGLE CRYSTAL STUDY

The single crystals of NH_4Cl and $(NH_4)_2SnCl_6$ both exhibited well defined growth faces, the orientations of which were indicated by the external crystal symmetry and confirmed by x-ray diffraction. Using these growth faces the crystals were optically oriented in the sample holder to an accuracy of a few degrees, their four-fold axes ([0,0,1]) being aligned along the axis of the sample probe. The [1,0,0] and [1,1,0] crystal directions were brought approximately along the applied field by rotation of the probe inside the dewar, the orientations then being sought at which the absorption lineshape showed minimum sensitivity to small angular deviations (the [1,0,0] and [1,1,0] are symmetry directions for a cubic crystal and so represent extrema in the lineshape).

III.5 SAMPLE MATERIALS

The chemicals used in this investigation, and their sources, are listed below. In the cases where some structural data is known, this is also given.

Ammonium chloride [NH_4Cl] can be prepared by double decomposition between an alkaline chloride and an ammonium salt (Adler, 1899). The material used was of "reagent ACS" grade and was supplied by Matheson Coleman and Bell Company. The room temperature crystal structure,as determined by x-ray studies, is simple cubic with a = 3.859 Å (Wyckoff, 1923).

Ammonium bromide [NH_4Br] can be obtained by the direct

reaction of an excess of ammonia gas with bromine (Bosetti, 1889). The material used in this study was of "reagent" grade, again supplied by Matheson Coleman and Bell Company. X-ray studies show the room temperature crystal structure to be cubic with a = 4.047 Å (Havighurst, Mack Jr., and Blake, 1925). Levy and Peterson (1953) performed a neutron diffraction study of four phases of ND_4Br. In the room temperature phase their results favoured a structure with orientational disorder among the ammonium ions and a space group Pm3m.

Ammoniom fluoride [NH_4F] can be prepared by crystallization from NH_4Cl and NaF solutions (Berzélius, 1828). The material used was of "Baker analyzed reagent" grade, supplied by J. T. Baker Chemical Company. At room temperature the crystal exhibits the zincite structure with two molecules per unit cell, where a = 4.39 Å and c = 7.02 Å (Zachariasen, 1927).

Ammonium selenate [$(NH_4)_2SeO_4$] can be obtained by the neutralization of selenic acid with a weak ammonium solution. Crystals form into monoclinic prisms with a:b:c = 1.758:1:1.206, β = 77°41' (Tutton, 1906). The material used was of "reagent" grade, supplied by Alfa Inorganics, Inc.

Ammonium diuranate [$(NH_4)_2U_2O_7$] can be obtained by the reaction of liquid ammonia at -33.5°C on uranium nitrate hexa- or di-hydrate (Watt, Jenkins and McCuiston, 1950). It is usually prepared industrially by the precipitation resulting from the addition of gaseous ammonia to a solution of uranyl nitrate.

The material used in this study was of "reagent" grade, supplied by Alfa Inorganics Inc.

Ammonium dichromate [$(NH_4)_2Cr_2O_7$] can be prepared by evaporation of a solution of one mole of ammonia and two moles of chromic anhydride (Abel, 1850). The material used in this study was a Fisher Scientific certified reagent. The crystals are monoclinic with a = 7.74 Å, b = 7.54 Å, c = 13.26 Å, β = 93°42' with four molecules per unit cell (Gossner and Mussgnug, 1930) and a space group C2/c (Wilhelmi, 1951). Specific heat measurements indicate two phase transitions at -2 °C and -120°C (Jaffray, 1952).

Ammonium persulphate [$(NH_4)_2S_2O_8$] results from anodic oxydation of a saturated solution of ammonium sulphite in dilute sulphuric acid (Berthelot, 1892). The material used in this study was "certified ACS" reagent supplied by Fisher Scientific Company. At room temperature the crystals are monoclinic (Fock, 1893), the bimolecular unit cell having dimensions a = 7.84 Å, b = 8.06 Å, c = 6.14 Å, β = 95°9' and the space group $P2_1/n$ (Wyckoff 1951a).

Ammonium trichlorostannite [NH_4SnCl_3] can be obtained by treating a solution of ammonium chloride with excess stannous chloride (Rimbach and Fleck, 1915). The material used in this study was of "reagent" grade, supplied by Alfa Inorganics Inc.

Ammonium hexachlorostannate [$(NH_4)_2SnCl_6$] can be obtained by the evaporation of a mixture of ammonium chloride

and stannic chloride solutions (Druce, 1918). The material used in this study was of "reagent" grade and was supplied by Alfa Inorganics Inc. The room temperature structure is face centred cubic with space group Fm3m (Engel, 1935).

Ammonium iodoplatinate $[(NH_4)_2PtI_6]$ can be obtained by treating tetravalent platinum iodide with ammonion iodide (Datta, 1913).

Ammonium hexanitratocerate $[(NH_4)_2Ce(NO_3)_6]$ was of "reagent" grade, supplied by Alfa Inorganics Inc.

Ammonium gallium tetrachloride $[(NH_4)GaCl_4]$ can be obtained by the action of HCl gas on trimethylmonoaminegallium $[(CH_3)_3GaNH_3]$ (Kraus and Toonder, 1933). The material used in this study was of "reagent" grade, and was supplied by Alfa Inorganics Inc.

Ammonium sulphate $[(NH_4)_2SO_4]$ can be prepared by the reduction of calcium sulphate in the presence of gaseous ammonia, carbon dioxide and water (Neumann, 1921). X-ray studies by Ogg and Hopwood (1919) show the room temperature structure to be orthorhombic with a = 5.951 Å, b = 10.560 Å, c = 7.729 Å, with a second order phase transition occurring at -50.7°C (Crenshaw and Ritter, 1932). The material used in this study was graded "primary standard" as supplied by Fisher SCientific Company.

Ammonium selenite $[(NH_4)_2SeO_3]$ can be obtained by evaporation of an aqueous solution of selenic acid saturated with ammonia gas (Muspratt, 1849). The material used in this

study was supplied by Alfa Inorganics Inc. as "reagent" grade.

Ammonium tetrafluoroberyllate [$(NH_4)_2BeF_4$] was supplied in "reagent" grade for this study by Alfa Inorganics Inc. Mukherjee (1944) found the room temperature structure to be orthorhombic with a = 7.49 Å, b = 10.39 Å, c = 5.89 Å. However, Okaya, Vedam and Pepinsky (1958) discovered a superstructuring which doubled the b and c dimensions and changed the space group from the basic Pnam to Acam.

Ammonium thiosulphate [$(NH_4)_2S_2O_3$] can be prepared by dissolving sulphur in a solution of the sulphite. The anhydrous crystals are monoclinic at room temperature with a:b:c = 1.5717:1:1.3500, and α = 85°25' (Fock and Kluss, 1889), with a space group C2/m (Brunt, 1946). The material used for this study was of "purified" grade, supplied by Fisher Scientific Company.

Ammonium nitrate [NH_4NO_3] can be obtained by the mutual neutralization and evaporation of acid and base. It forms flexible rhombohedral crystals at room temperature with a:b:c = 0.9092:1:1.0553 (Gossner, 1904). The room temperature phase is reported in Structure Reports (1960a) as orthorhombic with a = 5.75 Å, b = 5.45 Å and c = 4.96 Å and space group Pmmm . The material used in this study was of "analytical reagent" grade, supplied by British Drug Houses Limited.

Ammonium metavanadate [NH_4VO_3] can be prepared, for example, by neutralizing an acidic solution of vanadium anhydride

with excess ammonia, and adding an ammonium salt (Berzelius, 1831). The colourless crystals (Von Humboldt, 1804) are isomorphic to KVO_3 (Norblad, 1875). Structure Reports (1960b) gives the room temperature structure as orthorhombic with $a = 4.92$ Å, $b = 11.82$ Å, $c = 5.85$ Å and a space group Pmab. The material used in this study was of "reagent" grade, supplied by Alfa Inorganics Inc.

Impurities, in normal concentrations, will have virtually no effect on the nuclear absorption spectrum since the energy levels of only that small fraction of nuclei in the vicinity of the impurity will be affected. However, paramagnetic impurities can have a marked effect on the relaxation. The large magnetic moments of the unpaired electron spins in paramagnetic ions can couple quite strongly to the nuclear magnetic moments. Relaxation of the electron spin modulates this electron-nuclear coupling so allowing the nuclear Zeeman energy to relax to the electron system and hence to the lattice. The rapid establishment of a spin temperature among the nuclei by the nuclear spin-spin interaction means that the whole nuclear Zeeman system can be relaxed by relatively few impurities.

The electron spin-lattice relaxation is only slightly temperature dependent since the phonon spectrum inducing it is very broad. Hence, the nuclear relaxation through such paramagnetic centres is almost independent of temperature .

Therefore, at very high and very low temperatures where the thermal nuclear relaxation rate becomes slower than the paramagnetic relaxation rate, the latter dominates the relaxation, so limiting the value of T_1.

CHAPTER IV

CRYSTAL DATA

IV.1 INTRODUCTION

Most of the ammonium salts under consideration in this work have been studied only as powder samples, the relevant crystal classes to which they belong being given in Table VI (Chapter V). Since only NH_4Cl and $(NH_4)_2SnCl_6$ have been studied as single crystals, the crystal data for these salts alone will be presented in this chapter.

IV.2 AMMONIUM CHLORIDE [NH_4Cl]

The high and low temperature structures of this salt have been investigated by, for example, x-ray (Nagakura, 1957), neutron (Levy and Peterson, 1952) and electron (Kuwabara, 1959) diffraction. The crystal belongs to the cubic class with the nitrogen and chlorine atoms occupying a CsCl type lattice, the dimensions of whose unit cell is 3.866 Å at room temperature (Wyckoff, 1951b). The room temperature phase, existing between -30.5°C and 180.3°C, belongs to the space group Pm3m, while the low temperature phase, below -30.5°C, belongs to the space group P43m. The two possible orientations of the tetrahedral ammonium ion, in which the N-H bonds are directed towards the nearest neighbour

chlorine atoms, are occupied randomly in the room temperature phase, and regularly in the low temperature phase. The N-H distance in both cases is 1.03±0.02 Å. The possible configurations within a cell are shown in Figure 8(a).

IV.3 AMMONIUM HEXACHLOROSTANNATE [$(NH_4)_2SnCl_6$]

An x-ray diffraction study of this salt by Engel (1935), shows that at room temperature the crystal lattice is face centred cubic with a unit cell dimension of 10.038 Å. The crystal structure belongs to the space group Fm3m. The ammonium ion, surrounded tetrahedrally by four $SnCl_6$ ions, has twelve equidistant chlorine atoms as its nearest neighbours. The configuration of one octant of the unit cell is shown in Figure 8(b), where the ammonium ion orientation is only representational, there having been no precise determination of the hydrogen atom positions.

We are much indebted to Mr. H. C. Teh for supplying the crystal of NH_4Cl and to Dr. K. R. Jeffrey for the crystal of $(NH_4)_2SnCl_6$.

FIGURE 8

(a) Environment of the ammonion ion in NH_4Cl. The small closed, and small open circles show the two possible orientations of the NH_4^+ ion.

(b) Environment of the ammonium ion in $(NH_4)_2SnCl_6$, showing one octant of the unit cell. The hydrogen positions are only schematic.

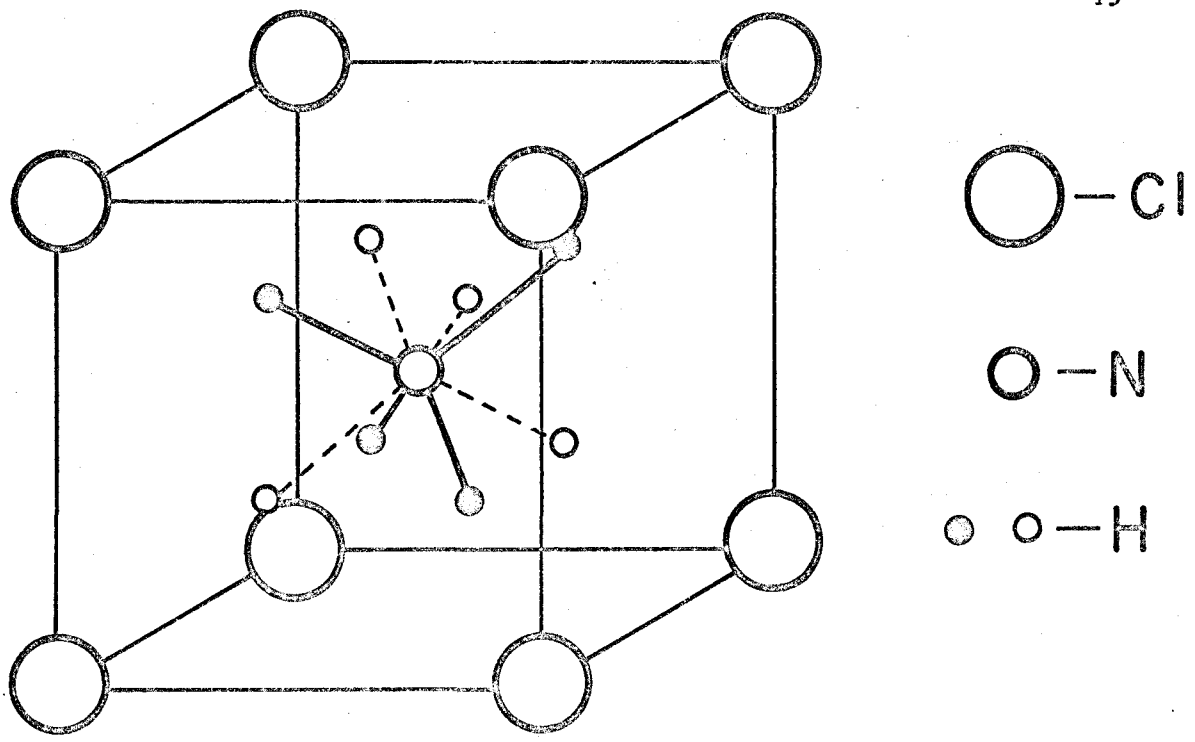

(a)

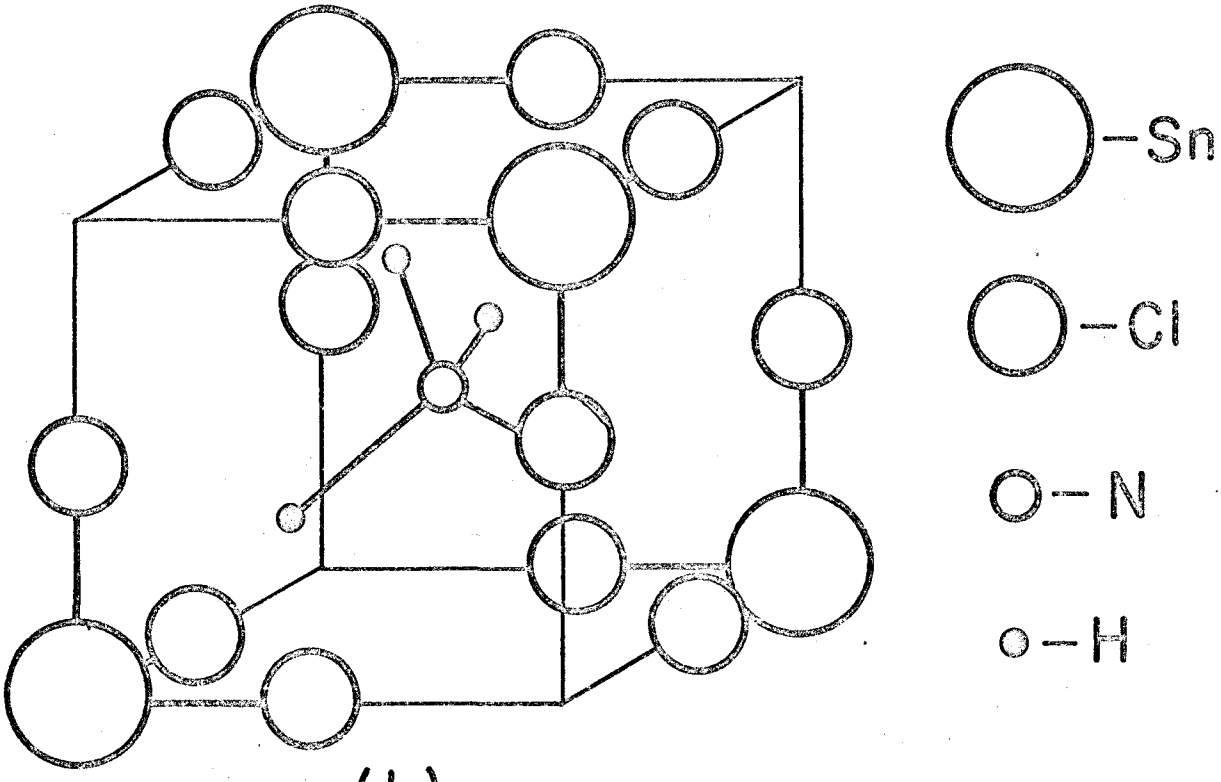

(b)

CHAPTER V

EXPERIMENTAL RESULTS

V.1 PROTON ABSORPTION MEASUREMENTS

The derivative of the proton absorption signals at 4.2°K for powdered samples of twenty ammonium salts were recorded. Those obtained for ammonium selenite [$(NH_4)_2SeO_3$], and ammonium tetrafluoroberyllate [$(NH_4)_2BeF_4$] are shown in Figures 9 and 10. These two have been chosen for explicit display because they are representative of the range of spectra obtained; from the very simple [$(NH_4)_2BeF_4$], to the more complicated [$(NH_4)_2SeO_3$].

The absorption spectra were obtained from these derivatives by computer integration and are shown in Figures 11 to 29 along with, in some cases, the theoretical spin isomer spectra (dashed curve) of closest fit (see Chapter VI). No correction for modulation distortion has been made, but the modulation amplitude is indicated in each figure. Only one half of each spectrum is given since all spectra were observed to be symmetrical about the origin, H_o.

Some gross features of each spectrum, such as line-width (δH), defined as the peak to peak field for the absorption derivative curve, and second moment (M_2) are listed in Table VI, as well as values for the activation energy (E_a)

TABLE VI

Powder parameters from absorption and relaxation data. Sources for the activation energies are given in the text. Second moments are measured at 4.2°K, except those referenced differently.

Material	Crystal Class	E_a (K cal/mole)	T_1 at 4.2°K (sec)	M_2-Low Temp. (G^2)	δH at 4.2°K (G)
NH_4Cl	cubic	4.7	220	49.5±0.5†	23.1±0.4
NH_4Br	cubic	4.00±0.16		48.0±0.5†	23.2±0.8
NH_4F	hex.			53 ±2	22 ±1
$(NH_4)_2SeO_4$	monoc.	4.7 ±0.2		50.6±1.2*	22.7±0.8
$(NH_4)_2U_2O_7$				25 ±1	2.9±0.1
$(NH_4)_2Cr_2O_7$	monoc.	2.0 ±0.2	600	7.59±0.35*	2.9±0.2
$(NH_4)_2S_2O_8$	monoc.	1.7 ±0.2	380	19.0±0.5	2.9±0.1
NH_4SnCl_3		1.7 ±0.5	10	9.6±0.5	2.1±0.1
$(NH_4)_2SnCl_6$	cubic	1.2 ±0.2	40	5.4±0.5	1.80±0.05
$(NH_4)_2PtI_6$	cubic			10 ±1	1.9±0.1
$(NH_4)_2Ce(NO_3)_6$	monoc.	1.6 ±0.2	160	3.0±0.2	1.5±0.1
NH_4GaCl_4				28 ±1	3.0±0.4
$(NH_4)_2SO_4$	rhomb.	} 3.9 2.7}	>1000	33.3±1.1*	4.6±0.2
$(NH_4)_2SeO_3$				38 ±1	22.2±0.8
$(NH_4)_2TeO_4$		4.7 ±0.2	13	26 ±1	5.1±0.4
$(NH_4)_2BeF_4$	rhomb.	}4.3 ±0.7 2.4 ±0.2}		25 ±1	6.8±0.4
$(NH_4)_2S_2O_3$	monoc.	}1.7 ±0.2 2.8 ±0.2}	520	26 ±1	3.3±0.2
NH_4NO_3	rhomb.	2.4 ±0.2	660	50.0±1.3*	7.7±0.2
NH_4VO_3		1.9 ±0.2	140	21.6±0.8*	11.2±0.2

*Richards and Schaefer (1961). $(NH_4)_2TeO_4$ measured at 90°K, the others at 20°K.

†Gutowsky, Pake and Bersohn (1954), at 77°K.

FIGURE 9

Derivative of the proton absorption spectrum, at 4.2°K, of powdered $(NH_4)_2SeO_3$.

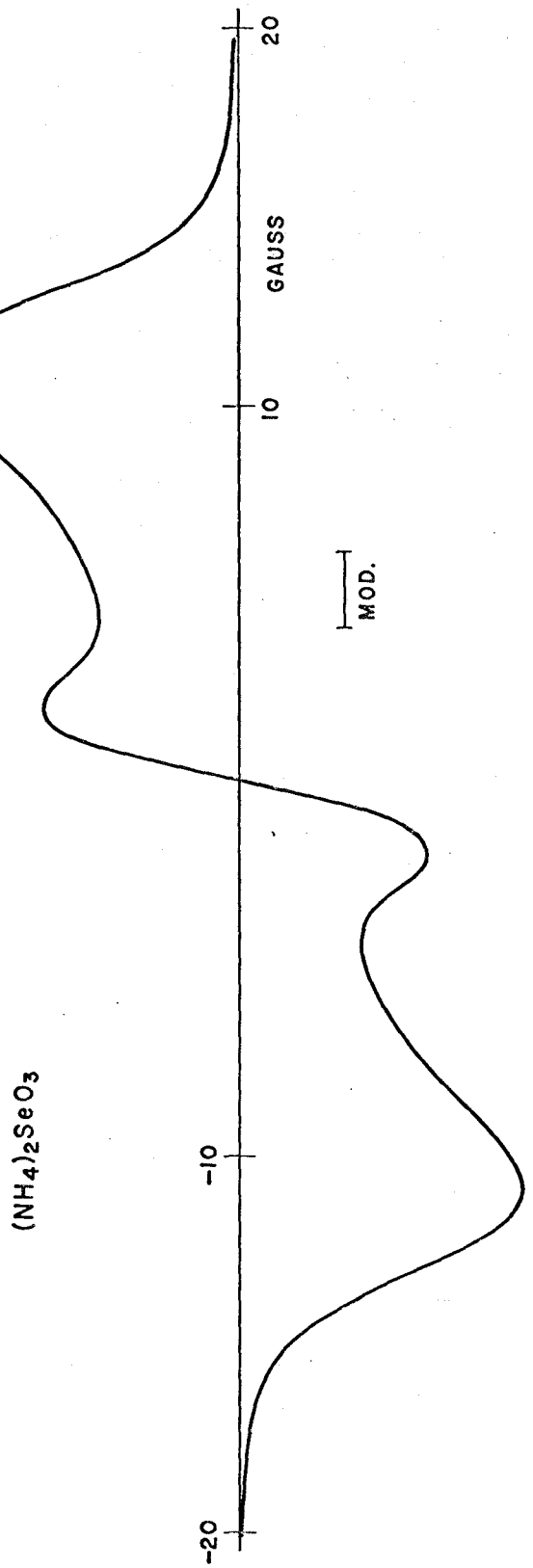
20
10
-10
-20
GAUSS
MOD.
$(NH_4)_2SeO_3$

FIGURE 10

Derivative of the proton absorption spectrum, at 4.2°K, of powdered $(NH_4)_2BeF_4$.

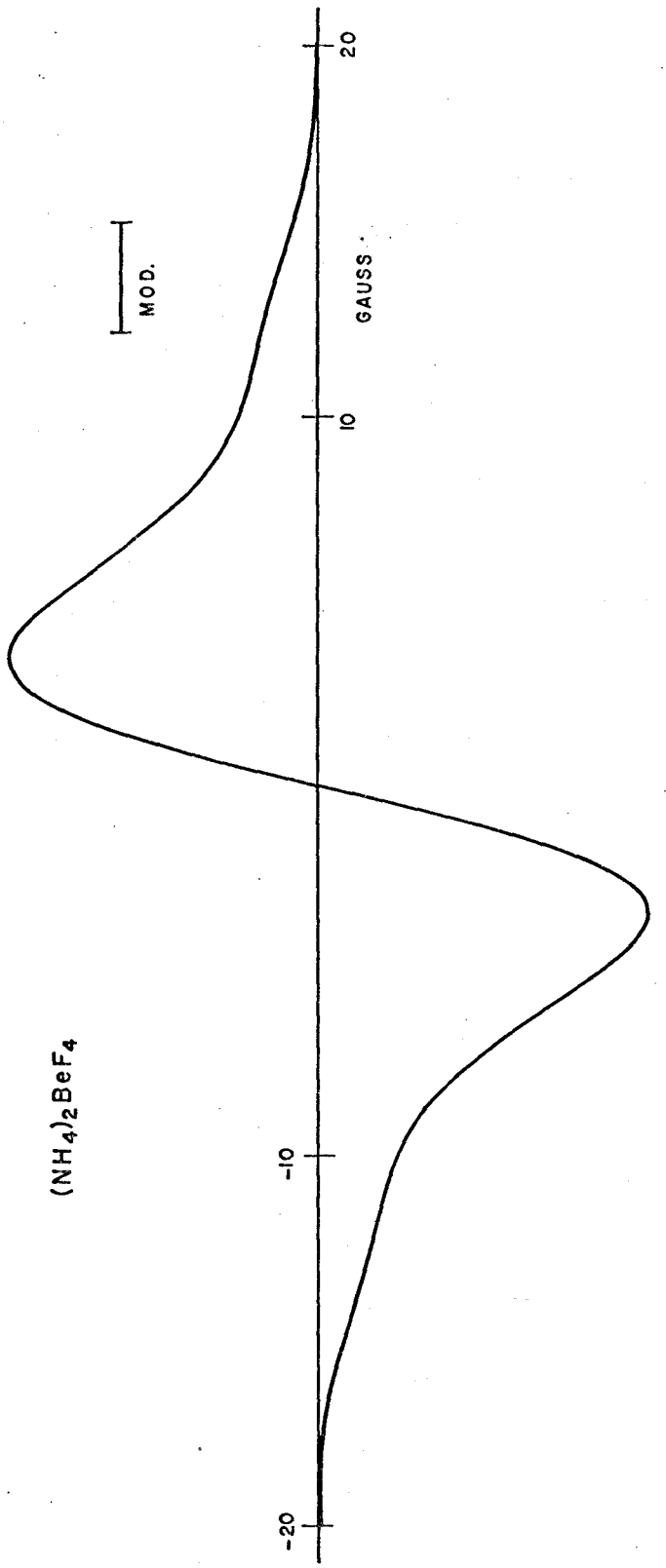
20
10
-10
-20
GAUSS
MOD.
$(NH_4)_2BeF_4$

FIGURE 11

Proton absorption spectrum, at 4.2°K, of powdered NH_4Cl.

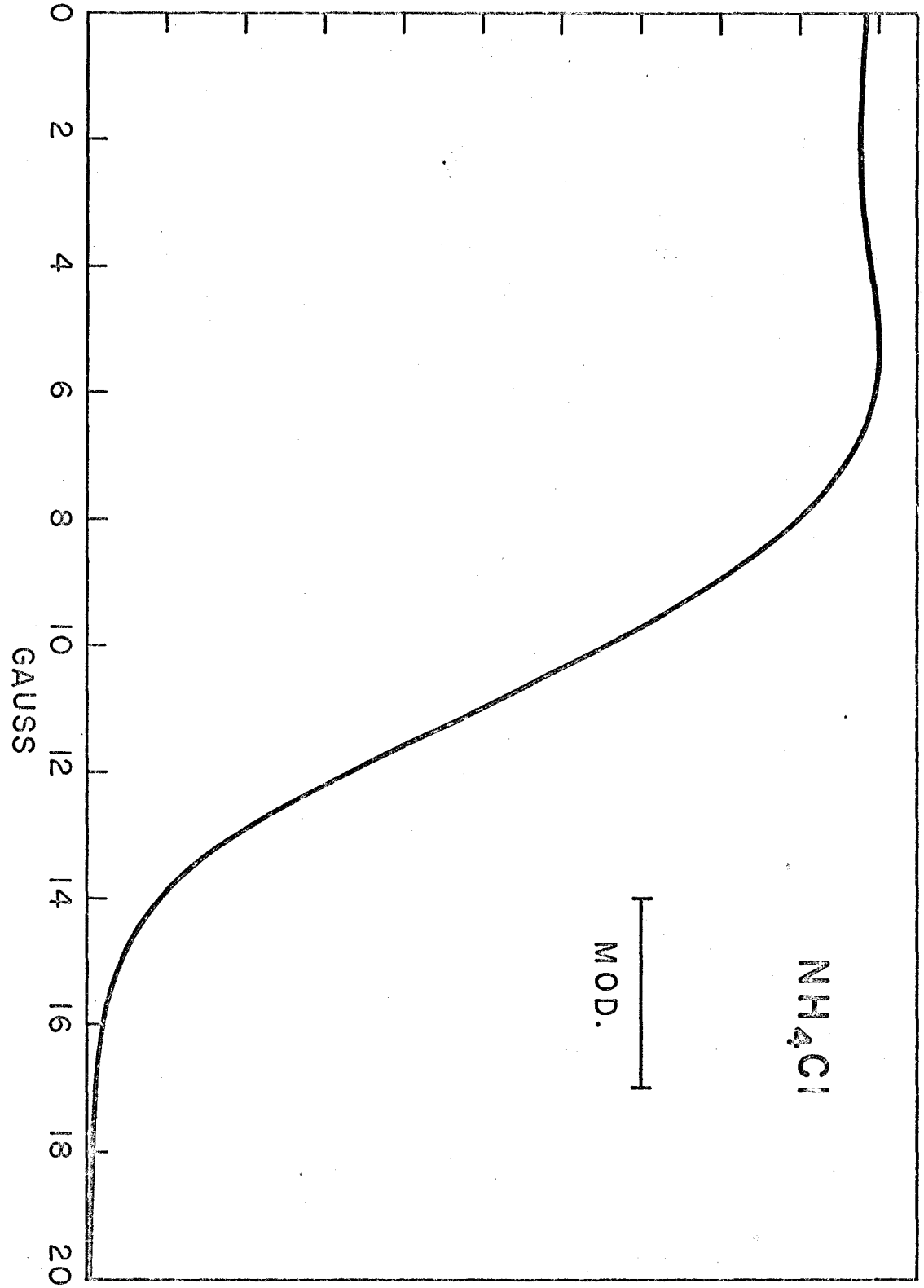
0
2
4
6
8
10
12
14
16
18
20
GAUSS
MOD.
NH4Cl

FIGURE 12

Proton absorption spectrum, at 4.2°K, of powdered NH_4Br.

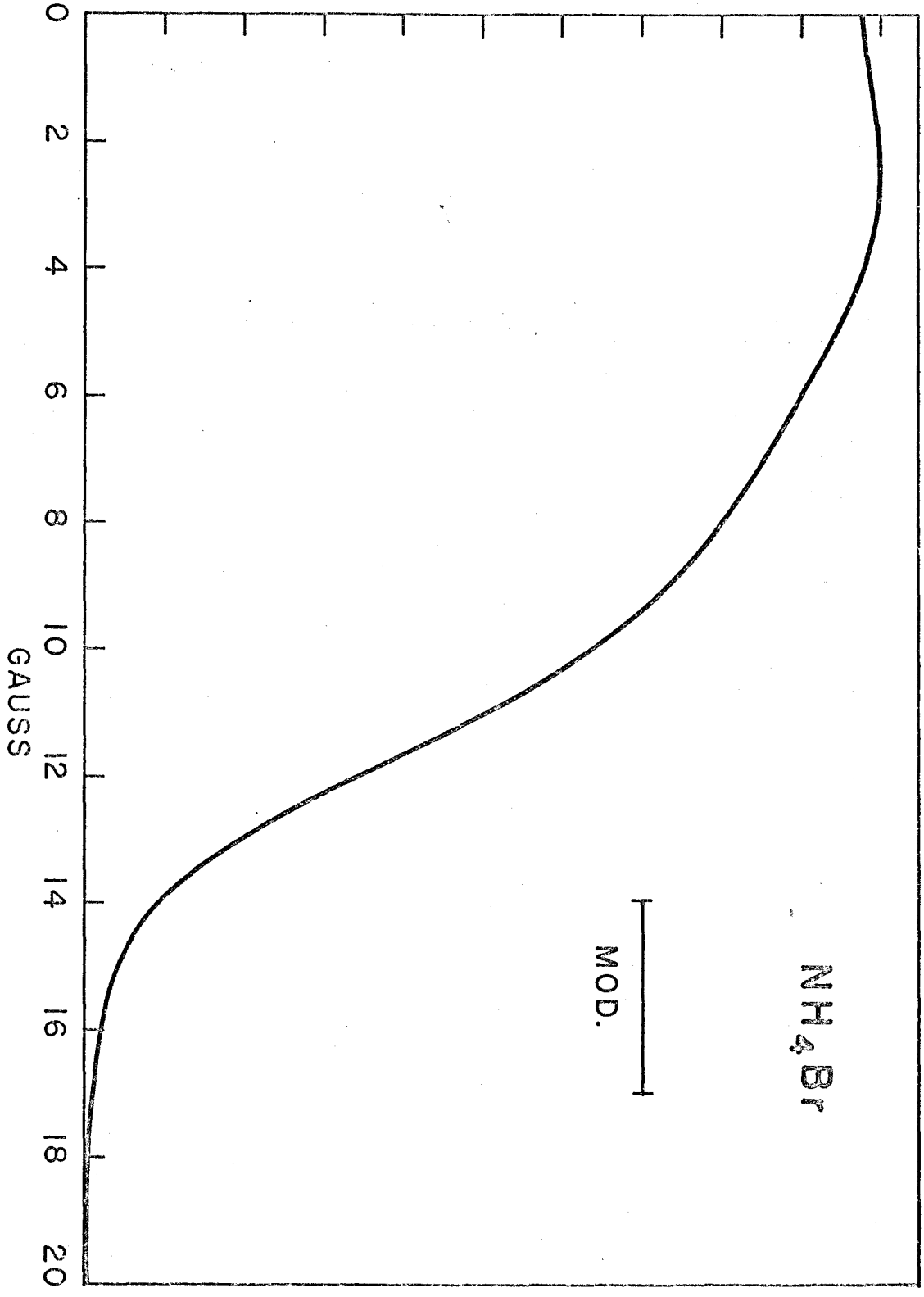
0
2
4
6
8
10
12
14
16
18
20
GAUSS
MOD.
NH4Br

FIGURE 13

Proton absorption spectrum, at 4.2°K, of powdered NH_4F.

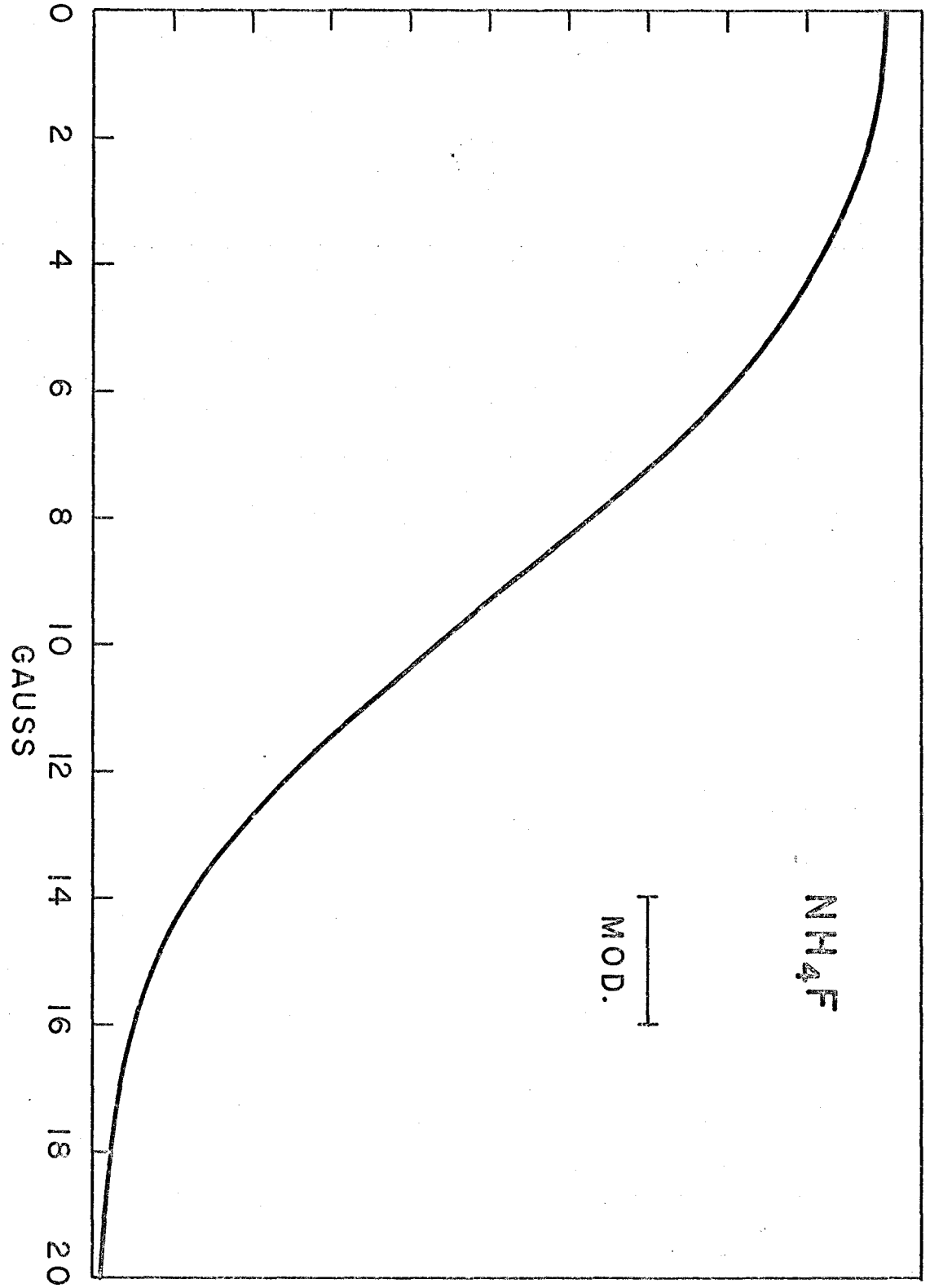
0
2
4
6
8
10
12
14
16
18
20
GAUSS
MOD.
NH4F

FIGURE 14

Proton absorption spectrum, at 4.2°K, of powdered $(NH_4)_2SeO_4$.

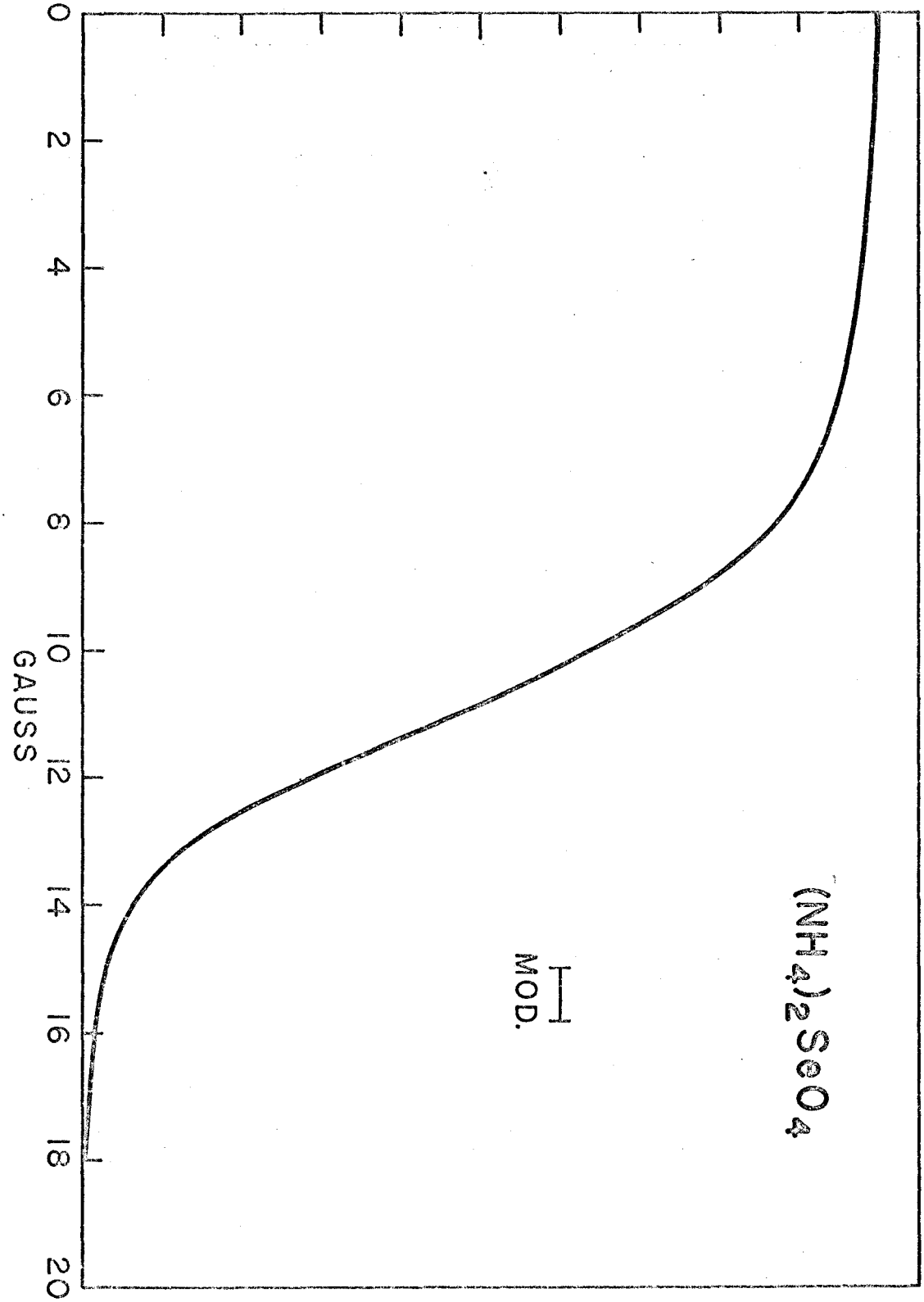
0
2
4
6
8
10
12
14
16
18
20
GAUSS
MOD.
(NH4)2SeO4

FIGURE 15

Proton absorption spectrum, at 4.2°K, of powdered $(NH_4)_2U_2O_7$ (full curve), and theoretical spin isomer spectrum for a $\langle \Delta H^2 \rangle$ of 4 G^2 (dashed curve).

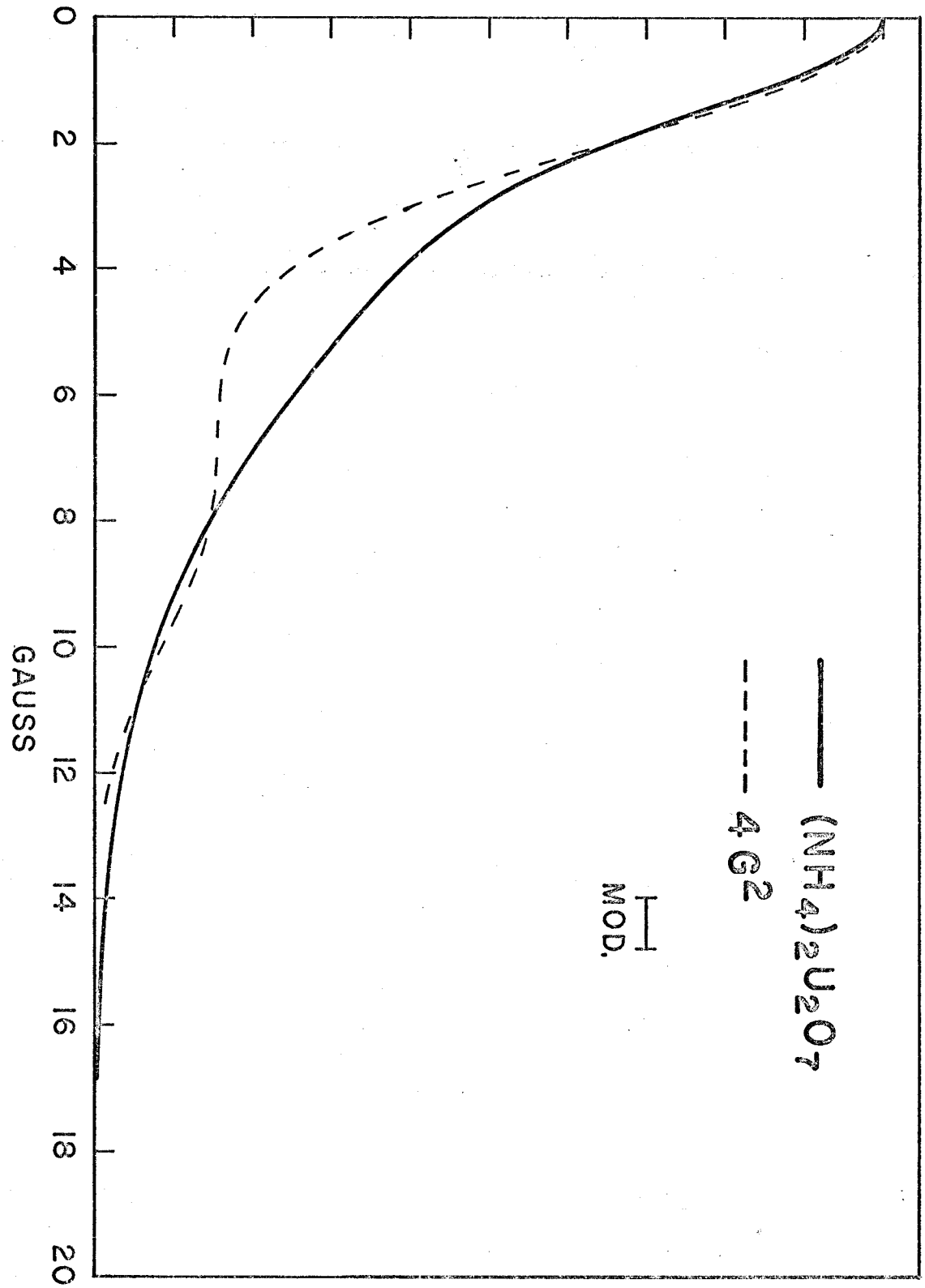
0
2
4
6
8
10
12
14
16
18
20
GAUSS
(NH4)2U2O7
4G2
MOD.

FIGURE 16

Proton absorption spectrum, at 4.2°K, of powdered $(NH_4)_2Cr_2O_7$ (full curve), and theoretical spin isomer spectrum for a $\langle \Delta H^2 \rangle$ of 2 G^2 (dashed curve).

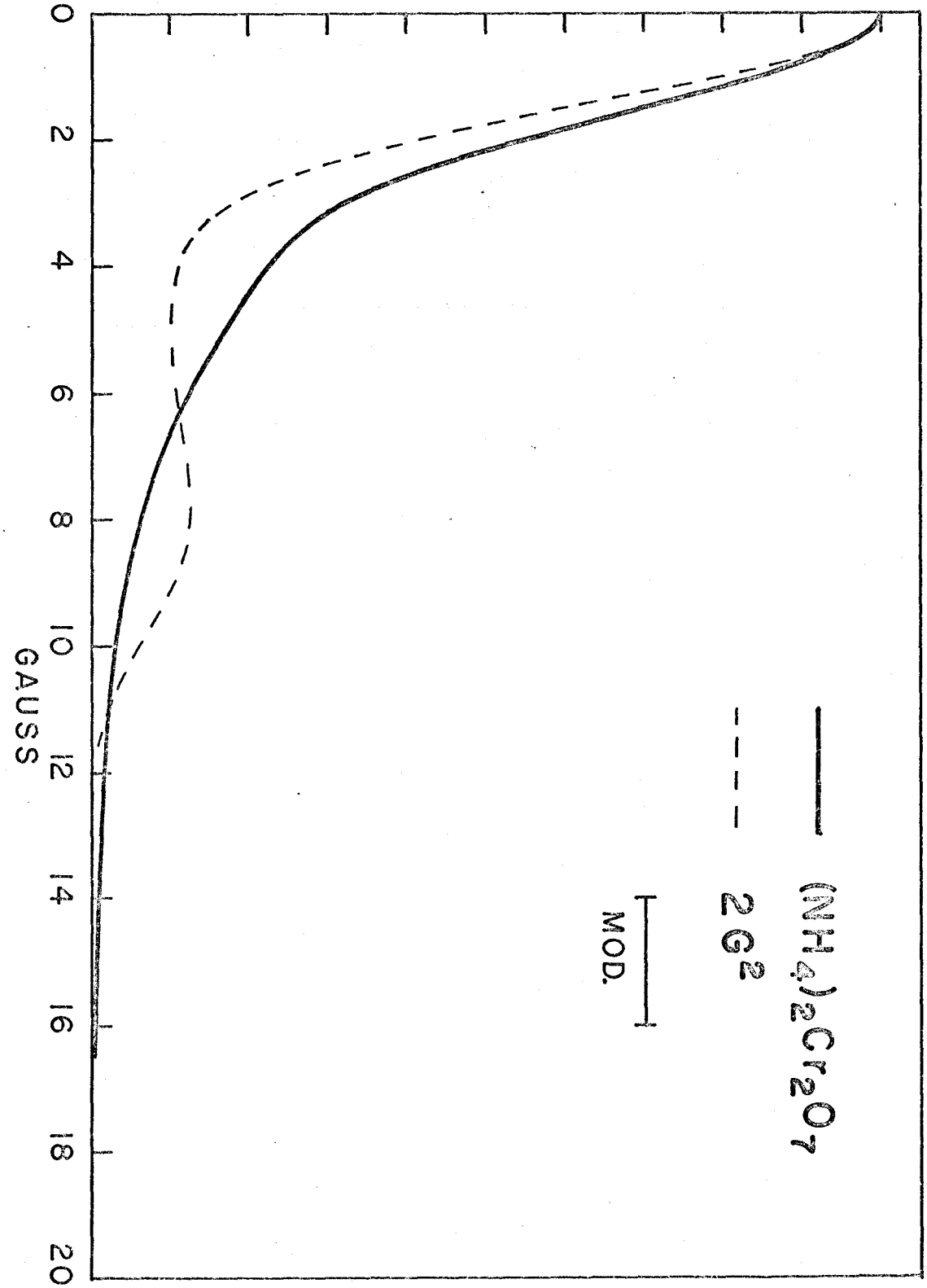
0
2
4
6
8
10
12
14
16
18
20
GAUSS
$(NH_4)_2Cr_2O_7$
2G2
MOD.

FIGURE 17

Proton absorption spectrum, at 4.2°K, of powdered $(NH_4)_2S_2O_8$ (full curve), and theoretical spin isomer spectrum for a $\langle \Delta H^2 \rangle$ of $2G^2$ (dashed curve).

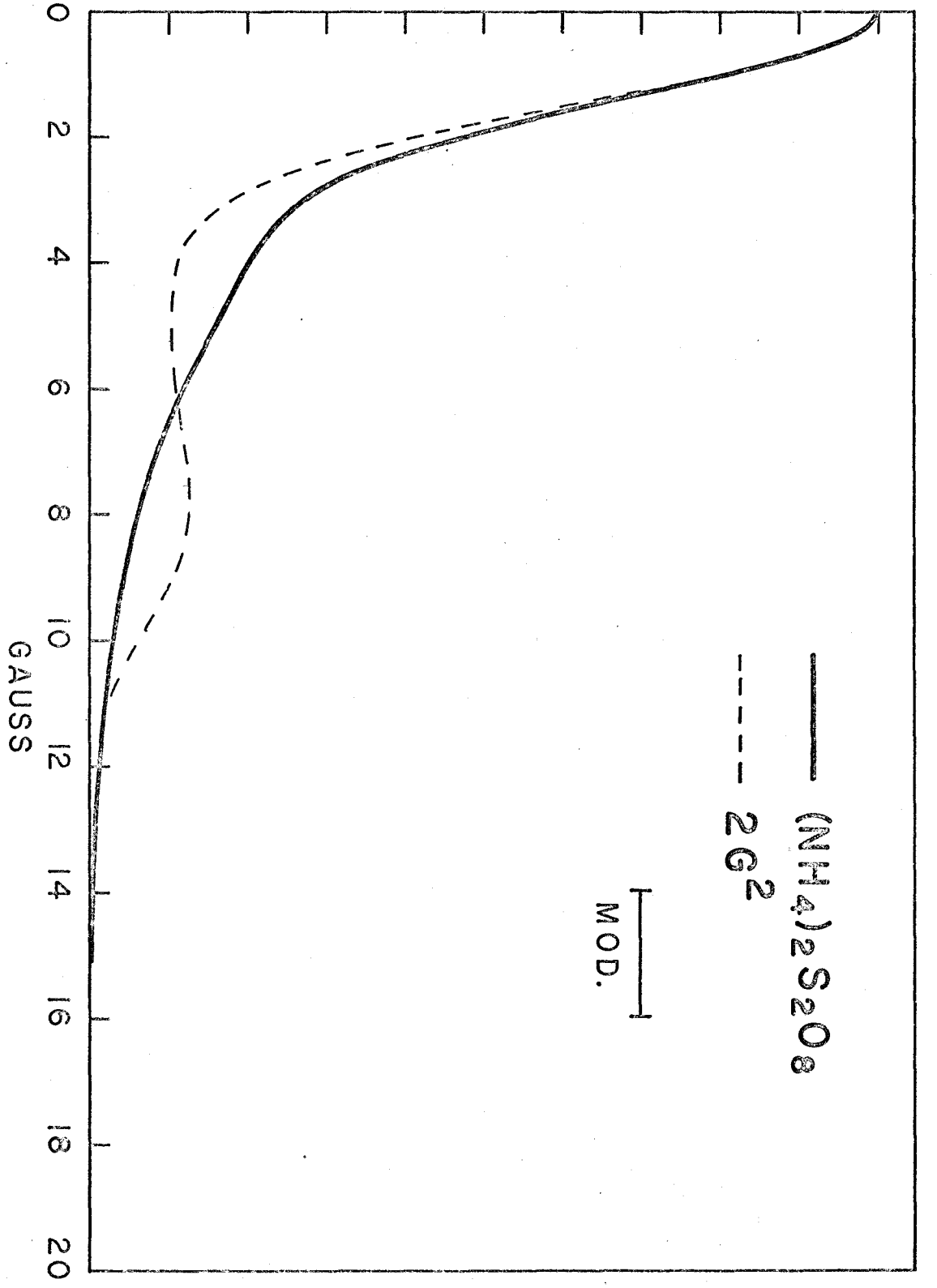
0
2
4
6
8
10
12
14
16
18
20
GAUSS
$(NH_4)_2S_2O_8$
2G2
MOD.

FIGURE 18

Proton absorption spectrum, at 4.2°K, of powdered NH_4SnCl_3 (full curve), and theoretical spin isomer spectrum for a $\langle \Delta H^2 \rangle$ of 2 G^2 (dashed curve).

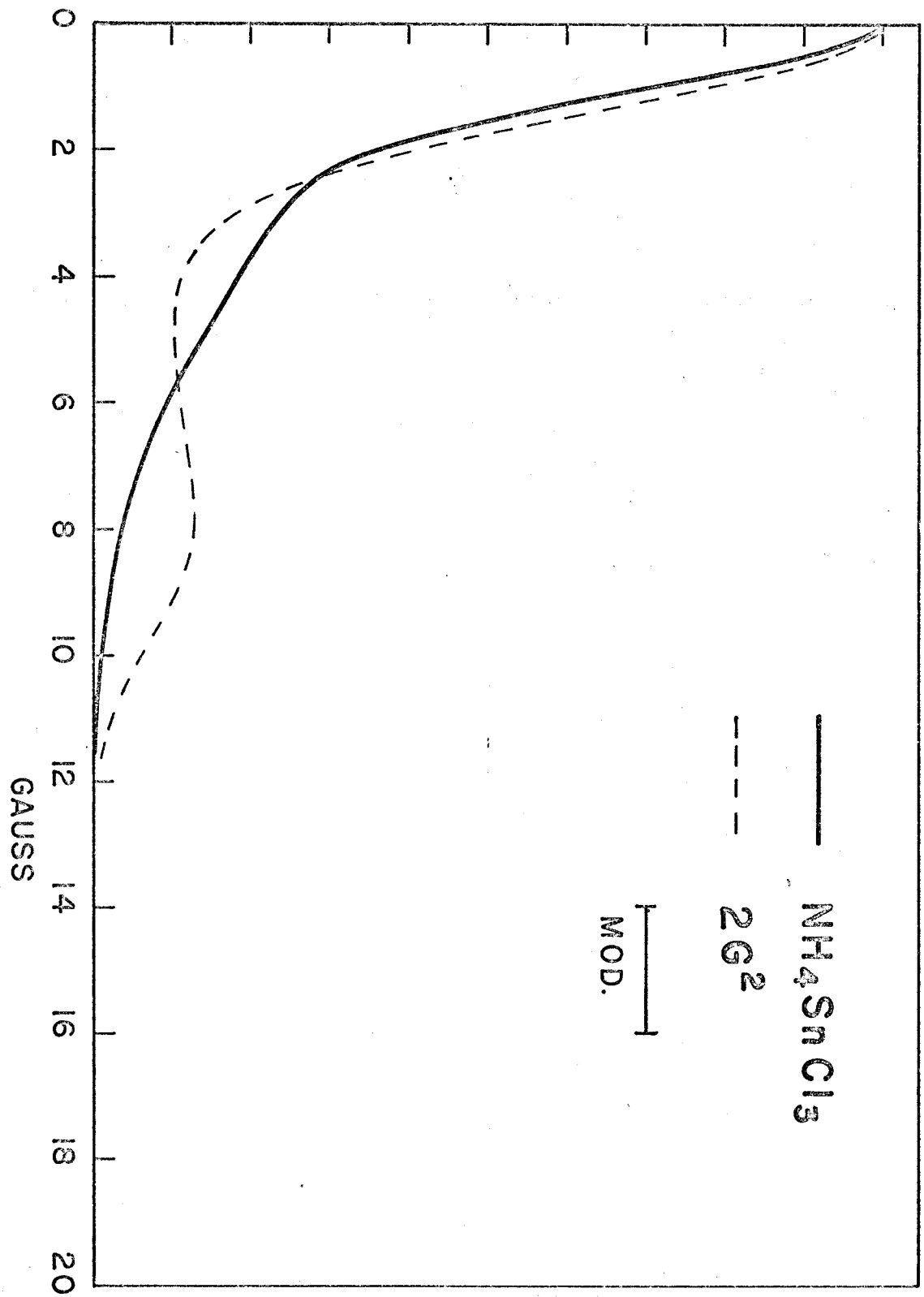
0
2
4
6
8
10
12
14
16
18
20
GAUSS
MOD.
2G2
NH4SnCl3

FIGURE 19

Proton absorption spectrum, at 4.2°K, of powdered $(NH_4)_2SnCl_6$ (full curve), and theoretical spin isomer spectrum with a $\langle \Delta H^2 \rangle$ of 1 G^2 (dashed curve).

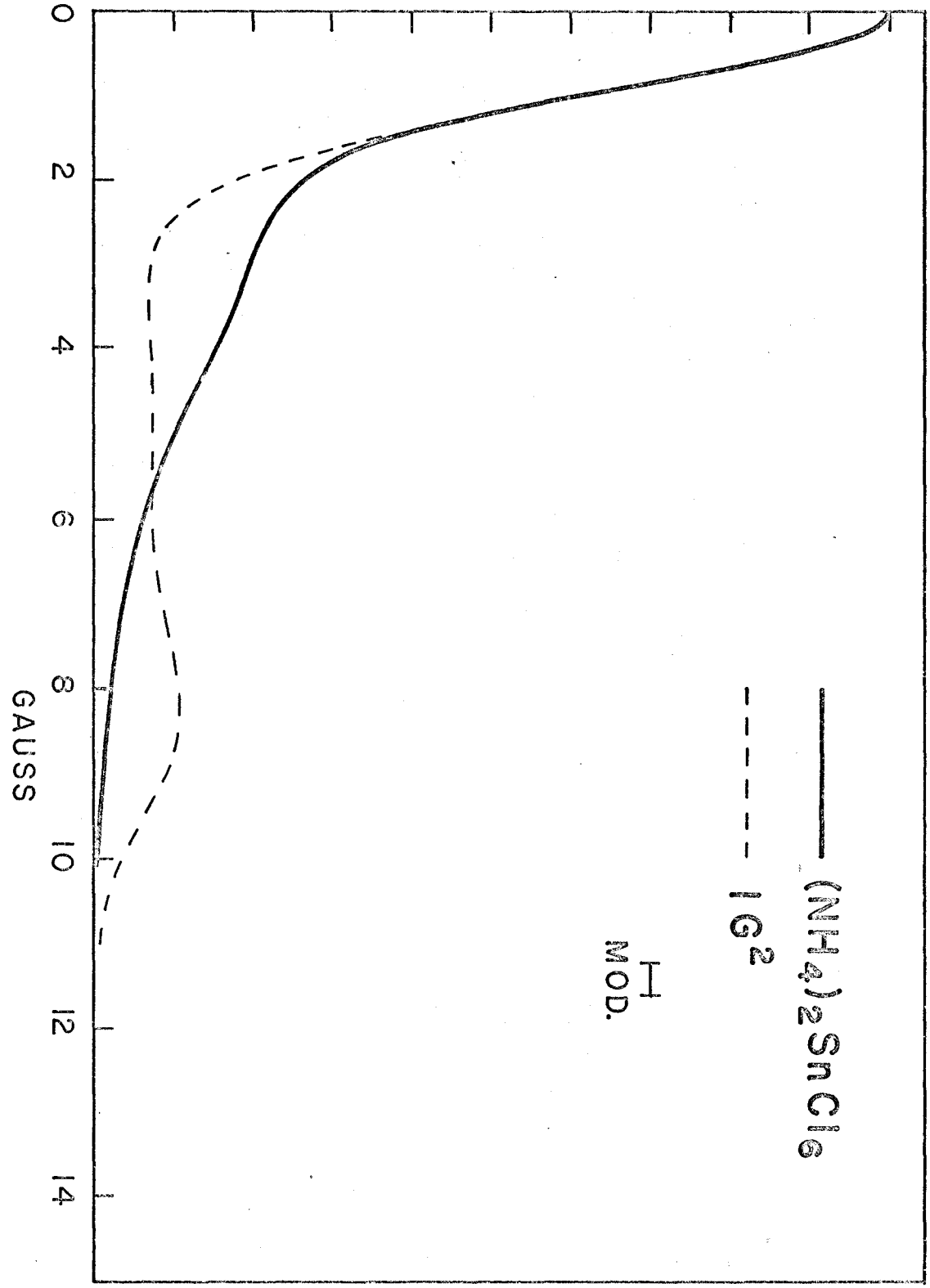
0
2
4
6
8
10
12
14
GAUSS
I
MOD.
G_2
$(NH_4)_2SnCl_6$

FIGURE 20

Proton absorption spectrum, at 4.2°K, of powdered $(NH_4)_2PtI_6$ (full curve), and theoretical spin isomer spectrum with a $\langle \Delta H^2 \rangle$ of 1 G^2 (dashed curve).

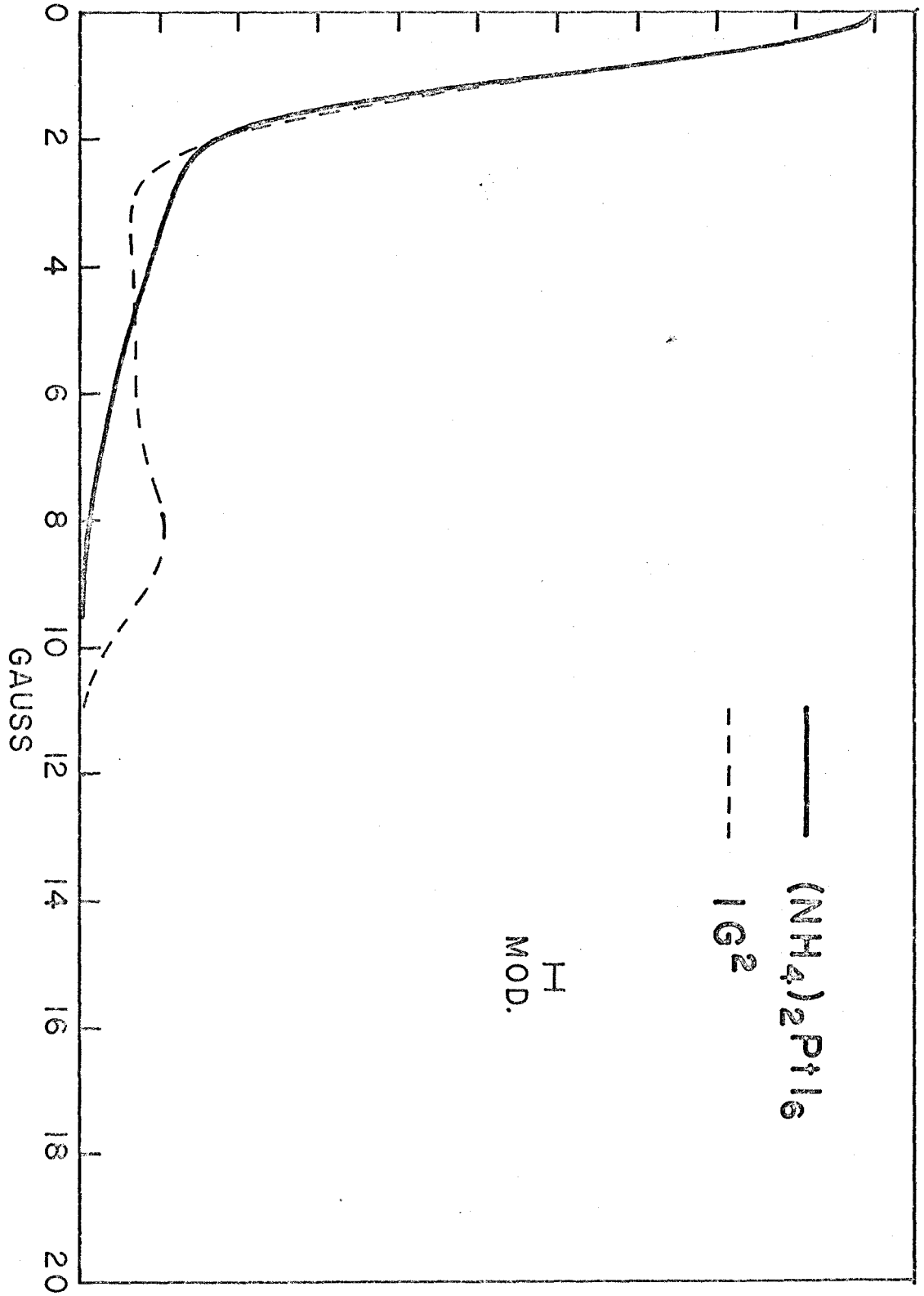
0
2
4
6
8
10
12
14
16
18
20
GAUSS
I
MOD.
$(NH_4)_2PtI_6$
I_{G_2}

FIGURE 21

Proton absorption spectrum, at 4.2°K, of powdered $(NH_4)_2Ce(NO_3)_6$ (full curve), and theoretical spin isomer spectrum with a $\langle \Delta H^2 \rangle$ of 1 G^2 (dashed curve).

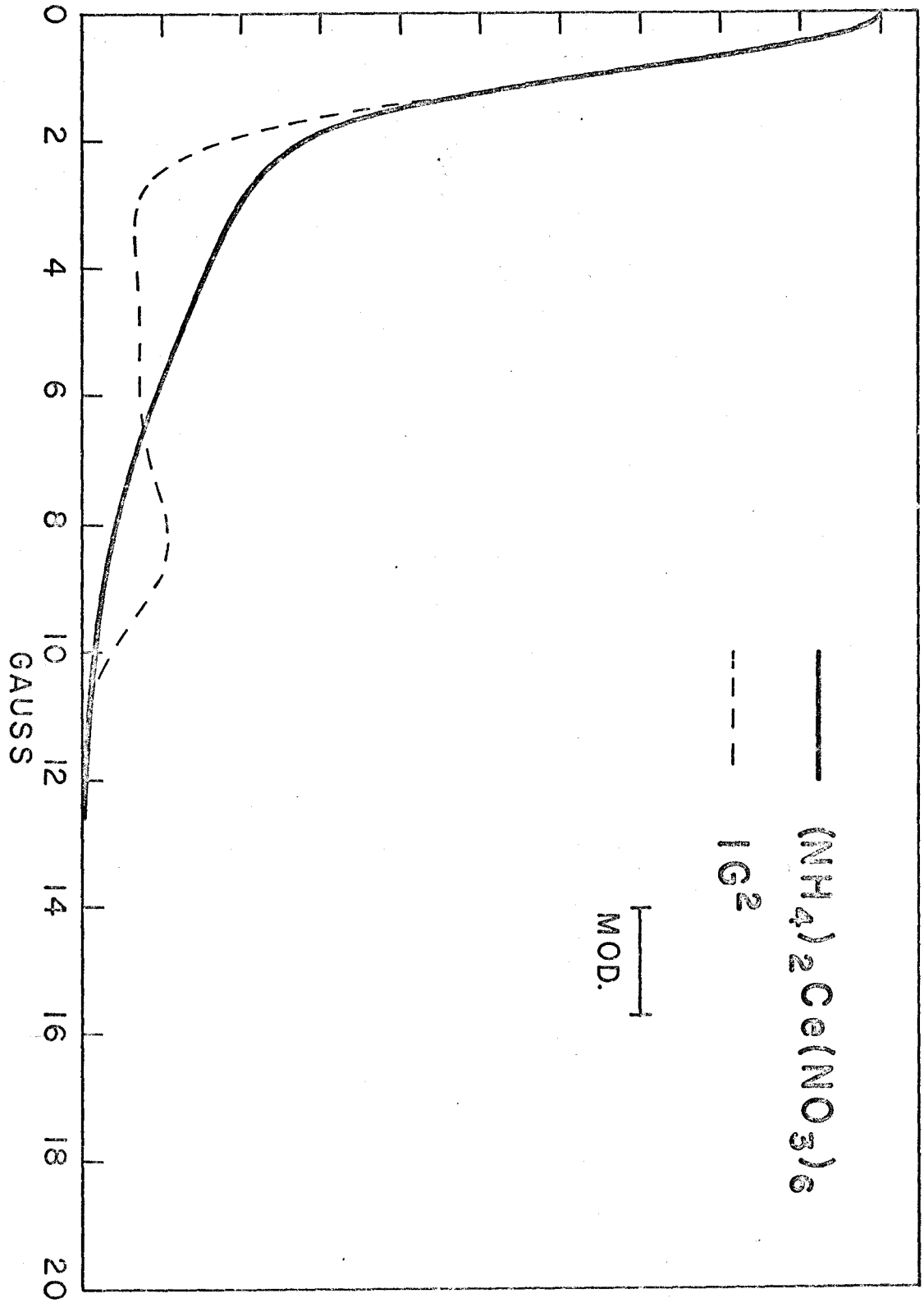
0
2
4
6
8
10
12
14
16
18
20
GAUSS
(NH4)2Ce(NO3)6
I G2
MOD.

FIGURE 22

Proton absorption spectrum, at 4.2°K, of powdered NH_4GaCl_4 (full curve), and theoretical spin isomer spectrum with a $\langle \Delta H^2 \rangle$ of 1 G^2 (dashed curve).

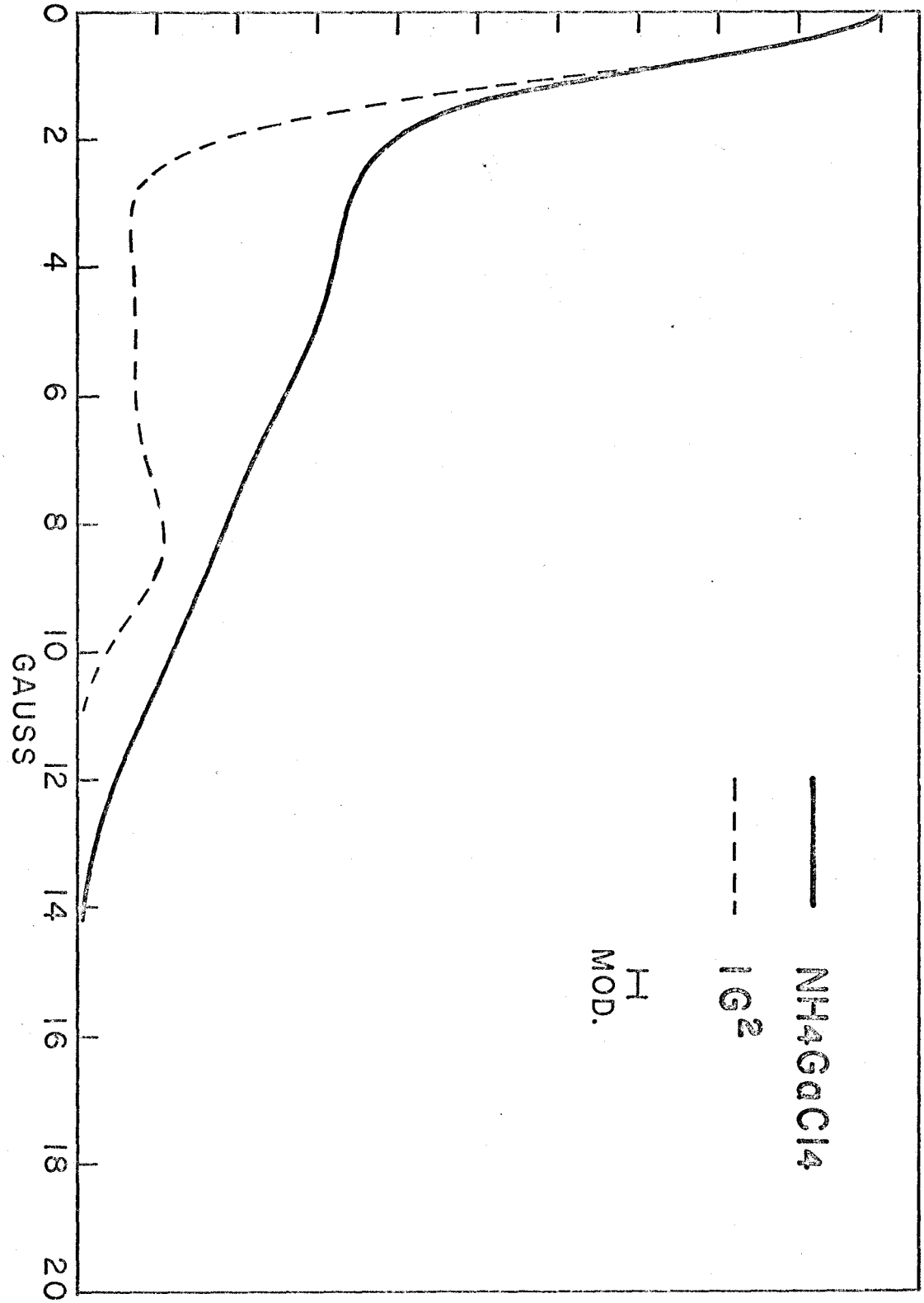
0
2
4
6
8
10
12
14
16
18
20
GAUSS
NH4GaCl4
IG2
H
MOD.

FIGURE 23

Proton absorption spectrum, at 4.2°K, of powdered $(NH_4)_2SO_4$ (full curve), and theoretical spin isomer spectrum with a $\langle \Delta H^2 \rangle$ of 8 G^2 (dashed curve).

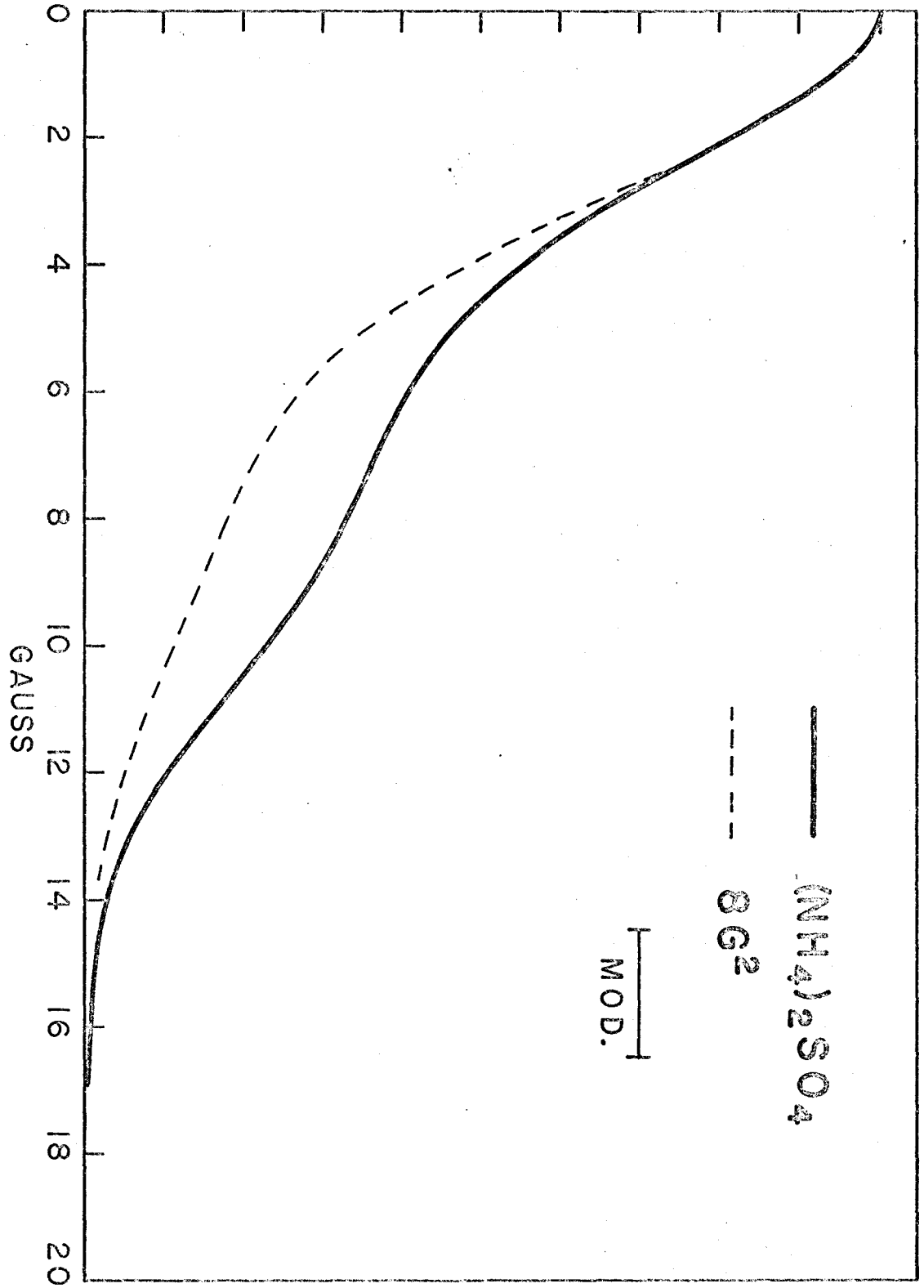
0
2
4
6
8
10
12
14
16
18
20
GAUSS
(NH4)2SO4
BG2
MOD.

FIGURE 24

Proton absorption spectrum, at 4.2°K, of powdered $(NH_4)_2SeO_3$.

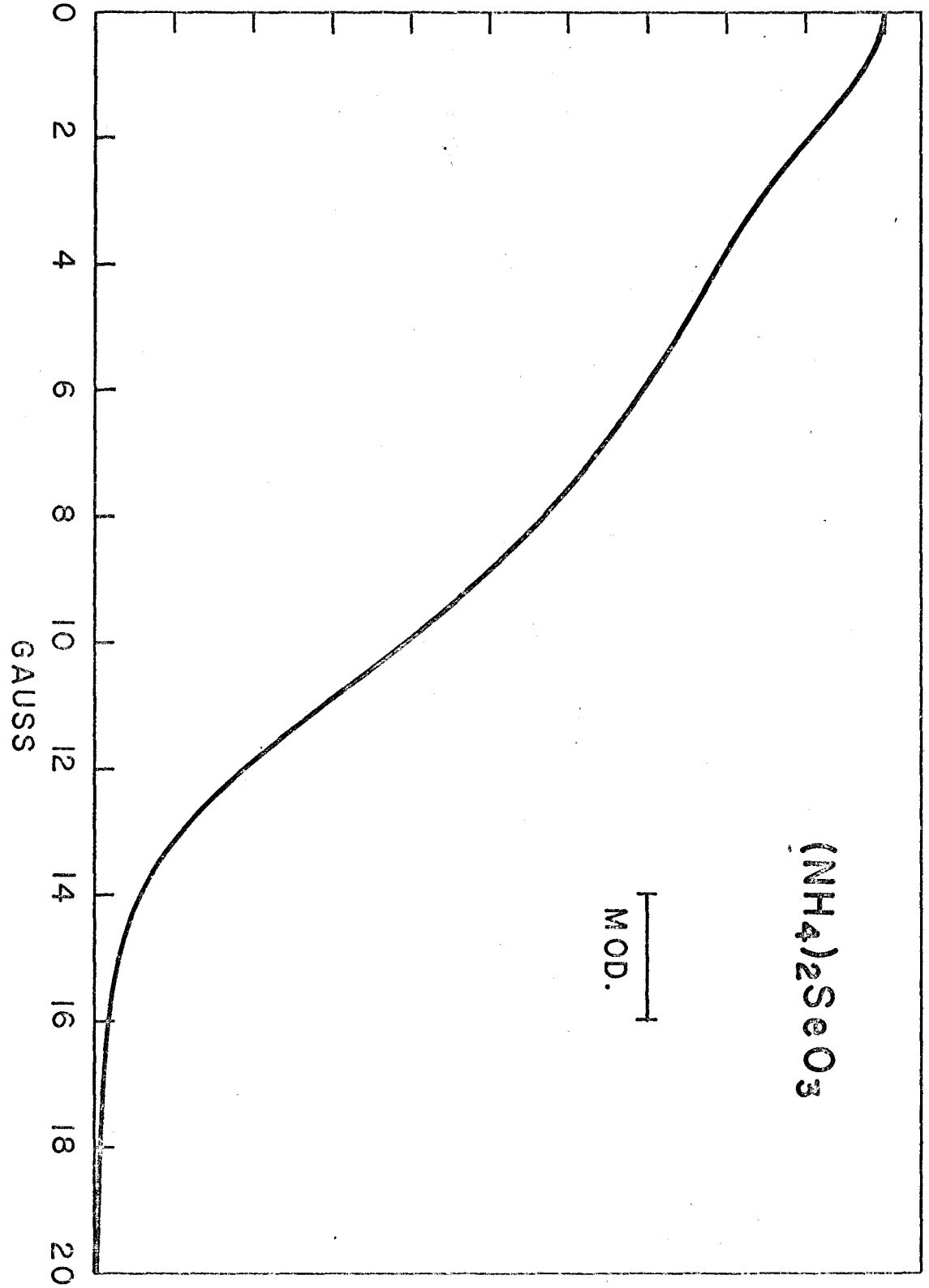
0
2
4
6
8
10
12
14
16
18
20
GAUSS
MOD.
(NH4)2SeO3

FIGURE 25

Proton absorption spectrum, at 4.2°K, of powdered $(NH_4)_2TeO_4$ (full curve), and theoretical spin isomer spectrum with a $\langle \Delta H^2 \rangle$ of 10 G^2 (dashed curve).

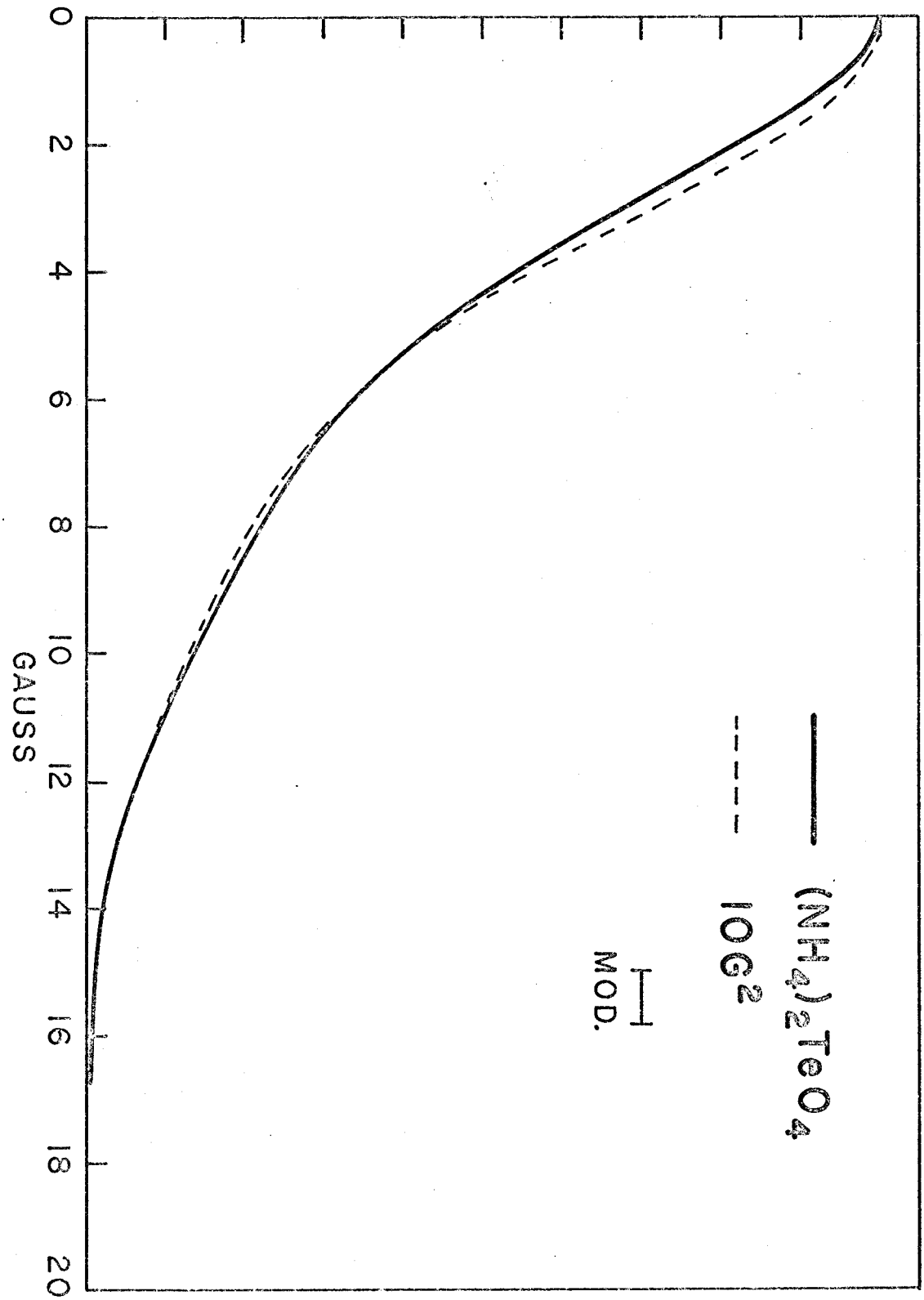
0
2
4
6
8
10
12
14
16
18
20
GAUSS
(NH4)2TeO4
TOG2
MOD.

FIGURE 26

Proton absorption spectrum, at 4.2°K, of powdered $(NH_4)_2BeF_4$ (full curve), and theoretical spin isomer spectrum with a $\langle \Delta H^2 \rangle$ of 10 G^2 (dashed curve).

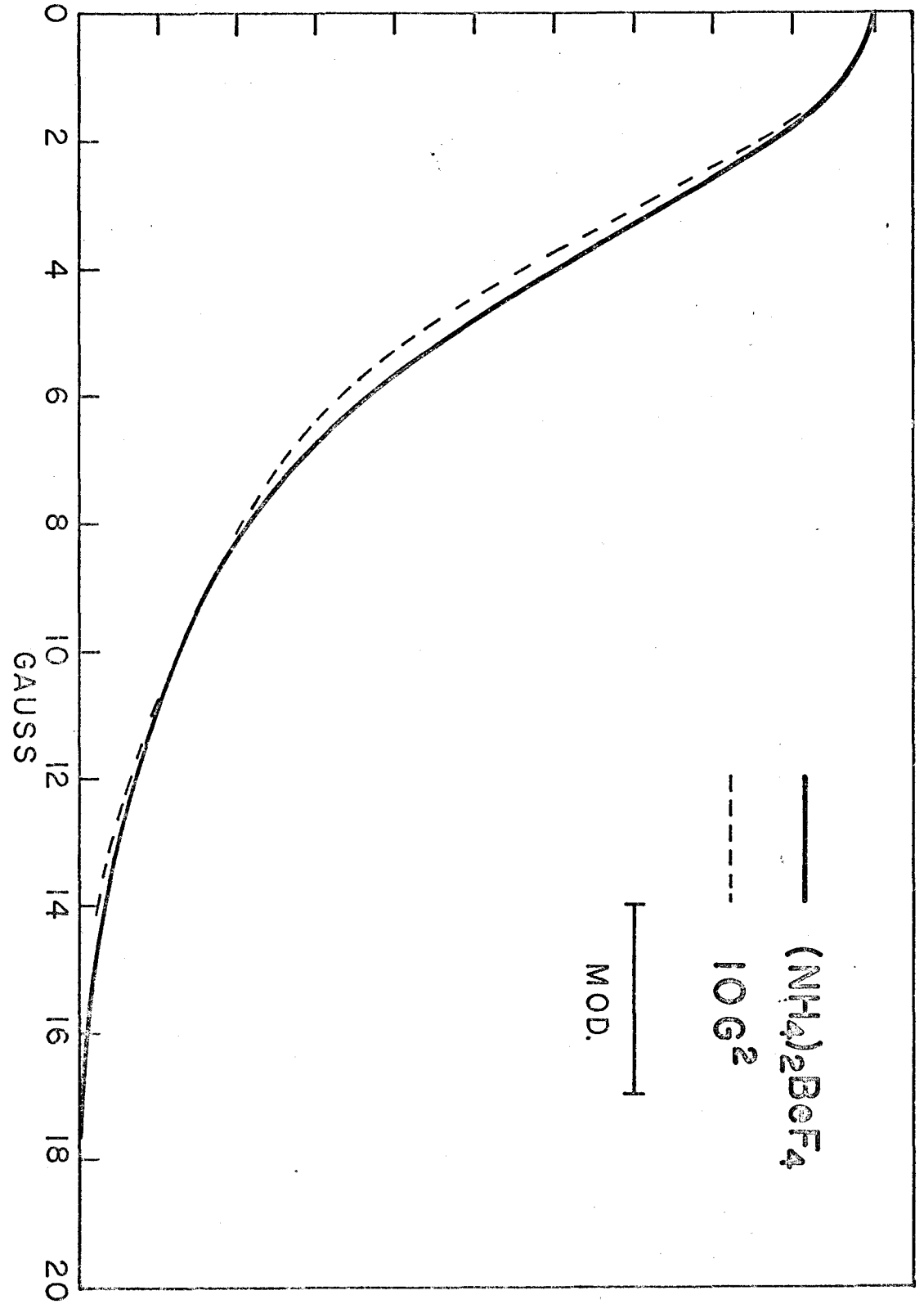
0
2
4
6
8
10
12
14
16
18
20
GAUSS
(NH4)2BeF4
IOG2
MOD.

FIGURE 27

Proton absorption spectrum, at 4.2°K, of powdered $(NH_4)_2S_2O_3$ (full curve), and theoretical spin isomer spectrum with a $\langle \Delta H^2 \rangle$ of 6 G^2 (dashed curve).

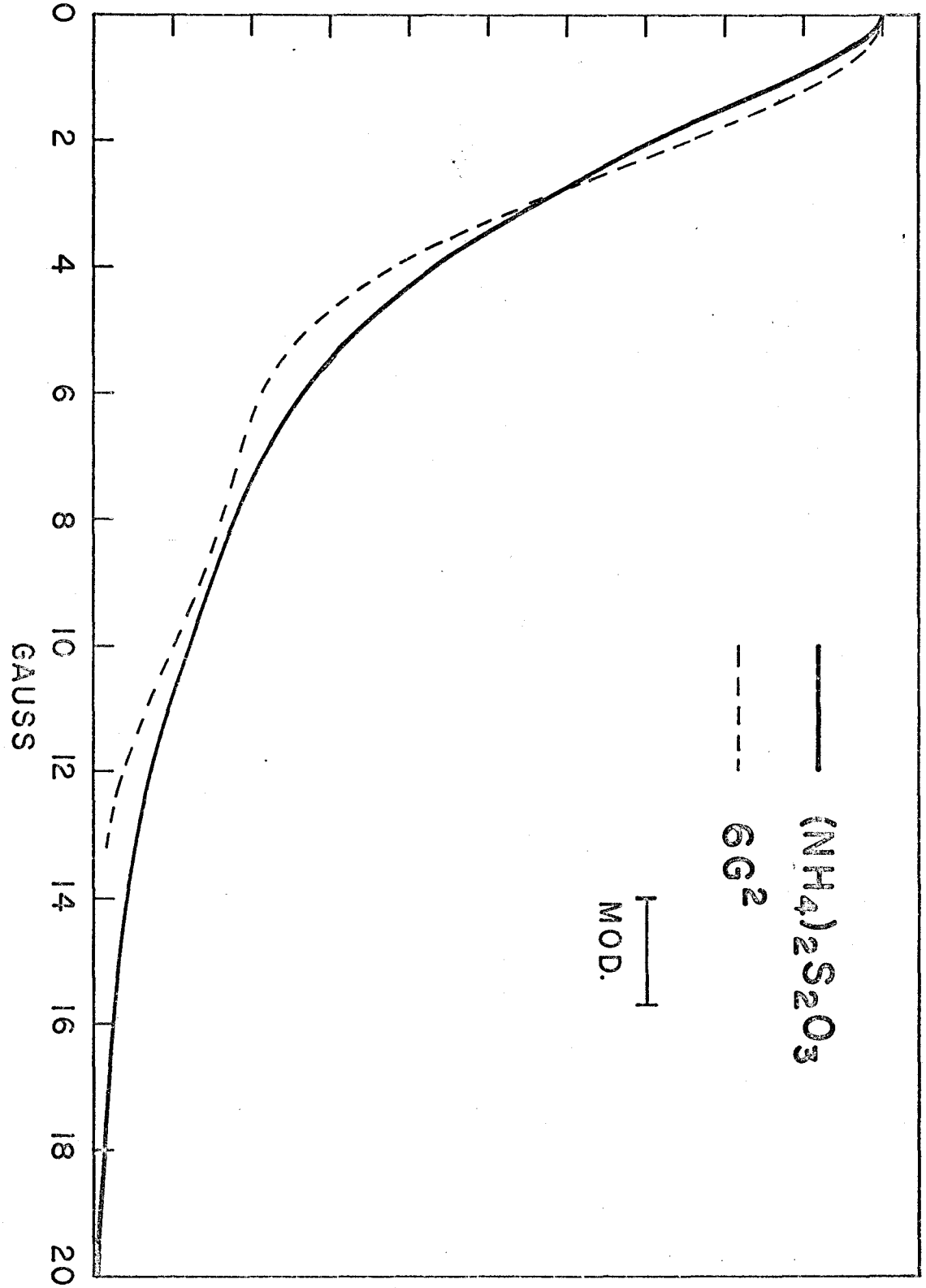
0
2
4
6
8
10
12
14
16
18
20
GAUSS
(NH4)2S2O3
6G2
MOD.

FIGURE 28

Proton absorption spectrum, at 4.2°K, of powdered NH_4NO_3 (full curve), and theoretical spin isomer spectrum with a $\langle \Delta H^2 \rangle$ of 16 G^2 (dashed curve).

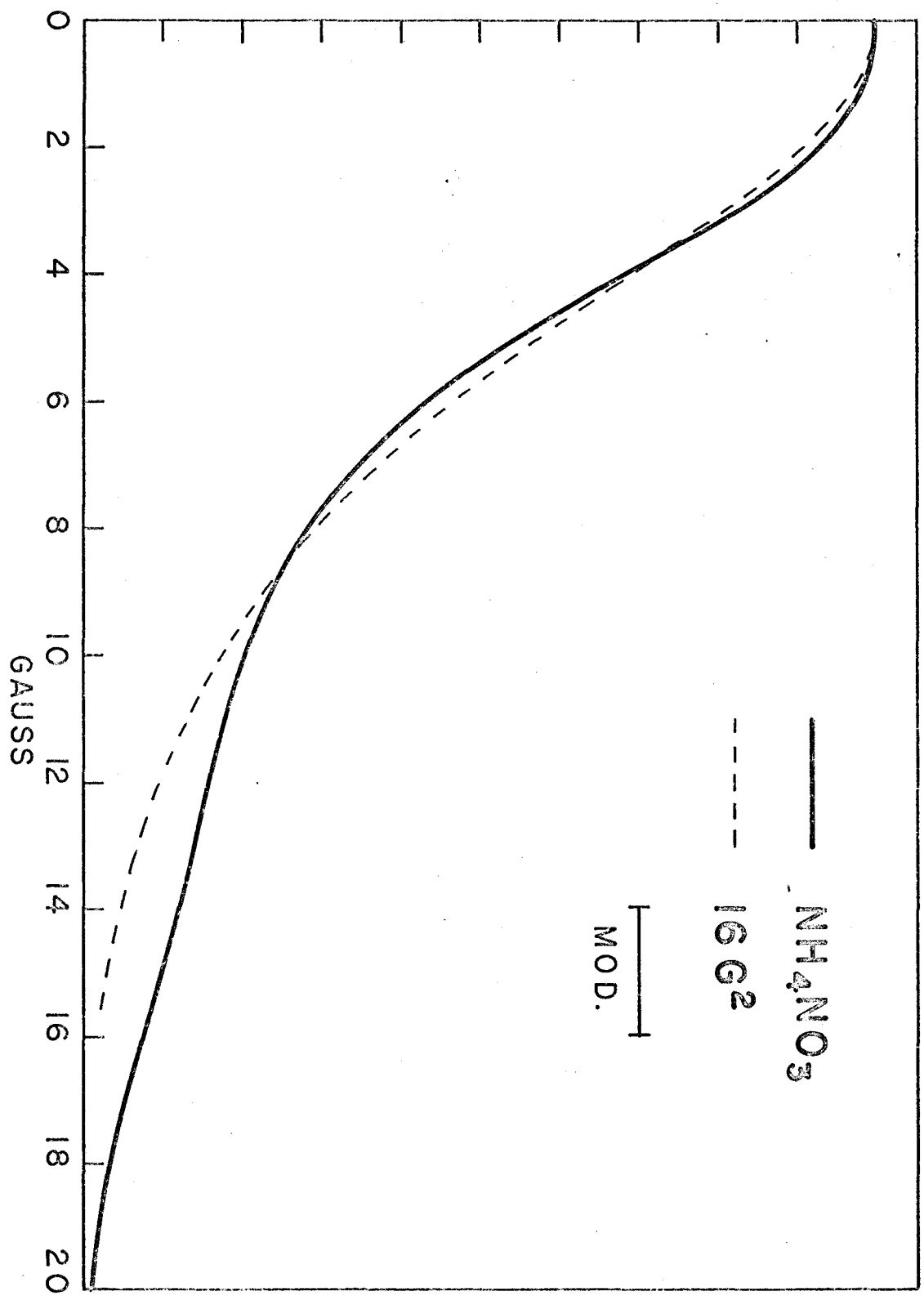
0
2
4
6
8
10
12
14
16
18
20
GAUSS
NH4NO3
IG G2
MOD.

FIGURE 29

Proton absorption spectrum, at 4.2°K, of powdered NH_4VO_3 (full curve), and theoretical spin isomer spectrum with a $\langle \Delta H^2 \rangle$ of 16 G^2 (dashed curve).

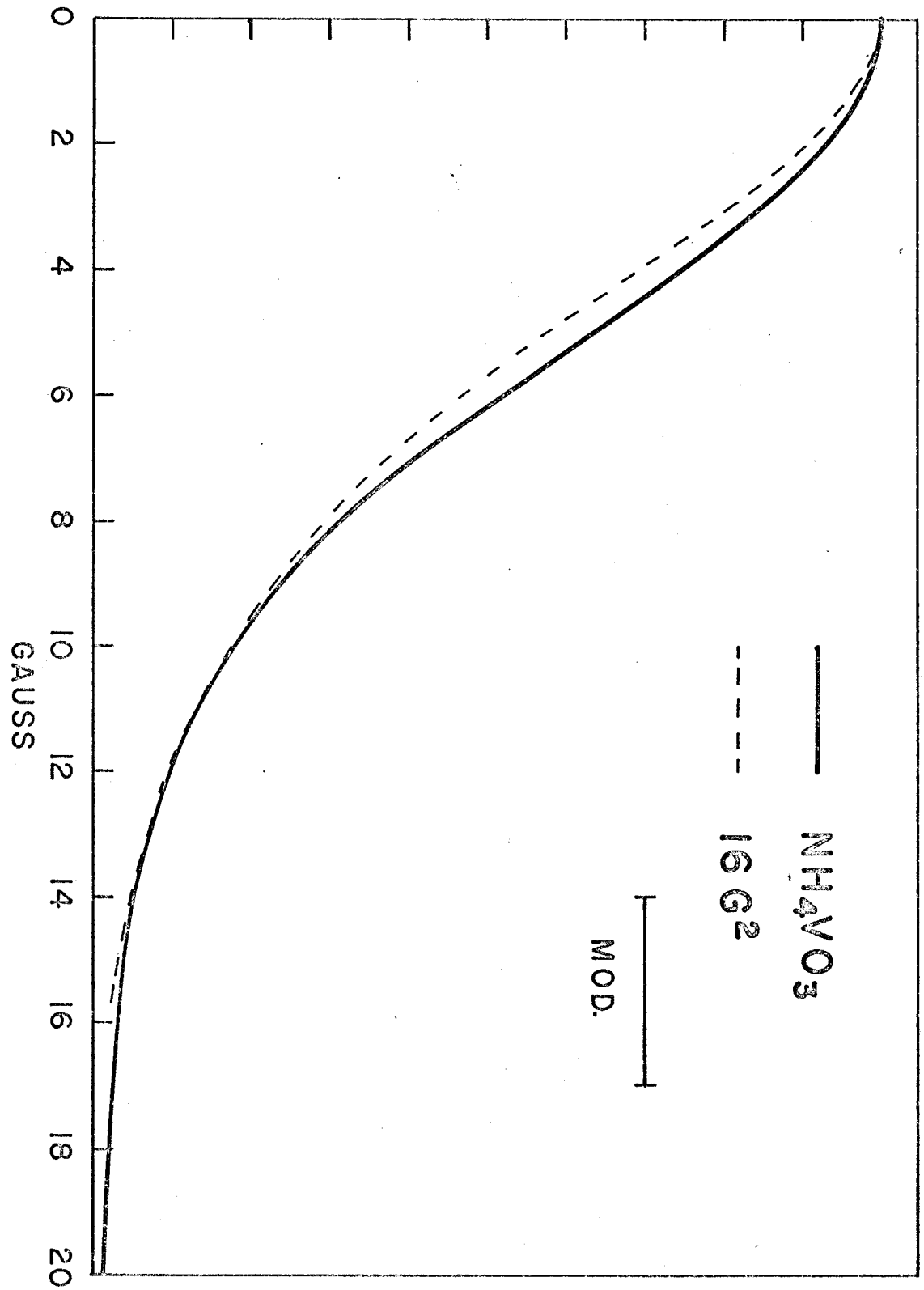
0
2
4
6
8
10
12
14
16
18
20
GAUSS
NH4VO3
16 G2
MOD.

and estimates, where available, of T_1 at 4.2°K obtained from the relaxation measurements. It should be noted that most of these salts have second moment values considerably less than the "rigid lattice" value of 50 G^2.

For each salt, the line shape itself constitutes a detailed characteristic, although it is not easily quantified, as are the gross features given in Table VI. Most spectra are characterized by a fairly narrow central gaussian component peak (1 to 2 G wide) and the semblance of some structure further out in the wings of the spectrum [e.g. $(NH_4)_2SnCl_6$, NH_4SnCl_3].

The line shapes stay fairly constant with increasing temperature up to about 30°K or 40°K when the wing structure disappears.

Some of the spectra however, such as NH_4Cl, NH_4Br, $(NH_4)_2SeO_4$, NH_4F are quite different in character from the above mentioned, having a very wide central peak ($\sim$ 10G), and no structure in the wings.

The spectra of a number of the salts showed no change over a period of days after initially reaching 4.2°K, the first observation being made about half an hour after the initial immersion in liquid helium. The mechanism responsible for the line shape must therefore establish equilibrium among the spins in a matter of minutes.

The absorption derivative spectra obtained at 4.2°K along the [1,0,0] and [1,1,0] directions are shown for a

single crystal of NH_4Cl in Figures 30 and 31, and for a single crystal of $(NH_4)_2SnCl_6$ in Figures 32 and 33. The corresponding absorption spectra are shown in Figures 34 to 37. The spectrum of NH_4Cl appears to consist of two angular dependent components symmetrically distributed about the Larmor field. For the [1,0,0] orientation, these components lie approximately 4G from the centre of the resonance, whereas for the [1,1,0] orientation they lie approximately 7G from the centre. The difference in character between the NH_4Cl and the $(NH_4)_2SnCl_6$ spectra is quite apparent. In the latter there appears to be a component centred at the Larmor field (H_o) in both orientations and two angular dependent components symmetrically distributed about H_o and lying at about 3.3 G for the [1,0,0] orientation, and 2.6G for the [1,1,0] orientation. There appears also to be two other symmetric components, more pronounced for the [1,1,0] orientation, at 4.8G from the centre.

In both cases the repetition of the same line shape on rotating the probe (and sample) through 90° confirmed that the [0,0,1] crystal direction was parallel to the probe axis.

V.2 RELAXATION TIME MEASUREMENTS

Spin-lattice relaxation time (T_1) measurements have been made for most of these salts. Those which have been published previously will not be shown explicitly but references will be given. Within the scope of the present work only such quantities as molecular correlation times and activation

FIGURE 30

Proton absorption derivative spectrum, at 4.2°K, for a single crystal of NH_4Cl. $\underline{H}_o$ is along the [1,0,0] direction.

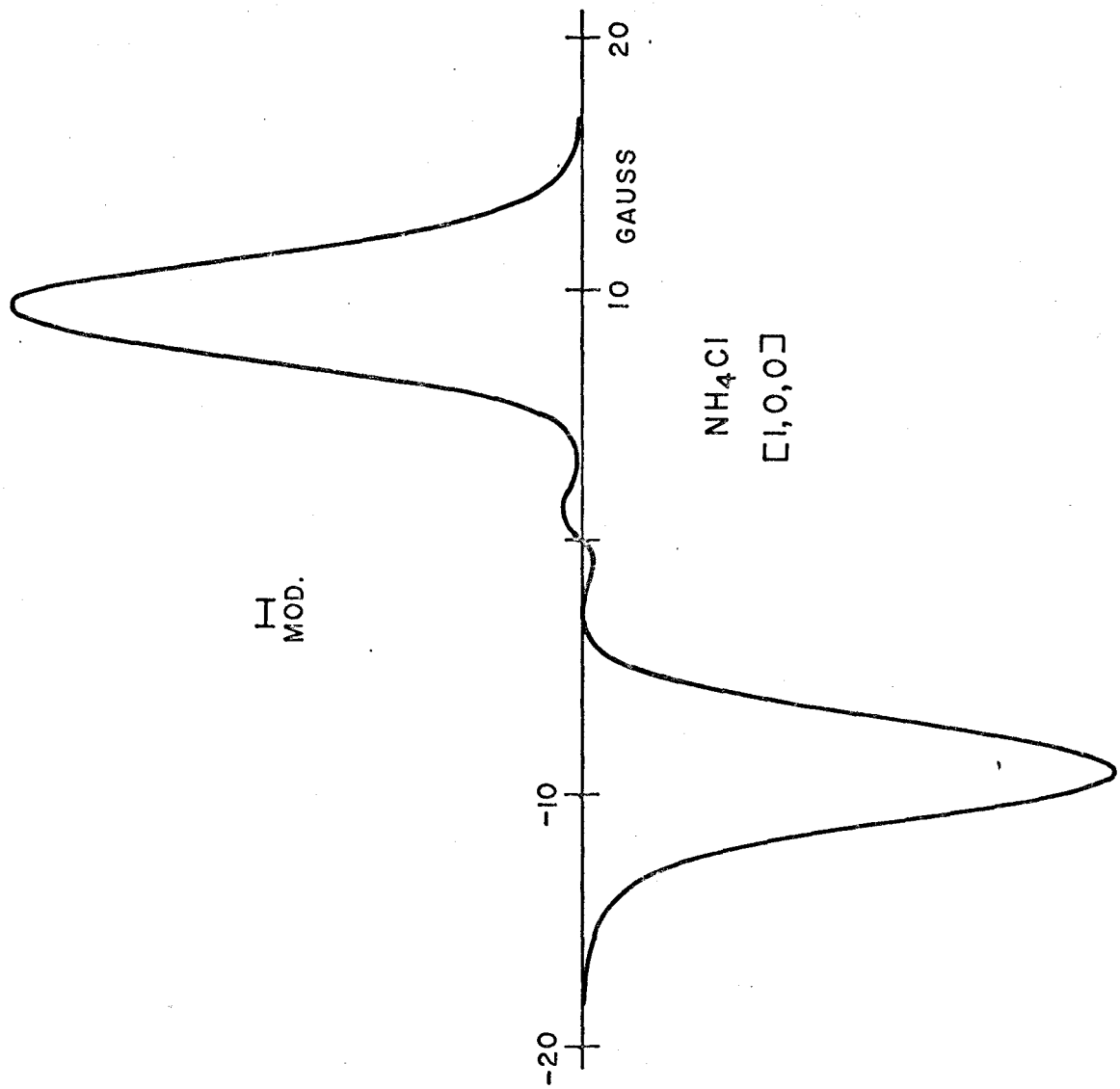
20
10 GAUSS
-10
-20
$I_{MOD.}$
NH_4Cl
[1,0,0]

FIGURE 31

Proton absorption derivative spectrum, at 4.2°K, for a single crystal NH_4Cl. $\underline{H}_o$ is along the [1,1,0] direction.

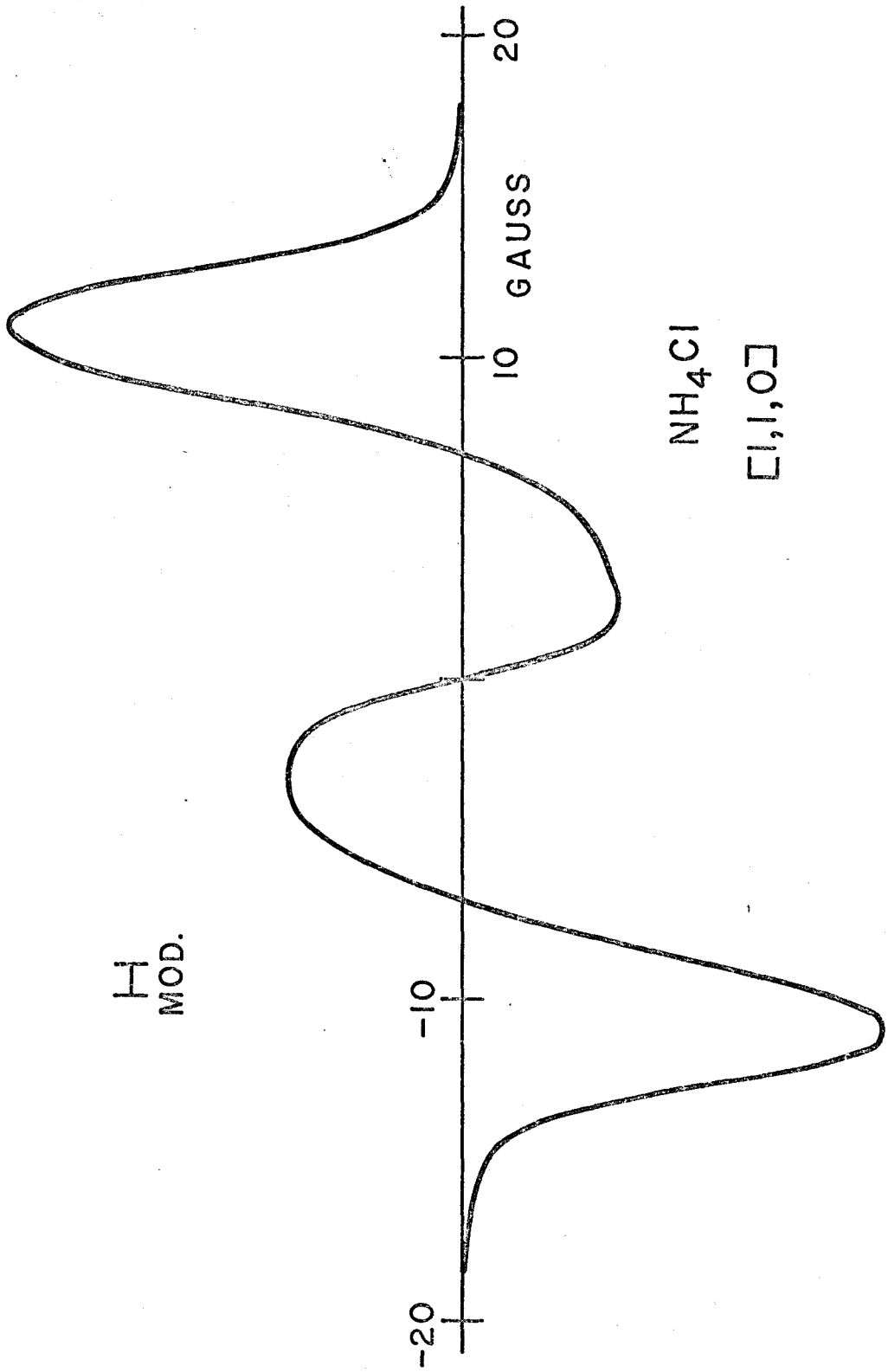
H
MOD.
-20
-10
10
20
GAUSS
NH4Cl
[1,1,0]

FIGURE 32

Proton absorption derivative spectrum, at 4.2°K, for a single crystal of $(NH_4)_2SnCl_6$. $\underline{H}_o$ is along the [1,0,0] direction.

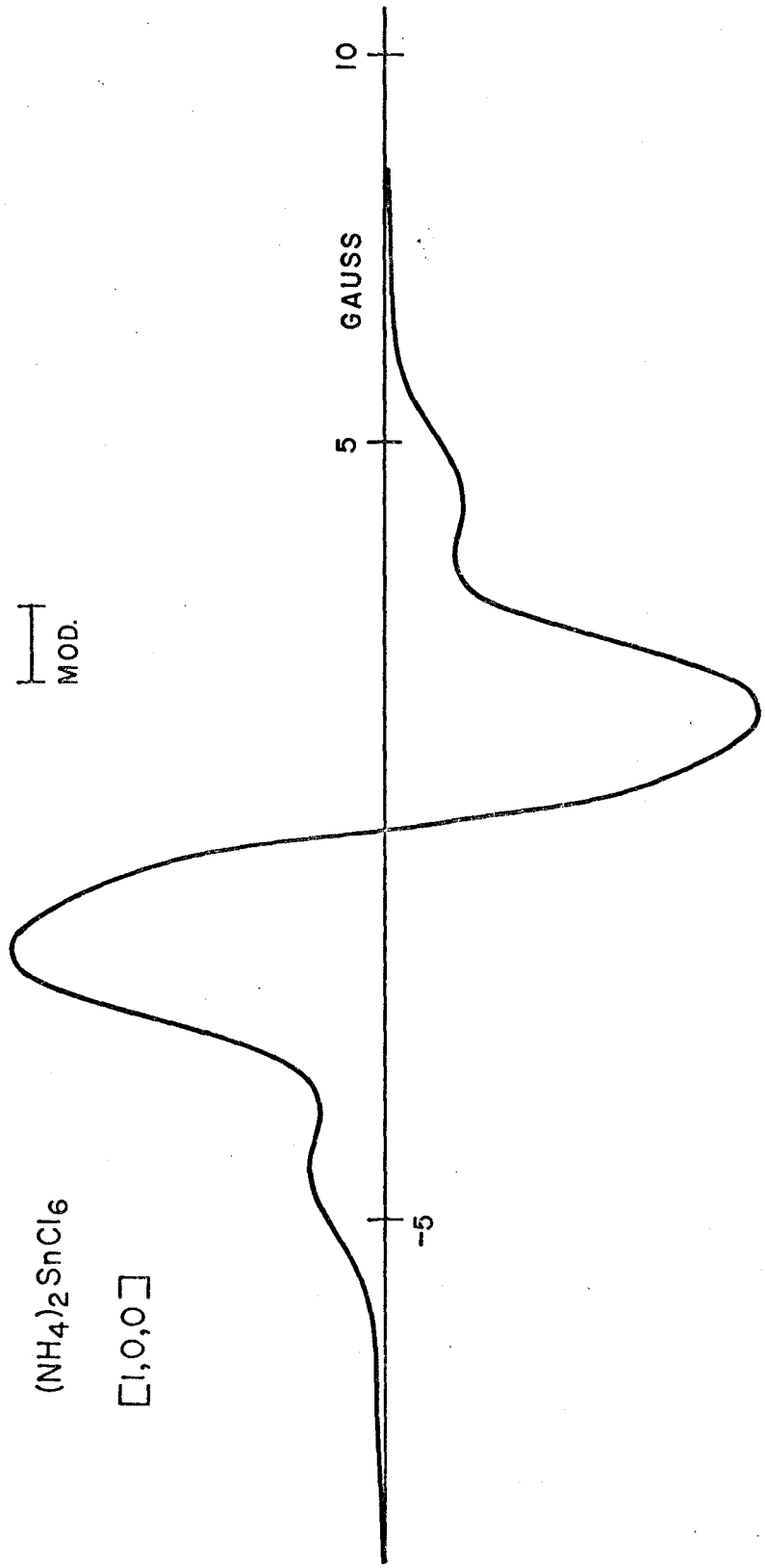
10
5
GAUSS
-5
MOD.
$(NH_4)_2SnCl_6$
[1,0,0]

FIGURE 33

Proton absorption derivative spectrum, at 4.2°K, for a single crystal of $(NH_4)_2SnCl_6$. $\underline{H}_o$ is along the [1,1,0] direction.

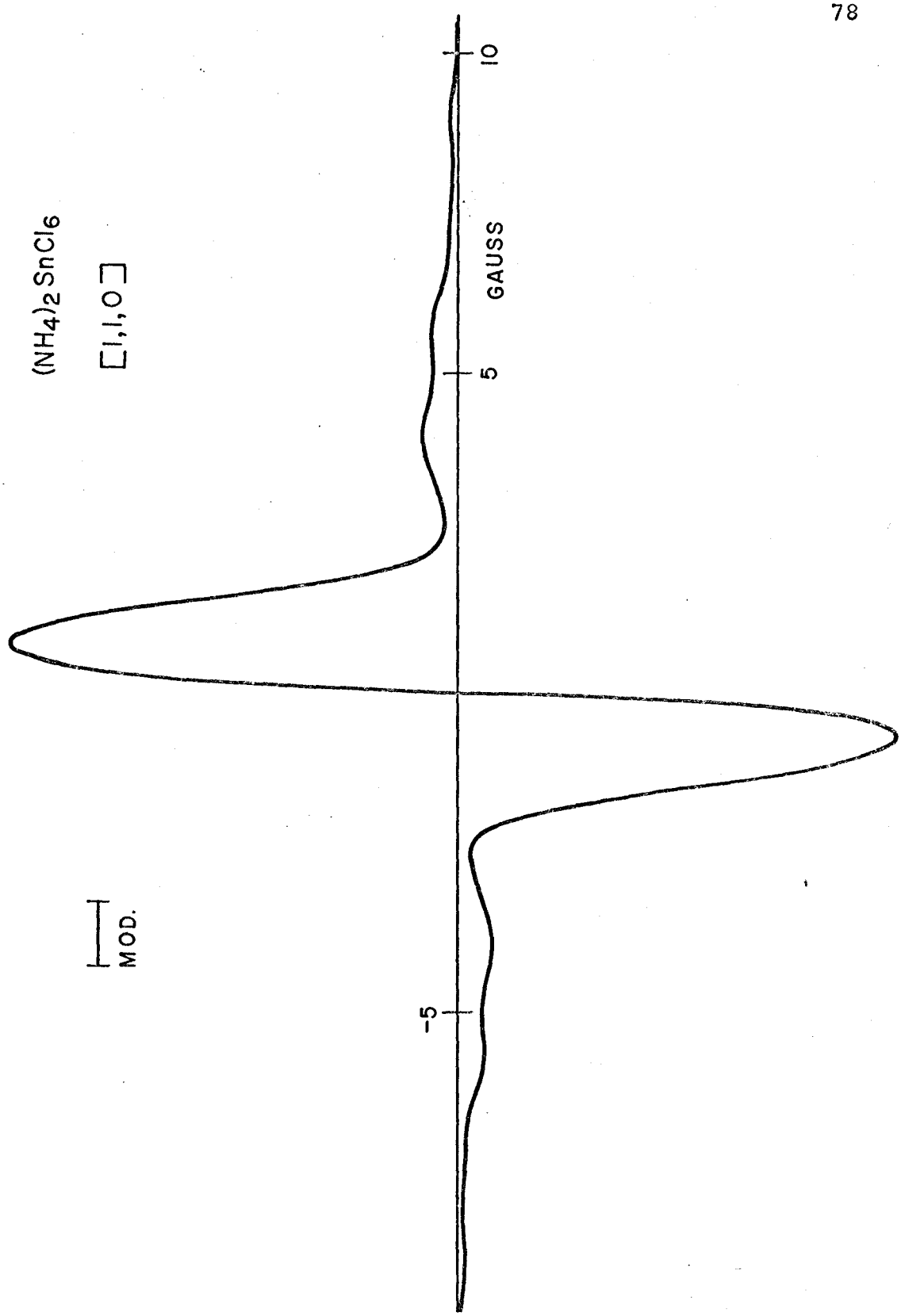
$(NH_4)_2SnCl_6$
[1,1,0]
10
5
GAUSS
-5
MOD.

FIGURE 34

Proton absorption spectrum, at 4.2°K, for the [1,0,0] field direction in a single crystal of NH_4Cl.

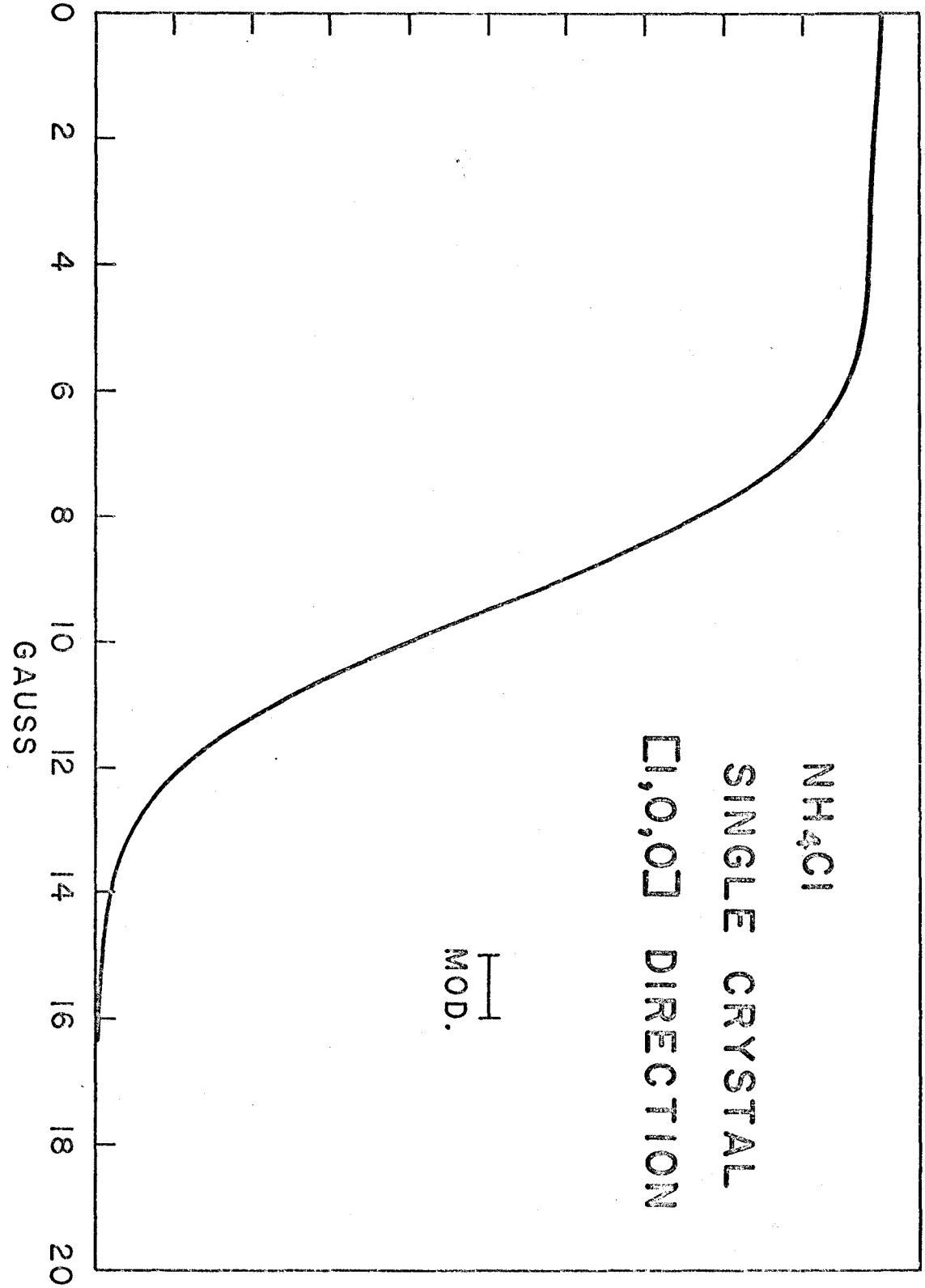
NH4Cl
SINGLE CRYSTAL
[1,0,0] DIRECTION
MOD.
0
2
4
6
8
10
12
14
16
18
20
GAUSS

FIGURE 35

Proton absorption spectrum, at 4.2°K, for the [1,1,0] field direction in a single crystal of NH_4Cl.

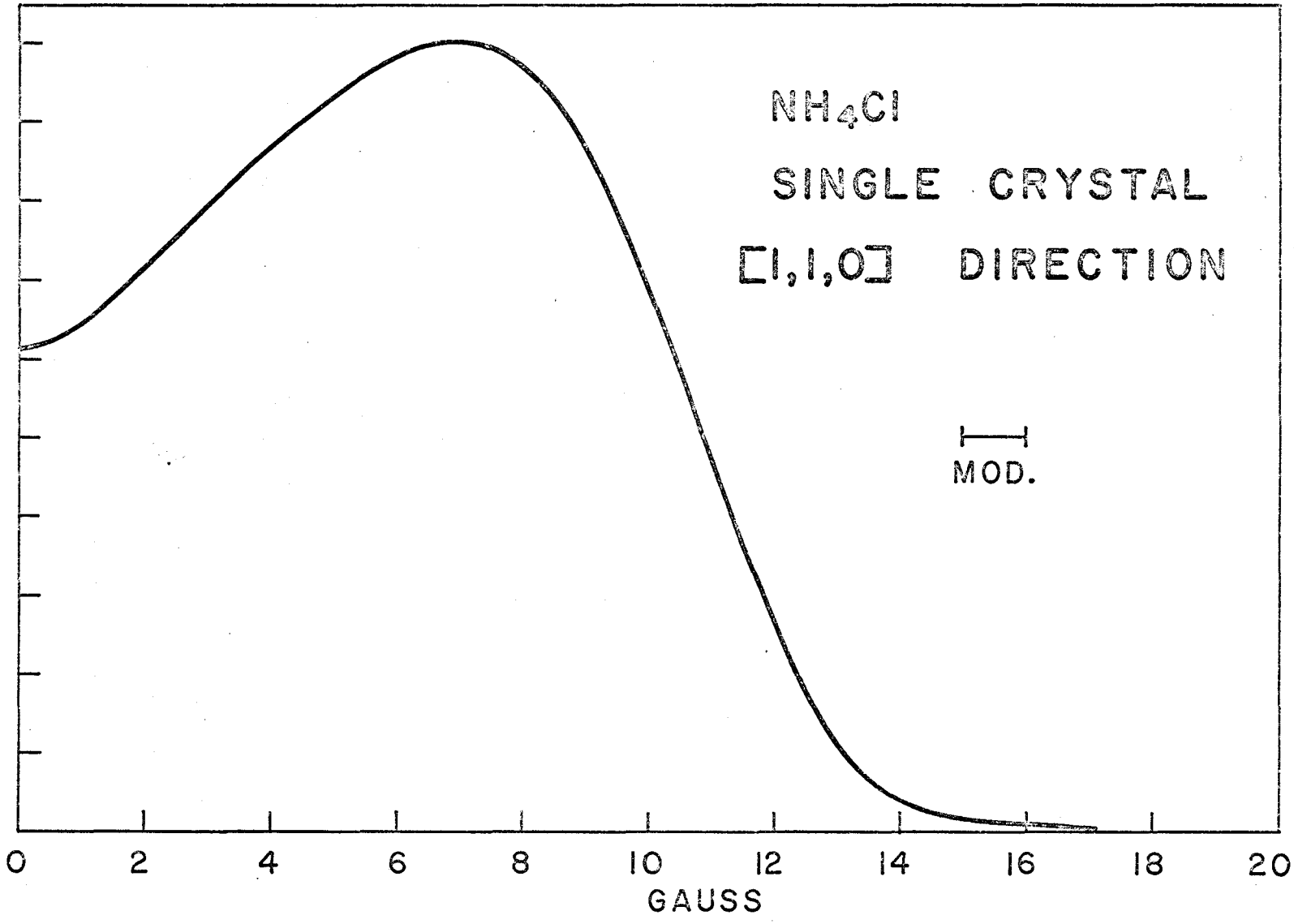
NH4Cl
SINGLE CRYSTAL
[1,1,0] DIRECTION
MOD.
0
2
4
6
8
10
12
14
16
18
20
GAUSS

FIGURE 36

Proton absorption spectrum, at 4.2°K, for the [1,0,0] field direction in a single crystal of $(NH_4)_2SnCl_6$.

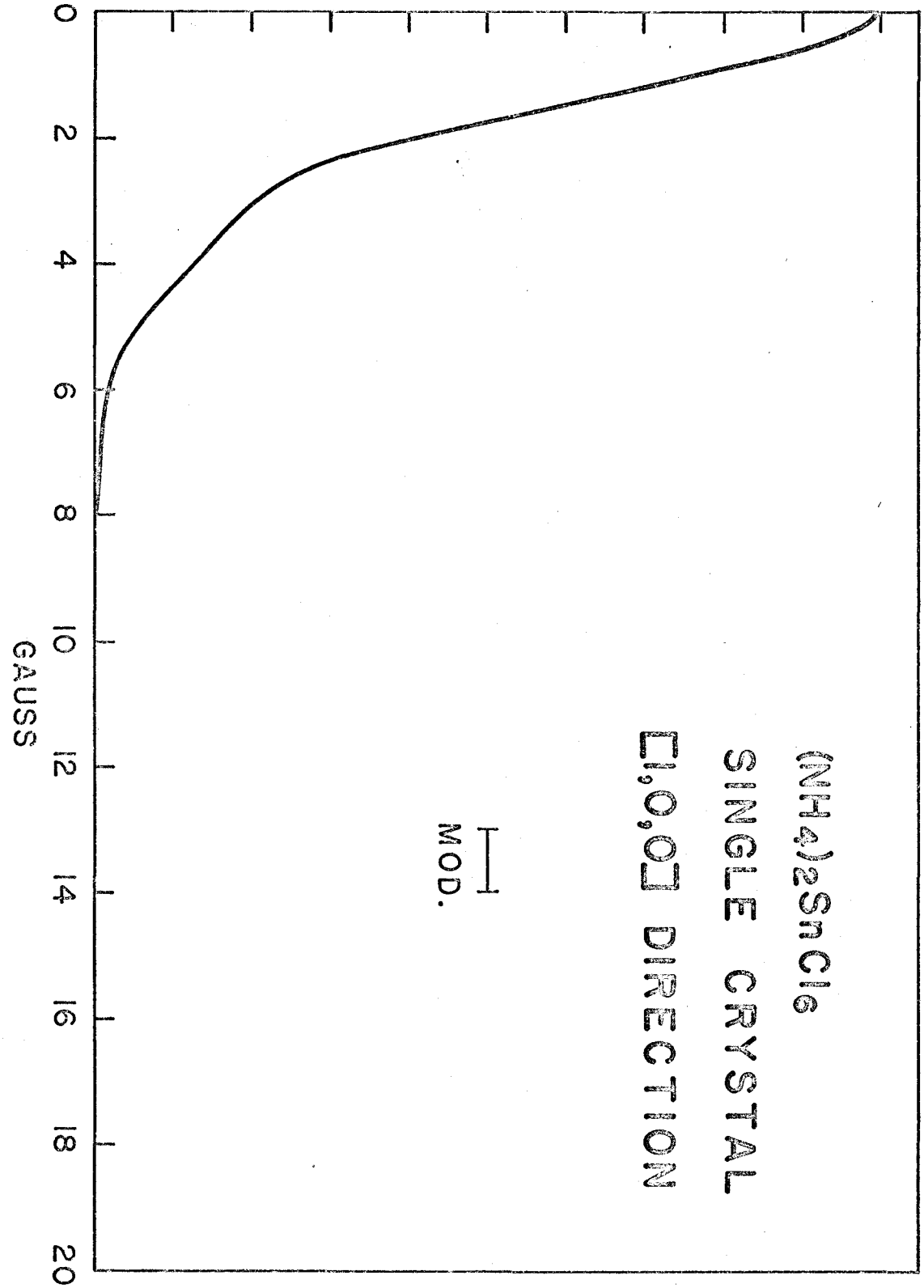
(NH4)2SnCl6
SINGLE CRYSTAL
[1,0,0] DIRECTION
MOD.
0
2
4
6
8
10
12
14
16
18
20
GAUSS

FIGURE 37

Proton absorption spectrum, at 4.2°K, for the [1,1,0] field direction in a single crystal of $(NH_4)_2SnCl_6$.

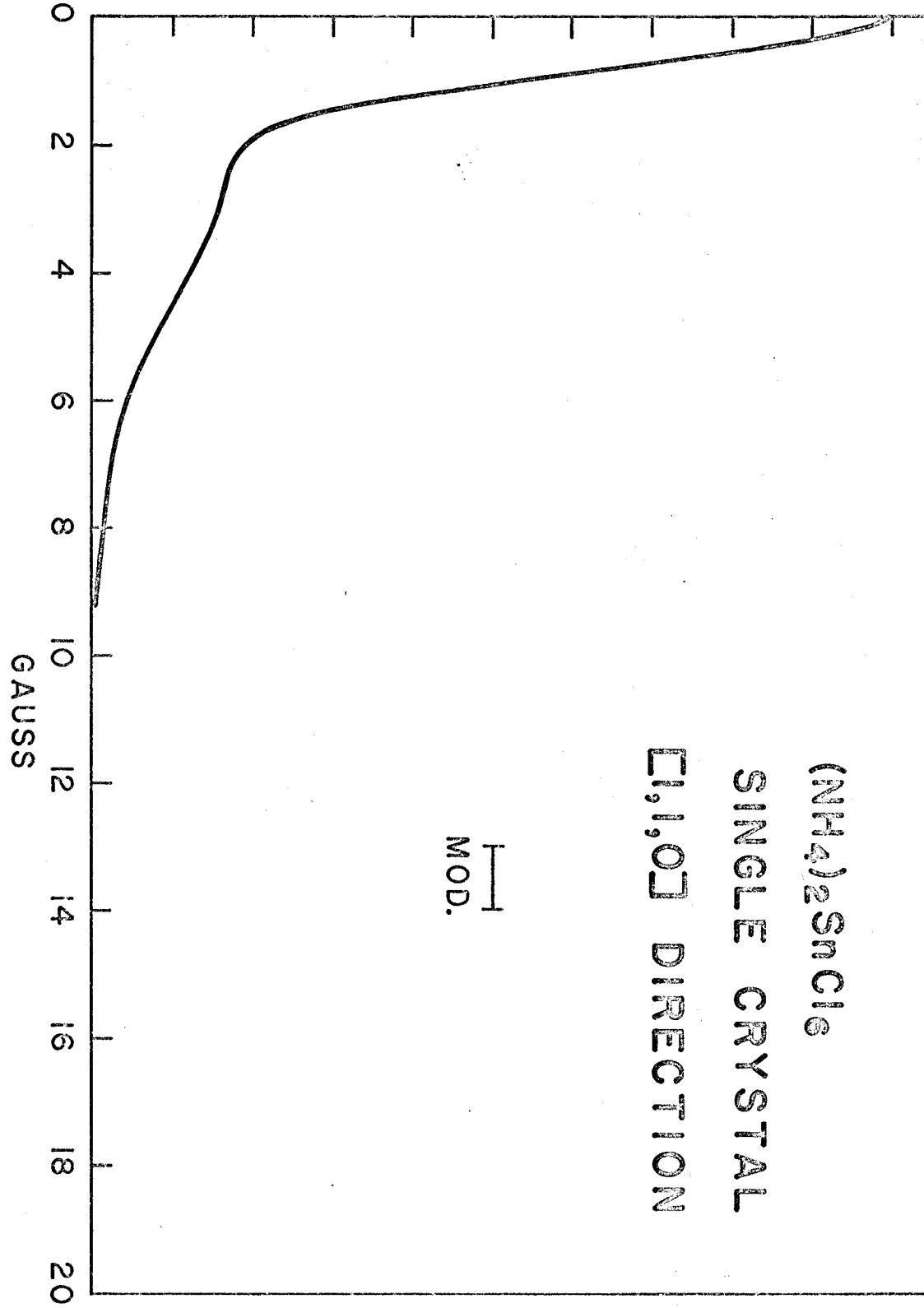
(NH4)2SnCl6
SINGLE CRYSTAL
[1,1,0] DIRECTION
MOD.
0
2
4
6
8
10
12
14
16
18
20
GAUSS

energies are of interest. Consequently, for the new data shown, only those features relevant to this objective will be emphasized. Aspects arising outside the scope of this work may be commented on, but any detailed discussion will be left for later publication by the various workers involved.

In the interest of brevity, the activation energies (E_a), calculated from the slopes of the linear portions of the $\ell n(T_1)$ vs. inverse temperature graphs, and the values of T_1 at 4.2°K, where available, are listed in Table VI.

Ammonium Tellurate $[(NH_4)_2TeO_4]$ - T_1 for this salt shows very little variation with temperature between 77°K and 300°K. This is probably a result of the presence of paramagnetic impurities dominating the relaxation. For this reason no activation energy was calculated, or data shown.

Ammonium Nitrate $[NH_4NO_3]$ - T_1 measurements have been reported by Riggin (1970).

Ammonium Metavanadate $[NH_4VO_3]$ - T_1's were measured at a frequency of 42 MHz in the temperature range from 77°K to 333°K, as shown in Figure 38. Of the two minima, one occurring at 123°K and the other at 192°K, the low temperature one can be attributed to reorientation of the ammonium

FIGURE 38

Temperature dependence of T_1 in NH_4VO_3 at 42 MHz.

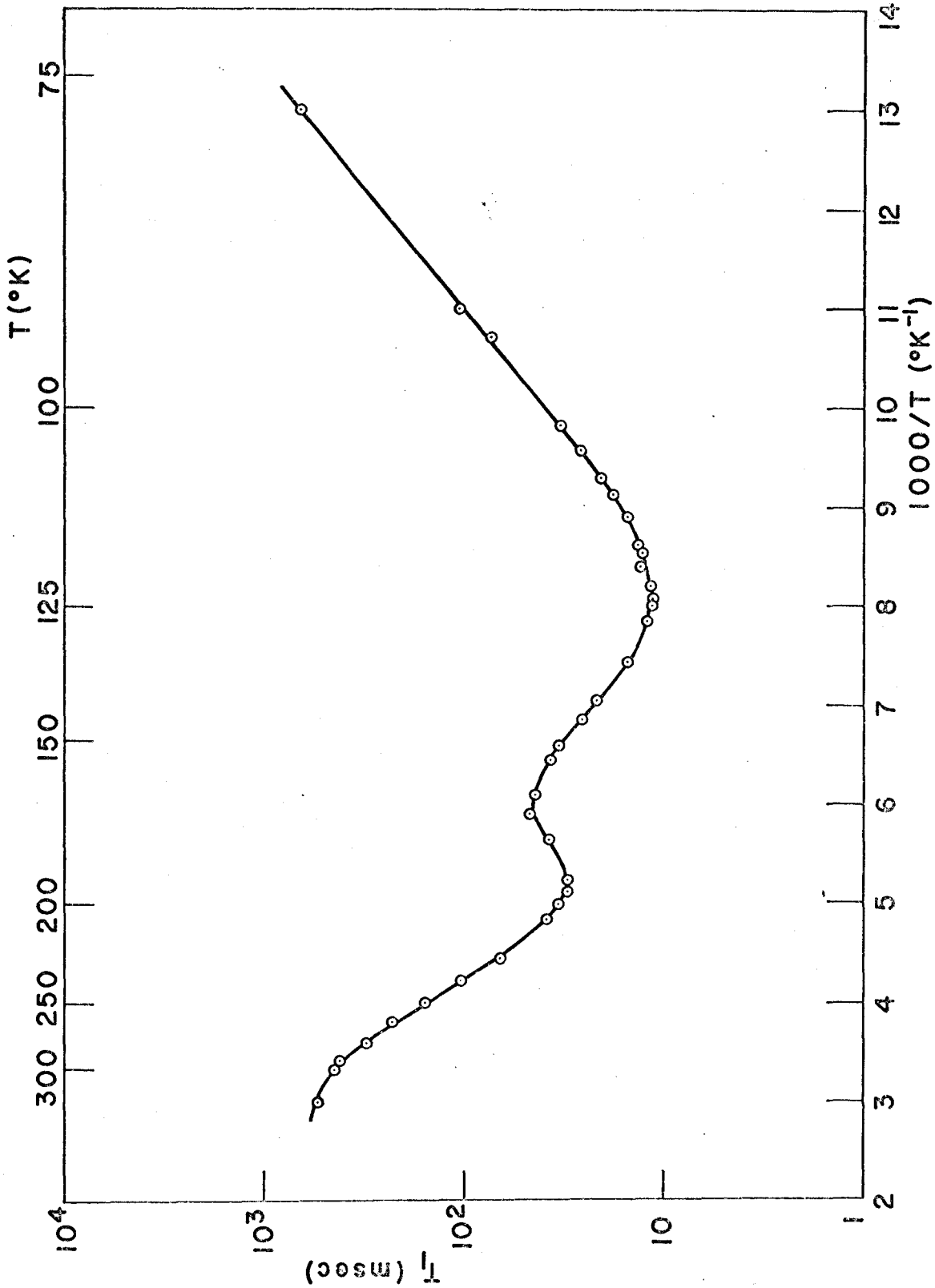
T (°K)
75
100
125
150
200
250
300
1000/T (°K⁻¹)
2
3
4
5
6
7
8
9
10
11
12
13
14
T1 (msec)
10⁴
10³
10²
10
1

ion.

Ammonium Dichromate [$(NH_4)_2Cr_2O_7$] - T_1's were measured at a frequency of 42 MHz in the temperature range from 77°K to 300°K, as shown in Figure 39. $\ell n(T_1)$ decreases linearly with increasing β(=1000/T) over much of the temperature range and approaches its minimum around 77°K, although the temperature range did not extend low enough to completely include the minimum.

Ammonium Persulphate [$(NH_4)_2S_2O_8$] - T_1's were measured at a frequency of 19 MHz in the temperature range from 77°K to 300°K, as shown in Figure 40. The temperature dependence is very similar to the dichromate with a minumum occurring around 80°K, which is again at the lower limit of the measured temperature range, and hence is ill-defined.

Ammonium Thiosulphate [$(NH_4)_2S_2O_3$] - T_1's were measured at a frequency of 20.7 MHz in the temperature range from 77°K to 300°K. Over this range the signal decay was non-exponential and was analyzed to give two unique T_1's as shown in Figure 41. This behaviour can be attributed to the existence of two inequivalent types of ammonium ion in this salt, each possessing its own spin temperature and relaxing independently to the lattice. The T_1 minimum for one ion type occurs around 116°K, but is only just beginning to appear for the other at the lower temperature limit of 77°K.

FIGURE 39

Temperature dependence of T_1 in $(NH_4)_2Cr_2O_7$ at 42 MHz.

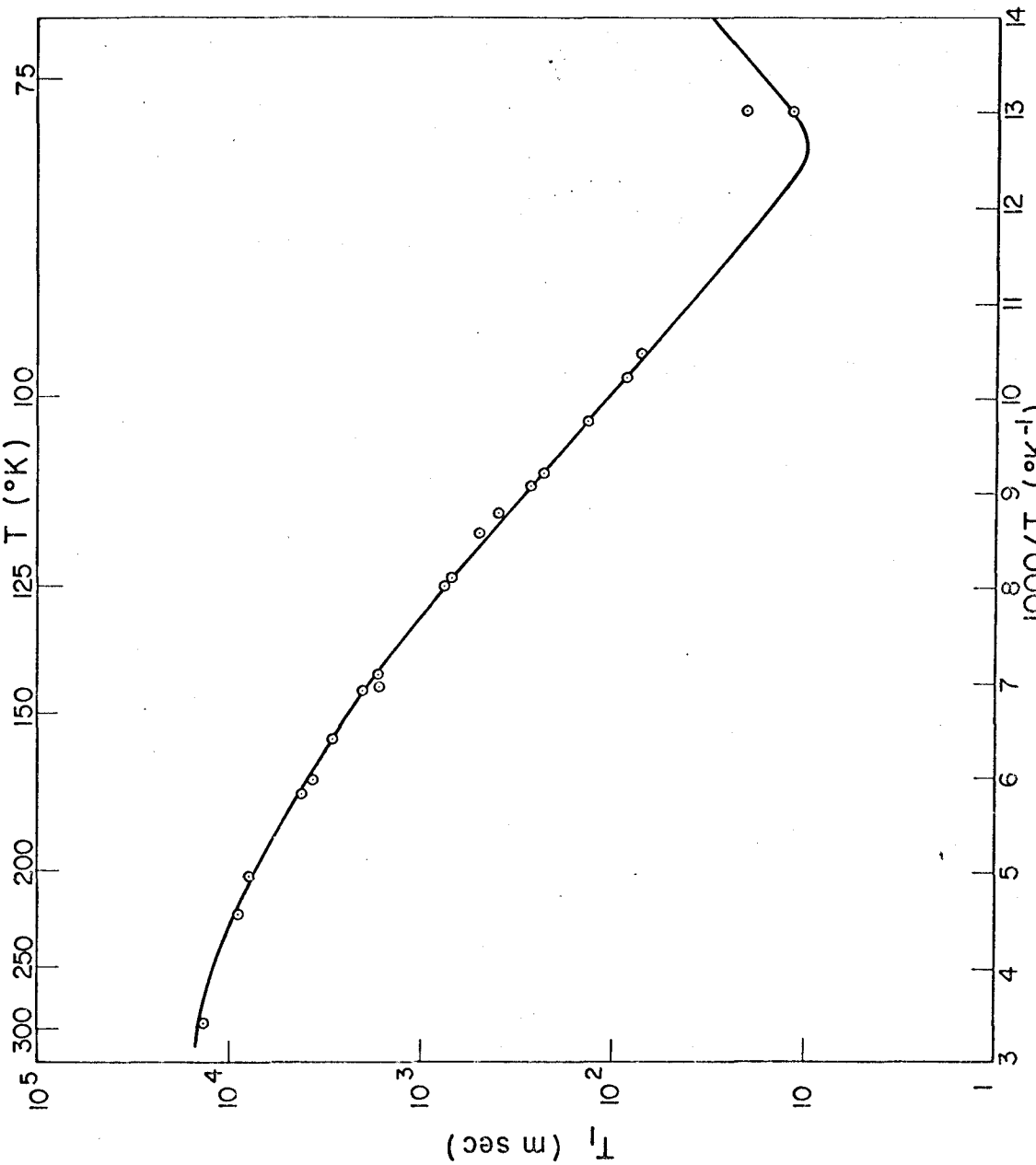
T (°K)
75
100
125
150
200
250
300
1000/T (°K⁻¹)
3
4
5
6
7
8
9
10
11
12
13
14
T₁ (m sec)
10⁵
10⁴
10³
10²
10
1

FIGURE 40

Temperature dependence of T_1 in $(NH_4)_2S_2O_8$ at 19 MHz.

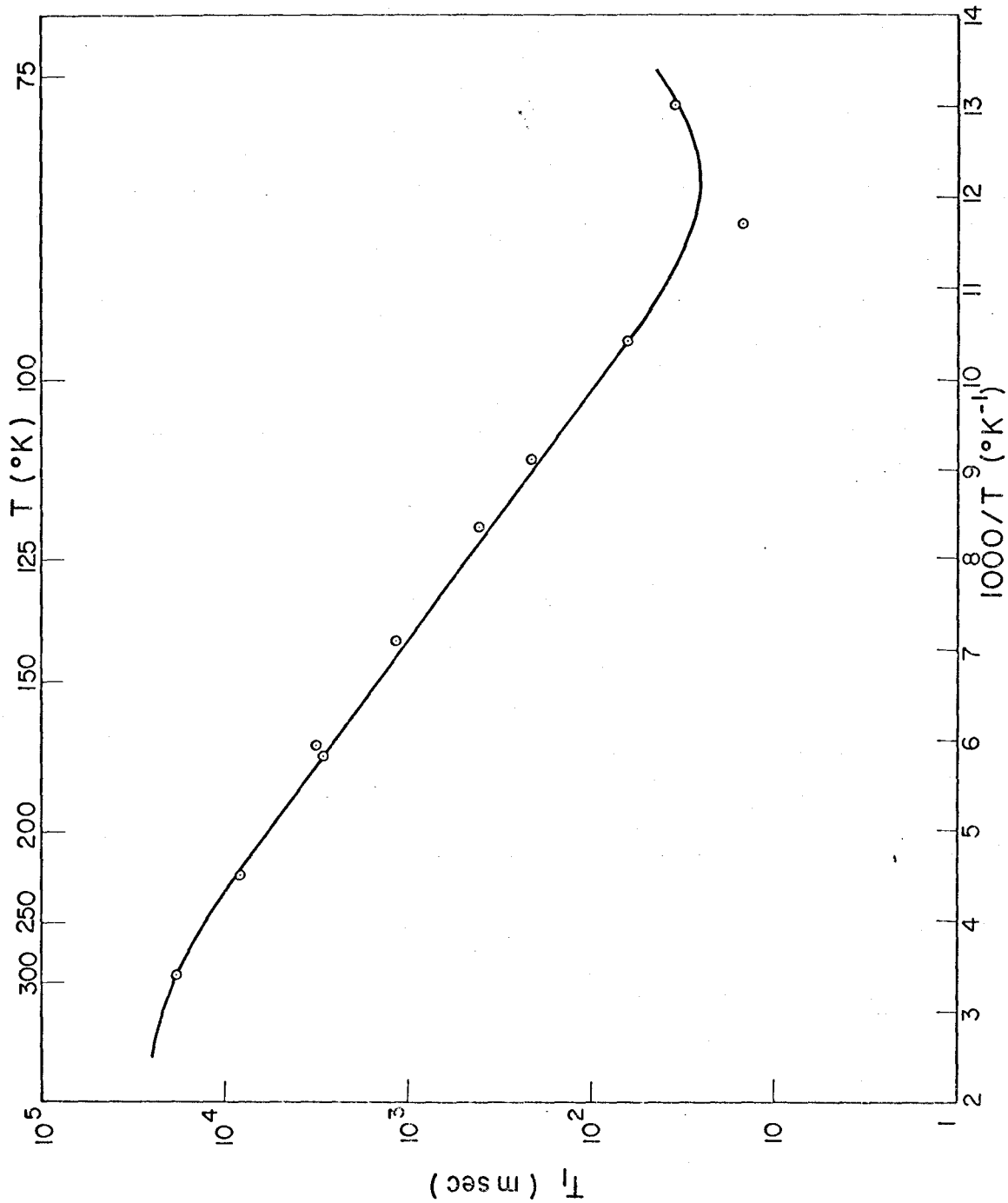
T_1 (msec)
10^5
10^4
10^3
10^2
10
1
2
3
4
5
6
7
8
9
10
11
12
13
14
1000/T (°K⁻¹)
75
100
125
150
200
250
300
T (°K)

FIGURE 41

Temperature dependence of $(NH_4)_2S_2O_3$ at 20.7 MHz. The signal decay was non-exponential over this range and was analysed to give the two T_1 dependences shown.

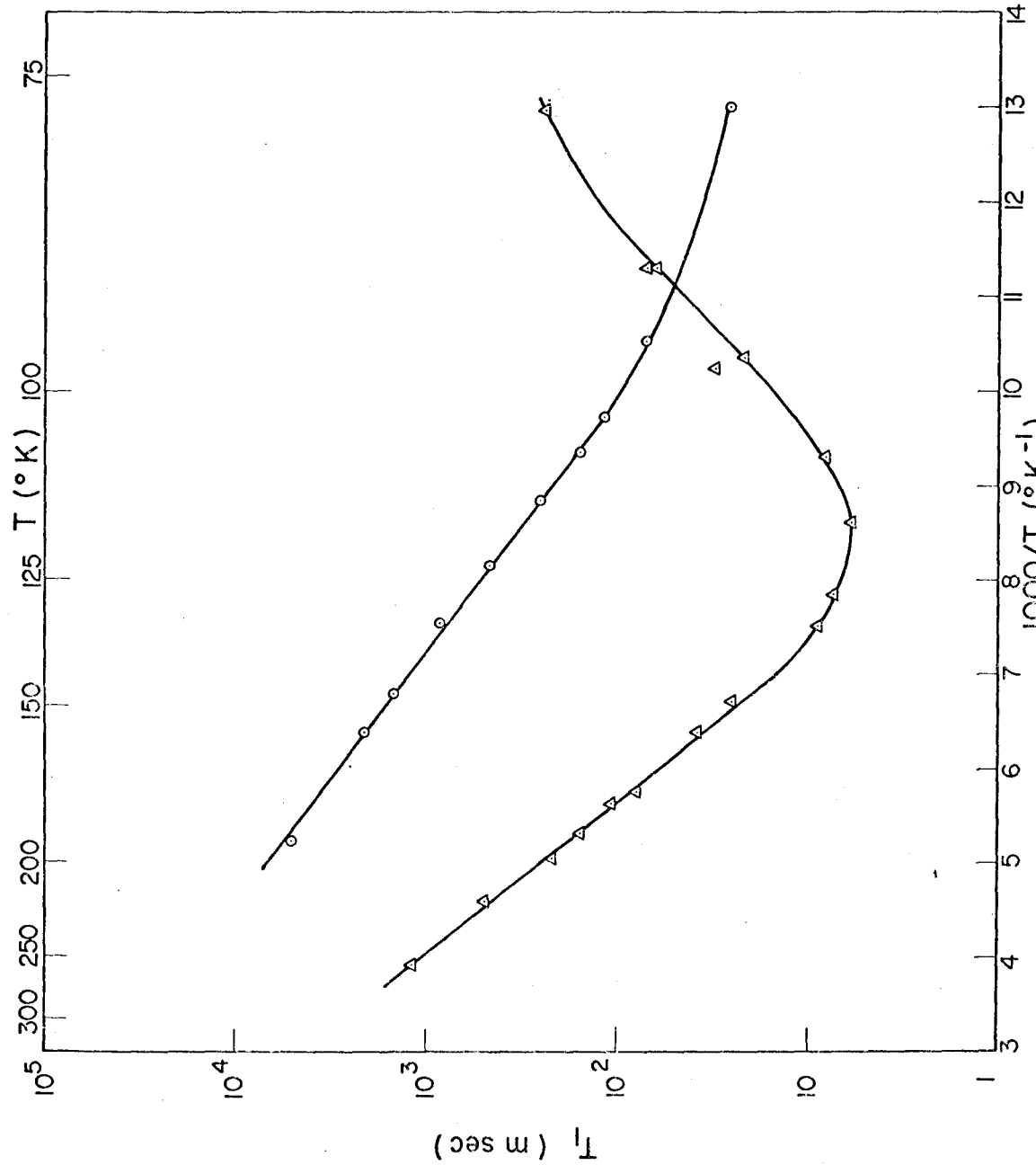
T_1 (m sec)
10^5
10^4
10^3
10^2
10
1
T (°K)
300
250
200
150
125
100
75
1000/T ($°K^{-1}$)
3
4
5
6
7
8
9
10
11
12
13
14

Ammonium Hexanitratocerate $[(NH_4)_2Ce(NO_3)_6]$ - T_1's were measured at a frequency of 5.4 MHz in the temperature range from 20°K to 300°K, as shown in Figure 42. On both sides of the minimum $\ell n(T_1)$ shows a linear dependence on inverse temperature. At very low temperatures, below 30°K, T_1 levels off as the paramagnetic impurities begin to dominate the relaxation.

Ammonium Selenate $[(NH_4)_2SeO_4]$ - T_1's were measured at a frequency of 20.7 MHz in the temperature range from 150°K to 350°K as shown in Figure 43. The T_1 minimum due to molecular reorientation occurs around 198°K.

Ammonium Hexachlorostannate $[(NH_4)_2SnCl_6]$ - T_1's were measured at a frequency of 5.4 MHz in the temperature range from 20°K to 125°K. Below about 70°K the signal decay was non-exponential and was analyzed to give two T_1's as shown in Figure 44. The data may be interpreted on the basis of two relaxation mechanisms: a reorientation of the ammonium group leading to a minimum in T_1 around 57°K and a tunneling assisted mechanism leading to a T_1 minimum at 29°K, which is too low a temperature for molecular reorientation to be evident.

Ammonium Trichlorostannite $[NH_4SnCl_3]$ - T_1's were measured at a frequency of 20.7 MHz in the temperature range from 77°K to 300°K. Over practically the whole of this range the signal decay was non-exponential, and was analyzed to give two

FIGURE 42

Temperature dependence in $(NH_4)_2Ce(NO_3)_6$ at 5.4 MHz.

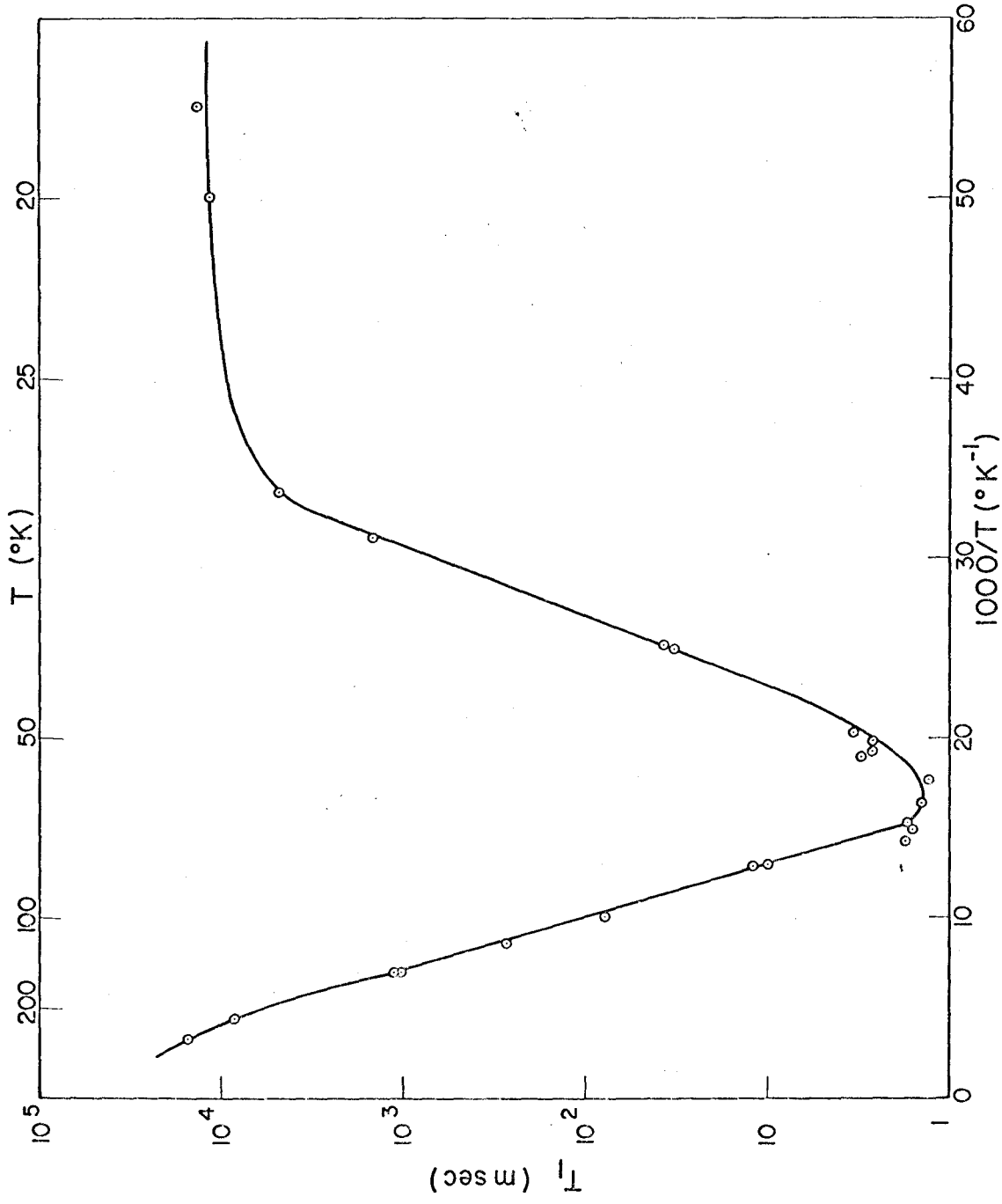
T_1 (msec)
10^5
10^4
10^3
10^2
10
1
T (°K)
200
100
50
25
20
0
10
20
30
40
50
60
1000/T (°K^{-1})

FIGURE 43

Temperature dependence of T_1 in $(NH_4)_2SeO_4$ at 20.7 MHz.

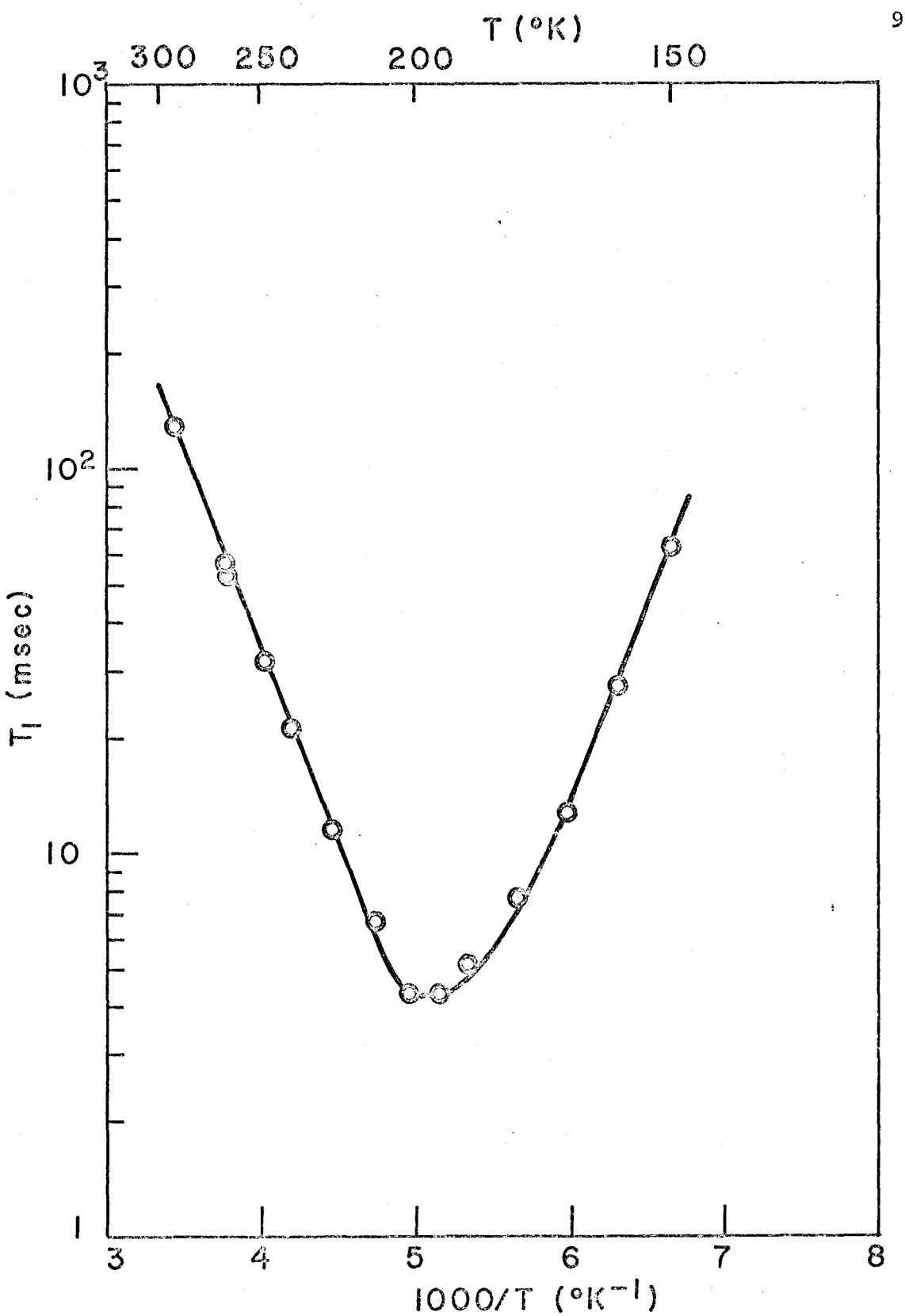
T (°K)
300
250
200
150
10^3
10^2
10
1
T_1 (msec)
3
4
5
6
7
8
1000/T (°K^{-1})

FIGURE 44

Temperature dependence of T_1 in $(NH_4)_2SnCl_6$ at 5.4 MHz. The signal decay in the region below 70°K is non-exponential, and was analysed to give the two T_1 dependences shown.

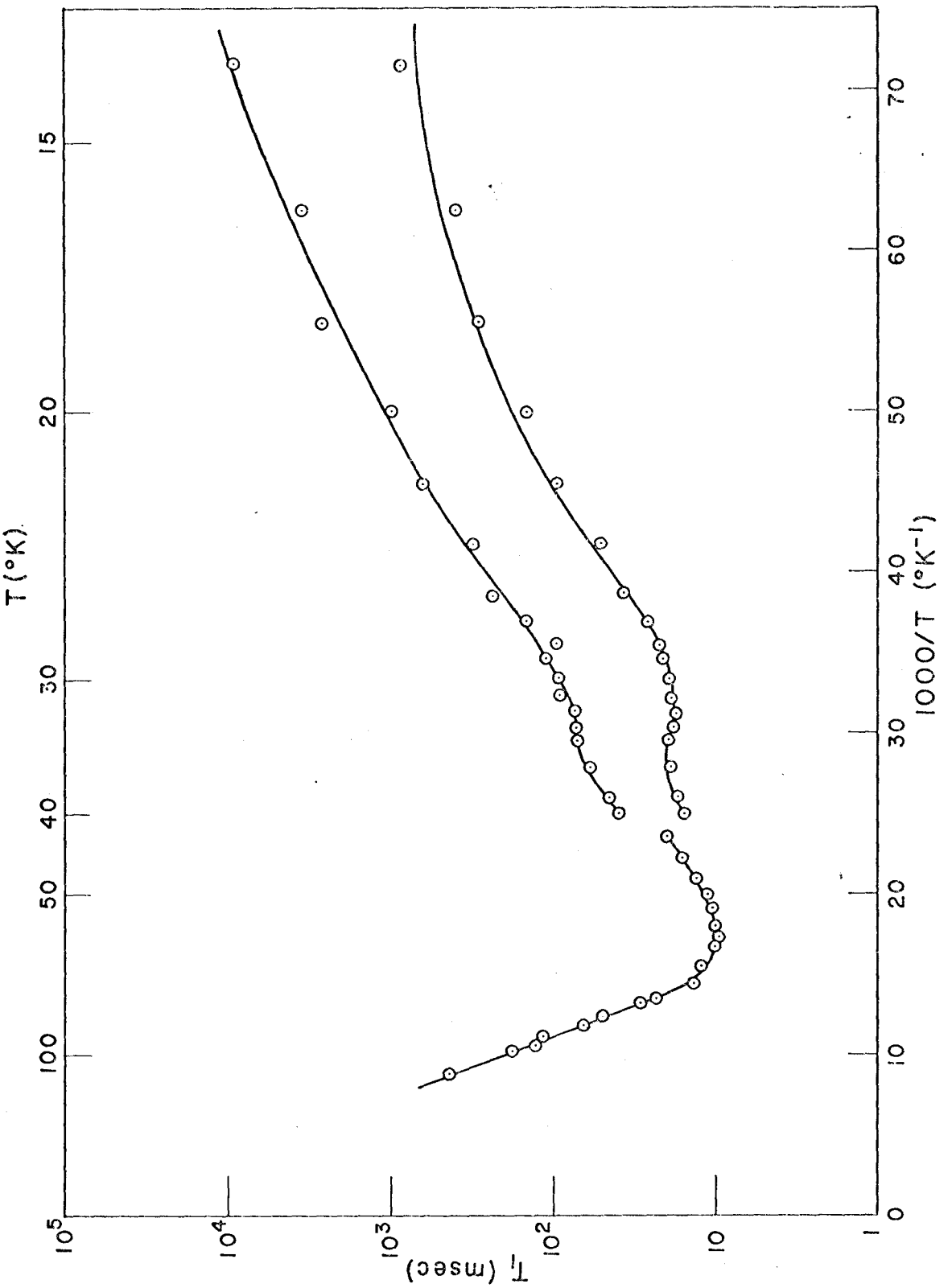
T (°K)
15
20
30
40
50
100
1000/T (°K⁻¹)
0
10
20
30
40
50
60
70
T₁ (msec)
10⁵
10⁴
10³
10²
10
1

T_1's as shown in Figure 45. In all cases the T_1 values found at each temperature were of the same order of magnitude, resulting in some inaccuracy of the extracted values. The inference is again of two inequivalent groups of ions relaxing independently to the lattice. The activation energy extracted from the small region around 150°K is, of course, inexact and can be taken only as a qualitative guide.

Ammonium Bromide [NH_4Br] - T_1 measurements have been reported by Woessner and Snowden (1967a).

Ammonium Chloride [NH_4Cl] - T_1 measurements have been reported by Woessner and Snowden (1967b).

Ammonium Sulphate [$(NH_4)_2SO_4$] - T_1 measurements have been reported by O'Reilly and Tsang (1967) for protons and by Kydon, Pintar and Petch (1967) for deuterons.

Ammonium Tetrafluoroberyllate [$(NH_4)_2BeF_4$] - T_1 measurements have been reported by Kydon et al (1969) for deuterons, and by O'Reilly, Peterson and Tsang (1967) for protons.

Ammonium Selenite [NH_4SeO_3] - No T_1 data is available for this salt.

Ammonium Diuranate [$(NH_4)_2U_2O_7$] - No T_1 data is given for this salt because the relaxation was dominated by paramagnetic impurities.

Ammonium Iodoplatinate [$(NH_4)_2PtI_6$] - No T_1 data is ayailable for this salt.

FIGURE 45

Temperature dependence of T_1 in NH_4SnCl_3 at 20.7 MHz. The two T_1 dependences represent an analysis of the non-exponential signal decay over the entire temperature range.

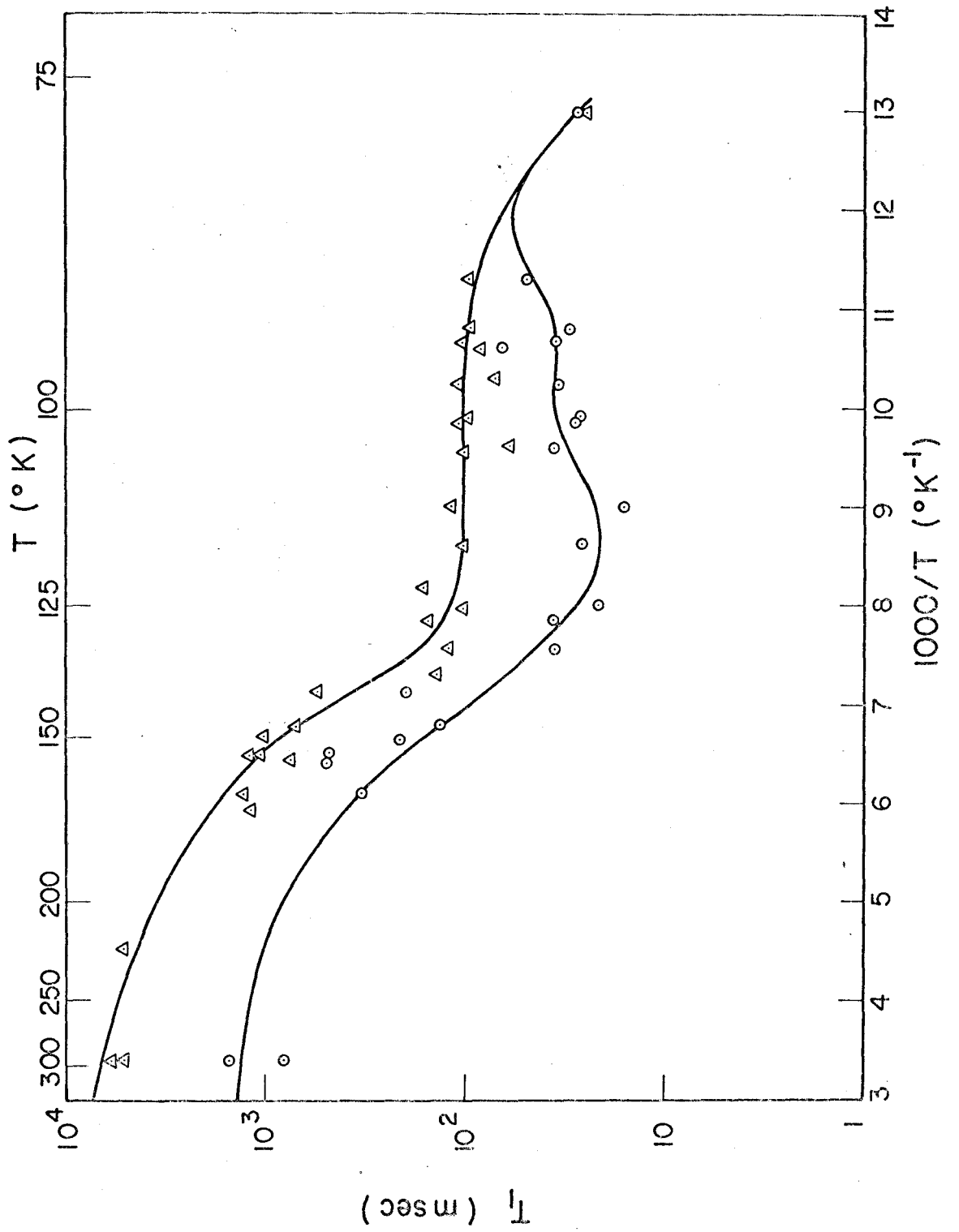
T (°K)
75
100
125
150
200
250
300
1000/T (°K⁻¹)
3
4
5
6
7
8
9
10
11
12
13
14
10^4
10^3
10^2
10
1
T_1 (msec)

Ammonium Chlorogallate [$(NH_4)_2GaCl_4$] - No T_1 data is available for this salt.

Ammonium Fluoride [NH_4F] - No T_1 data is available for this salt.

The effects of relaxation caused by paramagnetic impurities mentioned at the end of Chapter III can be seen in a number of these cases. At low temperatures the T_1 values of $(NH_4)_2Ce(NO_3)_6$ (Figure 42) and $(NH_4)_2SnCl_6$ (Figure 44) approach a limiting value of about 104 sec. as the paramagnetic relaxation begins to dominate. Similar limitation effects at high temperatures can be seen in NH_4VO_3 (Figure 38), $(NH_4)_2Cr_2O_7$ (Figure 39), $(NH_4)_2S_2O_8$ (Figure 40) and NH_4SnCl_3 (Figure 45). In the middle temperature ranges where T_1 is strongly temperature dependent the paramagnetic impurities play only a minor role in the relaxation which is dominated here by the thermally activated dipolar mechanisms.

For the particular case of $(NH_4)_2U_2O_7$ the constituent uranium ions themselves are paramagnetic and dominate the relaxation over the whole temperature range.

CHAPTER VI

DISCUSSION

VI.1 MOTIONAL EFFECTS

The calculation of the correlation frequency (defined as $1/2\pi\tau_c$) is illustrated for a few of the materials studied:-

The dipolar relaxation time for reorientation is given (Abragam, chapter VIII) by;

$$\left(\frac{1}{T_1}\right)_r = C_d\left[\frac{\tau_c}{1+\omega_L^2\tau_c^2} + \frac{4\tau_c}{1+4\omega_L^2\tau_c^2}\right] \qquad (6.1)$$

where C_d depends only upon the nuclei concerned and their configuration, τ_c is the correlation time for the reorientational process, and ω_L is the Larmor frequency.

From expression (6.1), a minimum in T_1 occurs when $\omega_L\tau_c = 0.62$. For ammonium selenate this minimum is observed to occur around 198°K at 20.7 MHz (Figure 43). Considering the reorientation as a thermally activated process, the Arrhenius expression

$$\tau_c = 3.2 \times 10^{-14} \exp\{2.4\beta\} \qquad (6.2)$$

is obtained for the reorientational correlation time in this salt. Using expression (6.2), the temperature at which the correlation frequency becomes less than the linewidth (which for these salts is ∿10G,or 40 KHz) can be calcualted. Hence we find that, for ammonium selenate, the lattice is effectively

rigid below 116°K.

For ammonium hexanitratocerrate the temperature at which T_1 reaches a minimum (around 50°K at 5.4 MHz - Figure 42) was one of the lowest among the salts measured. This fact, coupled with its very low activation energy (1.6 K cal/mole), would indicate that the "rigid lattice" temperature for this salt should be one of the lowest for the solids studied. A calculation analogous to the one for the selenate shows that the lattice of $(NH_4)_2Ce(NO_3)_6$ is effectively rigid below 35°K. Indeed, taking an extreme, hypothetical case, where the T_1 minimum at 20 MHz occurs at 50°K, with an activation energy of 1 K cal/mole (both quantities lower than those for any salt measured), the same calculation reveals that the lattice would be effectively rigid below 27°K. We may thus safely conclude that molecular reorientation, as a mechanism for line narrowing, can effectively be ruled out, for the ammonium salts studied here, at temperatures as low as 4.2°K.

VI.2 LINE SHAPES

From the theory of Chapter II, the proton absorption line shape for an ammonium group exhibiting spin isomerism is expected to display certain salient characteristics; a second moment considerably less than the "rigid lattice" value, a dominant central gaussian component, and either structure or broadening in the wings depending upon the inter-ionic second

moment. With one or two exceptions the ammonium salts studied fall naturally into three classes determined by the characteristics of their absorption spectra. Each salt will be discussed within the category to which its spectrum most closely conforms:

a) Wide Spectra

This category consists of the halogen salts NH_4Cl, NH_4Br and NH_4F plus the selenate $(NH_4)_2SeO_4$. Their spectra have no dominant central component and all are broad (Figures 11 to 14) with large second moments (comparable to the "rigid lattice" value). On the basis of their line shapes and second moment values we conclude that spin isomerism is not exhibited by any of the salts in this category.

The single crystal derivative spectra at 4.2°K of NH_4Cl for the [1,0,0] and [1,1,0] field directions (Figures 30 and 31) are identical with those obtained at 77°K by Bersohn and Gutowsky (1954) for the same orientations in this salt. They found good experimental agreement between their line shapes and a theoretical "4-spin 1/2" calculation, in which the entire matrix in Table II is diagonalized (protons are distinguishable - no symmetry restrictions on the wave function). They found better agreement for the [1,0,0] direction than the [1,1,0], and suggest that this may be the result of using the same inter-ionic broadening factor for each skeletal line of the isolated proton group spectrum, a criticism, however, which

applies equally to both orientations. A more probable explanation for the poorer agreement along [1,1,0] is that the contribution of the nitrogen nucleus, which they neglect, though zero for the [1,0,0] is non-zero for the [1,1,0] direction (see section II.13).

In view of this agreement for a single crystal we may conclude that the powder spectra at 4.2°K of all the salts in the present category, being qualitatively similar to that of NH_4Cl, are indicative of a "4-spin 1/2" system. This distinguishability shown by the protons is consistent with the high activation energies ($\gtrsim$ 4 K cal/mole) in these solids, which imply strong crystal fields and consequently small overlap of the spatial wave functions.

b) Narrow Spectra

The line shapes of all salts in this category are characterized by a very dominant, narrow ($\sim$1 G^2) central component, some exhibiting wing structure at about 4 or 5 G from the centre. They are shown in Figures 15 to 22, along with the theoretical spin isomer line shape (dashed curve) most closely fitting the central component. The values of the broadening factor, $\langle \Delta H^2 \rangle$, necessary to achieve this fit for each salt are: $(NH_4)_2U_2O_7$ (4 G^2-Figure 15) , $(NH_4)_2Cr_2O_7$ (2G^2 - Figure 16), $(NH_4)_2S_2O_8$ (2 G^2 - Figure 17), NH_4SnCl_3 (2 G^2 - Figure 18), $(NH_4)_2SnCl_6$ (1 G^2 - Figure 19), $(NH_4)_2PtI_6$ (1 G^2 - Figure 20), $(NH_4)_2Ce(NO_3)_6$ (1 G^2 - Figure 21),

NH_4GaCl_4 (1 G^2 - Figure 22). All have second moments much less than the "rigid lattice" value, and , with the exceptions of $(NH_4)_2U_2O_7$, $(NH_4)_2S_2O_8$, and NH_4GaCl_4, much less than the theoretical spin isomer value for a ratio (R) of meta:ortho of 5/3. Since all the salts in this group have very low activation energies ($\leq$ 2 K cal/mole) an attempt to explain these low second moments could be made by assuming that the spatial level splittings in such low crystal fields are so high that the Boltzman factor becomes important at 4.2°K. The effect of this would be to increase the population of the lower, meta, states, so decreasing the second moment (M_2 for the meta-transitions is just $\langle\Delta H^2\rangle$). However, the only effect this would have on the theoretical line shape would be to decrease the intensity of the ortho component - its associated wing structure would still occur in the same part of the spectrum, $\sim$9 G from the centre. This is in disagreement with the observed spectra of all the salts in this group, whose wing structure is observed to occur around 4 or 5 G from the centre.

$(NH_4)_2SnCl_6$ is a typical salt of this category. Its absorption spectrum for the [1,0,0] field direction (which is particularly easy to interpret because of the absence of the nitrogen contribution) can be approximated very closely in the central region by a spin isomer spectrum with a $\langle\Delta H^2\rangle$ of 2 G^2 - Figure 36. However, the theoretical structure occuring at $\sim$9 G is completely absent, while only a semblance of that at $\sim$5 G remains. The lack of agreement for the single crystal

between the experimental and theoretical line shapes is, as for the powders, in the location as well as the amount of wing structure.

We can conclude that the spin isomeric spectrum is exhibited by none of the salts in this category, although the protons can clearly not be regarded as distinguishable. The presence of a central meta component is apparent, but the ortho component, which is responsible for the wing structure, is much narrower than the theoretical ortho-isomer component. It is probable that "tunneling" of the ammonium ion in the low crystal fields of these solids, which would not affect the meta transitions, is responsible for the observed narrowing of the ortho component.

c) Broad-Gaussian

The salts in this category are all characterized by a broad ($\geq$ 6 G^2) central component with either broadening or structure in the wings.

The central component of the $(NH_4)_2SO_4$ spectrum is best reproduced by a theoretical spin isomeric line shape with a $\langle \Delta H^2 \rangle$ of 8 G^2 - Figure 23. A calculation of the inter-ionic proton contribution to the second moment for proton-proton separations of up to 20 Å was made using the proton positions given by Schlemper and Hamilton (1966). A value of 5.2 G^2 was obtained, and considering the remaining protons, and the nitrogen contributions, 8 G^2 is not an unreasonable estimate

for $\langle \Delta H^2 \rangle$. However, the experimentally observed wing structure is too pronounced to be consistent with the theoretical spin isomer line shape obtained with this broadening factor. There are, however, two inequivalent ammonium ions in this salt (Schlemper and Hamilton); one tightly bound (E_a = 3.9 K cal/mole), the other more loosely bound (E_a = 2.7 K cal/mole - Table VI). It is possible that each ion is exhibiting a different type of absorption spectrum, the experimentally observed one being their superposition. To account for the larger second moment of this salt (33.3 G^2), one of these component spectra would have to be the "4-spin 1/2" type of category a), having a second moment $\sim$50 G^2. If the other component were spin isomeric with a second moment of 23 G^2 (15 G^2 for the isolated group plus 8 G^2 broadening), the observed second moment, being the average for the two types, would be $\sim$37 G^2, which though higher than the observed value, is of the right order. However, had the second component not been spin isomeric, but of the type observed in category b), with a second moment $\sim$10 G^2, the observed second moment would have been $\sim$30 G^2, which is also of the right order, though smaller than observed. On the basis of these results, no definite conclusion can be drawn as to the nature of this narrower component in the spectrum of $(NH_4)_2SO_4$. Any wing detail that may confirm or refute it as spin isomeric in character is masked by the broad component.

The spectrum of $(NH_4)_2SeO_3$ is qualitatively similar to that of $(NH_4)_2SO_4$ (Figure 24) and a similar proposition can be forwarded of two spectral types being present in the observed line shape. Although there is more of the broad component present in this case, the consequently higher second moment (38 ± 1 G^2) agrees well with that predicted above (37 G^2) for a 1:1 mixing of "4-spin 1/2" with spin isomeric sites. No structural data is presently available on this material, so this proposition cannot be substantiated.

$(NH_4)_2TeO_4$ and $(NH_4)_2BeF_4$ spectra are both approximated very closely by a spin isomeric spectrum with a broadening factor, $\langle \Delta H^2 \rangle$, of 10 G^2 - Figures 25 and 26. Both these salts have second moments, 26 ± 1 G^2 and 25 ± 1 G^2 respectively, consistent with that predicted for spin isomerism (15 G^2 for the intra-protonic group plus the 10 G^2 broadening) with a ratio of meta:ortho of 5:3 (spatial splitting << kT at 4.2°K). However, not only is an inter-ionic second moment of 10 G^2 questionably high, but in the tetrafluoroberyllate at least, the situation is again complicated by the presence of two inequivalent ammonium groups with different activation energies (Table VI). It is possible that in these salts too the observed spectra are the composites of two components, the narrower one being broadened sufficiently by the inter-ionic second moment to give an apparent agreement with the theoretical spin isomeric spectrum.

The closest fit of a theoretical spin isomeric line shape to the spectrum of $(NH_4)_2S_2O_3$ is achieved with a $\langle\Delta H^2\rangle$ of 6 G^2 - Figure 27. The agreement is very poor,both in the central region (which is apparently non-gaussian) and in the wings, which are experimentally observed to be much wider and less structured than those of the spin isomer spectrum.

To approximate the spectra of NH_4NO_3 and NH_4VO_3 by a spin isomeric line shape a $\langle\Delta H^2\rangle$ of at least 16 G^2 must be used (Figures 28 and 29), which is an unrealistically high value. With this amount of broadening, no wing structure would be observed, whereas the NH_4NO_3 spectrum in particular, still exhibits quite pronounced wing structure.

Although the low second moments at 4.2°K indicate some indistinguishability among the protons in all the salts of this category, it is unlikely that any of them exhibit solely isomeric spin states. All their spectra may, in fact, be composites of the spectra from two inequivalent proton groups - one distinguishable, the other not.

VI.3 CONCLUDING REMARKS

A mechanism for line narrowing at 4.2°K is not characteristic of all ammonium salts. Those of category a) exhibit the "4-spin 1/2" line shape characteristic of distinguishable ammonium group protons, their high hindering potentials being consistent with such an interpretation.

The spectra of the salts in category b) show their ammonium group protons to be indistinguishable, although spin isomerism is not the sole mechanism responsible for the line shape. The extreme narrowness of the spectrum of some of these salts indicates some other mechanism, probably "tunneling" of the ammonium groups through the low hindering potentials, is modifying the spin isomeric line shape.

Similarly, for the salts in category c), with the possible exception of $(NH_4)_2TeO_4$ and $(NH_4)_2BeF_4$, spin isomerism is not the sole mechanism responsible for the line narrowing at 4.2°K. However, the spectra of $(NH_4)_2TeO_4$ and $(NH_4)_2BeF_4$ are indicative of spin isomerism in these salts, although the large broadening factor involved would tend to obscure the wing structure (ortho component) in which tunneling effects would manifest themselves.

The splitting of the A, E and 3T spatial levels, which is responsible for the separation of the different spin symmetry states, is a result of the overlap of the spatial wave functions from one equilibrium orientation of the ion to another - the conventional tunneling of the ion between equilibrium sites. If this splitting is much greater than the natural absorption linewidth, transitions between different spin symmetry states then give rise to very weak components in the absorption spectrum far removed from the Larmor frequency which become lost in the noise of the wings, thus narrowing the resonance

line and the second moment . In a crystal field of tetrahedral or higher symmetry the 3T levels remain degenerate so that none of the allowed transitions between the different T states are lost in the wings. This situation is implicit in our description of spin isomerism. However, in a crystal field of symmetry lower than tetrahedral the degeneracy of the 3T levels is at least partially removed (see page 11). If the splitting of these levels is much greater than the natural linewidth certain transitions among them will again give rise to unobserved components far removed from the Larmor frequency, resulting in a further narrowing of the observed spectrum. This is the situation we have previously referred to as "tunneling", but it must be emphasized that it is in fact only a removal, by the crystal field symmetry, of the residual degeneracy of the 3T levels. The conventional tunneling of the ammonium ion is already responsible for the separation of these levels from the A and E types.

The extreme narrowness of the ortho components in category b) suggest that this "tunneling" situation may be present in these salts and that the initial decoupling of the spin and space eigenfunctions employed by Tomita with the subsequent diagonalisation of the spin state representation of the dipolar Hamiltonian is not justified. A future attempt to describe this mechanism should involve an initial coupling

of spin and space eigenfunctions to form physically real states, followed by diagonalisation of the matrix representative of the dipolar Hamiltonian in this spin-space basis.

APPENDIX A

MATRIX ELEMENTS

A.I NOTATION

To condense the expressions involved in this appendix to a convenient length the following abbreviated notation will be defined:

a) The symmetry adapted states ${}_M\phi_i^R$ will be represented by a vector of the form $\{a_1, a_2, \ldots\}$ where the a_i's are the coefficients of the states $|m_1 m_2 m_3 m_4\rangle$ in the reduction to ${}_M\phi_i^R$ defined in Table I. e.g. the state;

$$ {}_1\phi_1^A = \frac{1}{2} [|-+++\rangle + |+-++\rangle + |++-+\rangle + |+++-\rangle] $$

will be represented by;

$$ {}_1\phi_1^A = \frac{1}{2} \{1,1,1,1\} $$

b) The matrix elements will be linear combinations of the A_{ij}'s and will be represented by a vector $(b_1, \ldots b_6)$, where the b's are the coefficients of the A_{ij}'s in these linear combinations. e.g. from Table II;

$$ a_2 = -\frac{1}{4} (A_{12}+A_{23}+A_{13}+A_{14}+A_{24}+A_{34}) $$

will be represented by:

$$ a_2 = -\frac{1}{4} (1,1,1,1,1,1) $$

A.II MATRIX ELEMENTS OF H_{dp}

From section II.3;

$$H_{dp} = \sum_{\substack{i>j \\ =1}}^{4} A_{ij}[I_{iz}I_{jz} - \frac{1}{4}(I_i^+I_j^- + I_i^-I_j^+)] \qquad (A.1)$$

The relevant operator properties are (for $m_i = \pm \frac{1}{2}$);

$$\left.\begin{aligned} I_{iz}I_{jz}|m_1m_2m_3m_4\rangle &= m_im_j|m_1m_2m_3m_4\rangle \\ I_1^+I_2^-|m_1m_2m_3m_4\rangle &= |-m_1\,-m_2,m_3,m_4\rangle \end{aligned}\right\} \qquad (A.2)$$

for $m_1 = -\frac{1}{2}$ and $m_2 = +\frac{1}{2}$ and is zero otherwise.

Consider, for example, $|{}_1\phi_1^T\rangle$ where, from Table I;

$$|{}_1\phi_1^T\rangle = \frac{1}{2\sqrt{3}}\{1,1,1,-3\} \qquad (A.3)$$

Operating with (A.1) and using (A.2) we find;

$$H_{dp}|{}_1\phi_1^T\rangle = \frac{1}{8\sqrt{3}}\{(-2,1,-2,2,1,1),(-2,-2,1,1,2,1),$$

$$(1,-2,-2,1,1,2),(-3,-3,-3,2,2,2)\}$$

Also;

$$|{}_1\phi_2^T\rangle = \frac{1}{\sqrt{6}}\{1,1,-2,0\}$$

Hence;

$$f = \langle {}_1\phi_2^T | H_{dp} | {}_1\phi_1^T \rangle$$

$$= \frac{1}{24\sqrt{2}} [(-2,1,-2,2,1,1)+(-2,-2,1,1,2,1)-2(1,-2,-2,1,1,2)]$$

$$= \frac{1}{24\sqrt{2}} (-6,3,3,1,1,-2)$$

The other matrix elements of H_{dp} are obtained in an identical manner.

A-III MATRIX ELEMENTS OF H_{dn}

From section II.13;

$$H_{dn} = \sum_{i=1}^{4} A_{i0} I_{iz} I_{nz} \qquad (A.4)$$

The relevant operator properties are;

$$I_{iz} I_{nz} | m_1 m_2 m_3 m_4 \rangle_n = n m_i | m_1 m_2 m_3 m_4 \rangle_n \qquad (A.5)$$

where the modified states $|m_1 m_2 m_3 m_3\rangle_n$ are defined in section II.13. The same notation defined in section A.I and extended to this case gives, for example;

$$| {}_1\phi_3^T \rangle = \frac{1}{\sqrt{2}} \{1,-1,0,0\}$$

Then operating with (A.4) and using (A.5) we get, for n = 1,

$$H_{dn} | {}_1\phi_3^T \rangle = \frac{1}{2\sqrt{2}} \{(-1,1,1,1),-(1,-1,1,1),0,0\}$$

Hence;

$$\ell' = \langle {}_1\phi_3^T | H_{dn} | {}_1\phi_3^T \rangle$$

$$= \frac{1}{4} [(-1,1,1,1) + (1,-1,1,1)]$$

$$\ell' = (0,0,1,1)$$

The other matrix elements of H_{dn} are obtained in an identical manner.

APPENDIX B

A_{ij} AND A_{i0} IN SPHERICAL CO-ORDINATES

B.I A_{ij}

In the reference frame defined by Figure 1 a unit vector $\underline{h}$ along the applied field $\underline{H}_o$ has co-ordinates;

$$(x,y,z) = (\sin\theta\cos\phi, \sin\theta\sin\phi, \cos\theta) \qquad (B.1)$$

θ and ϕ being the spherical angular co-ordinates of $\underline{h}$. Unit vectors $\hat{\underline{r}}_{ij}$ along the proton-proton vectors $\underline{r}_{ij}$ are given by

$$\left.\begin{aligned}
\hat{\underline{r}}_{12} &= \frac{1}{\sqrt{2}}(\underline{i} + \underline{j}) \\
\hat{\underline{r}}_{13} &= \frac{1}{\sqrt{2}}(\underline{i} - \underline{k}) \\
\hat{\underline{r}}_{14} &= \frac{1}{\sqrt{2}}(\underline{j} - \underline{k}) \\
\hat{\underline{r}}_{23} &= -\frac{1}{\sqrt{2}}(\underline{j} + \underline{k}) \\
\hat{\underline{r}}_{24} &= -\frac{1}{\sqrt{2}}(\underline{i} + \underline{k}) \\
\hat{\underline{r}}_{34} &= \frac{1}{\sqrt{2}}(-\underline{i} + \underline{j})
\end{aligned}\right\} \qquad (B.2)$$

$\underline{i}$, $\underline{j}$, $\underline{k}$, being the unit vectors along x,y,z.

Now, if θ_{ij} is the angle $\underline{r}_{ij}$ makes with $\underline{H}_o$, then $\cos\theta_{ij} = \hat{\underline{r}}_{ij} \cdot \underline{h}$ and therefore, from (B.2) and (B.1);

$$\left.\begin{aligned}
\cos\theta_{12} &= \frac{1}{\sqrt{2}}\sin\theta(\cos\phi+\sin\phi)\\
\cos\theta_{13} &= \frac{1}{\sqrt{2}}(\sin\theta\cos\phi-\cos\theta)\\
\cos\theta_{14} &= \frac{1}{\sqrt{2}}(\sin\theta\sin\phi-\cos\theta)\\
\cos\theta_{23} &= -\frac{1}{\sqrt{2}}(\sin\theta\sin\phi+\cos\theta)\\
\cos\theta_{24} &= -\frac{1}{\sqrt{2}}(\sin\theta\cos\phi+\cos\theta)\\
\cos\theta_{34} &= \frac{1}{\sqrt{2}}\sin\theta(\sin\phi-\cos\phi)
\end{aligned}\right\} \qquad (B.3)$$

But $A_{ij} = \frac{\gamma^2\hbar^2}{r_{ij}^3}(1-3\cos^2\theta_{ij})$, which on substituting equations (B.3) gives;

$$A_{12} = A[1 - \tfrac{3}{2}\sin^2\theta(\cos\phi+\sin\phi)^2]$$

$$A_{13} = A[1 - \tfrac{3}{2}(\sin\theta\cos\phi-\cos\theta)^2]$$

$$A_{14} = A[1 - \tfrac{3}{2}(\sin\theta\sin\phi-\cos\theta)^2]$$

$$A_{23} = A[1 - \tfrac{3}{2}(\sin\theta\sin\phi+\cos\theta)^2]$$

$$A_{24} = A[1 - \tfrac{3}{2}(\sin\theta\cos\phi+\cos\theta)^2]$$

$$A_{34} = A[1 - \tfrac{3}{2}\sin^2\theta(\sin\phi-\cos\phi)^2]$$

where $A = \frac{\gamma^2\hbar^2}{r^3}$, r being the proton-proton distance $|\underline{r}_{ij}|$.

In the same reference frame, Figure 1, the unit vectors $\hat{r}_{i0}$ along the nitrogen-proton vectors $\underline{r}_{i0}$ are:

$$\left.\begin{aligned} \hat{\underline{r}}_{10} &= \frac{1}{\sqrt{3}}(-\underline{i}-\underline{j}+\underline{k}) \\ \hat{\underline{r}}_{20} &= \frac{1}{\sqrt{3}}(\underline{i}+\underline{j}+\underline{k}) \\ \hat{\underline{r}}_{30} &= \frac{1}{\sqrt{3}}(\underline{i}-\underline{j}-\underline{k}) \\ \hat{\underline{r}}_{40} &= \frac{1}{\sqrt{3}}(-\underline{i}+\underline{j}-\underline{k}) \end{aligned}\right\} \qquad (B.4)$$

Since $\cos\theta_{i0} = \hat{\underline{r}}_{i0}\cdot\underline{h}$, substituting from (B.1) and (B.4) gives;

$$\left.\begin{aligned} \cos\theta_{10} &= \frac{1}{\sqrt{3}}\{-\sin(\cos\phi+\sin\phi)+\cos\theta\} \\ \cos\theta_{20} &= \frac{1}{\sqrt{3}}\{\sin\theta(\cos\phi+\sin\phi)+\cos\theta\} \\ \cos\theta_{30} &= \frac{1}{\sqrt{3}}\{\sin\theta(\cos\phi-\sin\phi)-\cos\theta\} \\ \cos\theta_{40} &= \frac{1}{3}\{\sin\theta(-\cos\phi+\sin\phi)-\cos\theta\} \end{aligned}\right\} \qquad (B.5)$$

Now $A_{i0} = \frac{\gamma\gamma_n\hbar^2}{r_{\rho n}^3}(1-3\cos^2\theta_{i0})$, so substituting for the θ_{i0} from (B.5) gives

$$A_{10} = A_o[-\sin^2\theta\sin2\phi+\sin2\theta(\sin\phi+\cos\phi)]$$

$$A_{20} = A_o[-\sin^2\theta\sin2\phi-\sin2\theta(\sin\phi+\cos\phi)]$$

$$A_{30} = A_o[\sin^2\theta\sin2\phi-\sin2\theta(\sin\phi-\cos\phi)]$$

$$A_{40} = A_o[\sin^2\theta\sin2\phi+\sin2\theta(\sin\phi-\cos\phi)]$$

where

$$A_o = \frac{\gamma\gamma_n\hbar^2}{r_{\rho n}^3}$$

APPENDIX C

TRANSITION PROBABILITIES

C.I PERTURBING OPERATOR

The relevant operator inducing transitions among the states ${}_M\phi_i^R$ is the x-component of the total spin operator;

$$I_x = I_{1x} + I_{2x} + I_{3x} + I_{4x}$$

$$= \frac{1}{2}(I_1^+ + I_1^- + I_2^+ + I_2^- + I_3^+ + I_3^- + I_4^+ + I_4^-) \qquad (C.1)$$

where $I_i^+ = I_{ix} + iI_{iy}$ is the spin raising operator for proton i, and $I_i^- = I_{ix} - iI_{iy}$ is the spin lowering operator for proton i.

C.II META-TRANSITIONS

As an example, take the meta-transition ${}_2\phi_1^A \rightarrow {}_1\phi_1^A$, with transition probability (from equation (2.2)) of;

$$P_A(2\rightarrow 1) = |\langle {}_2\phi_1^A | I_x | {}_1\phi_1^A \rangle|^2 \qquad (C.2)$$

Applying (C.1) to the state ${}_1\phi_1^A$ defined in Table I gives;

$$I_x|{}_1\phi_1^A\rangle = |++++\rangle + \frac{1}{2}\{|--++\rangle + |+--+\rangle + |-+-+\rangle$$

$$+ |-++-\rangle + |+-+-\rangle + |++--\rangle\}$$

$$= |{}_2\phi_1^A\rangle + \frac{\sqrt{6}}{2}|{}_0\phi_1^A\rangle. \qquad (C.3)$$

Therefore, applying (C.3) to (C.2) gives;

$$P_A(2 \to 1) = 1$$

In a similar way the transition ${}_1\phi_1^A \to {}_0\phi_1^A$ occurs with a probability;

$$P_A(1 \to 0) = |\langle {}_0\phi_1^A | I_x | {}_1\phi_1^A \rangle|^2$$

which, by (C.3) gives;

$$P_A(1 \to 0) = \frac{3}{2} .$$

The negative M transitions are treated identically.

C.III ORTHO-TRANSITIONS

Applying (C.1) to the state ${}_0\phi_1^T$ defined in Table I gives;

$$I_x | {}_0\phi_1^T \rangle = \frac{1}{2\sqrt{6}} \{ |-+++\rangle + |+-++\rangle + |++-+\rangle - 3|+++-\rangle$$

$$- |+---\rangle - |-+--\rangle - |--+-\rangle + 3|---+\rangle\}$$

$$= \frac{1}{\sqrt{2}} (|{}_1\phi_1^T\rangle - |{}_{-1}\phi_1^T\rangle) \qquad (C.4)$$

Substituting this in the expression for the transition probability;

$$P_T(\pm 1 \rightleftarrows 0) = |\langle {}_{\pm 1}\phi_1^T | I_x | {}_0\phi_1^T \rangle|^2$$

gives;

$$P_T(\pm 1 \rightleftarrows 0) = \frac{1}{2} .$$

It is also clear from (C.4) that

$$\langle {}_{\pm 1}\phi_i^T | I_x | {}_0\phi_1^T \rangle = 0 \quad \text{unless } i=1$$

The same treatment applies, with the same results, for the other ortho-transitions.

APPENDIX D

ROOTS OF A CUBIC EQUATION

D.I EIGENVALUE EQUATION

To find the roots of the equation (2.4);

$$x^3 - \frac{3}{16}x + \frac{1}{32}\cos\Psi(\theta,\phi) = 0 \qquad (D.1)$$

we make use of the identity;

$$x^3-3pqx+p^3+q^3=(x+p+q)(x+\varepsilon p+\varepsilon^2 q)(x+\varepsilon^2 p+\varepsilon q) \qquad (D.2)$$

where $1,\varepsilon, \varepsilon^2$ are the cube roots of unity, and;

$$1 + \varepsilon + \varepsilon^2 = 0$$

(i.e. $\varepsilon = \exp\{2\pi i/3\}$).

Comparing (D.1) with (D.2) we set;

$$\left.\begin{aligned} pq &= \frac{1}{16} \\ p^3+q^3 &= \frac{1}{32}\cos\Psi \end{aligned}\right\} \qquad (D.3)$$

Eliminating q from (D.3) and substituting $t = p^3$ we obtain;

$$16^3t^2 - 128\cos\Psi\cdot t + 1 = 0$$

whence:

$$t = \frac{1}{64}(\cos\Psi \pm i\sin\Psi) = p^3 \qquad (D.4)$$

Writing p in the form;

$$p = P\exp\{i\chi\} \qquad (D.5)$$

substituting into (D.4) and equating real and imaginary parts we get;

$$P^3\cos 3\chi = \frac{1}{64}\cos\Psi$$

$$P^3\sin 3\chi = \pm\frac{1}{64}\sin\Psi$$

from which;

$$P = \frac{1}{4} \text{ and } \chi = \pm\frac{\Psi}{3}.$$

Therefore, from (D.5) and (D.3);

$$p = \frac{1}{4}\exp(\pm i\frac{\Psi}{3}) = \frac{1}{4}(\cos\frac{\Psi}{3} \pm i\sin\frac{\Psi}{3})$$

$$q = \frac{1}{4}\exp(\mp i\frac{\Psi}{3}) = \frac{1}{4}(\cos\frac{\Psi}{3} \mp i\sin\frac{\Psi}{3}).$$

Inserting these values into (D.2) we therefore find the only real solutions to (D.1) are;

$$x_1 = -p-q = -\frac{1}{2}\cos\frac{\Psi}{3}$$

$$x_{2,3} = -(\varepsilon p+\varepsilon^2 q) = -\frac{1}{2}\cos(\frac{2\pi}{3} \pm \frac{\Psi}{3}).$$

But since $\cos(\chi-\pi) = -\cos\chi$;

$$x_1 = -\frac{1}{2}\cos\frac{\Psi}{3}$$

$$x_2 = \frac{1}{2}\cos(\frac{\pi-\Psi}{3})$$

$$x_3 = \frac{1}{2}\cos(\frac{\pi+\Psi}{3})$$

D.II ROOTS OF $\Theta = f$

We need to find the roots of the cubic equation;

$$\Theta = \xi(1-\xi)^2 = f \tag{D.6}$$

To eliminate the term in ξ^2 and so transform (D.6) to the form (D.2) we make the substitution;

$$\xi = z + \frac{2}{3} \tag{D.7}$$

Then D.6 becomes;

$$z^3 - \frac{1}{3} z + \frac{2}{27} - f = 0. \tag{D.8}$$

From which, by comparison with (D.2), we set;

$$\left.\begin{aligned} pq &= \frac{1}{9} \\ p^3+q^3 &= \frac{2}{27} - f \end{aligned}\right\} \tag{D.10}$$

Eliminating q from (D.10) and substituting $t = p^3$ we obtain;

$$9^3t^2 + 27(27f-2)t + 1 = 0$$

from which;

$$t = \frac{1}{54} [2-27f \pm \sqrt{27f(27f-4)}] = p^3 \tag{D.11}$$

But f lies in the region

$$\frac{4}{27} \geq f \geq 0$$

from which it can be seen that solution (D.11) for t is complex.

Substituting $\rho = P\exp(i\chi)$ into (D.11) and equating real and imaginary parts gives;

$$P^3\cos 3\chi = \frac{1}{54}(2-27f)$$

$$P^3\sin 3\chi = \frac{1}{54}\sqrt{27f(4-27f)}$$

from which;

$$\left.\begin{aligned} P &= \frac{1}{3} \\ \sin 3\chi &= \frac{1}{2}\sqrt{27f(4-27f)} \\ \cos 3\chi &= \frac{1}{2}(2-27f) \end{aligned}\right\} \qquad (D.12)$$

where

and

$$\left.\begin{aligned} p &= \frac{1}{3}\exp(i\chi) \\ q &= \frac{1}{3}\exp(-i\chi) \end{aligned}\right\} \qquad (D13)$$

from (D.10).

From (D.2), the only real solution for z is therefore;

$$z = -p-q = -\frac{2}{3}\cos\chi$$

and so, by (D.7);

$$\xi = \frac{2}{3}(1-\cos\chi)$$

where χ is given by (D.12).

APPENDIX E

BEHAVIOUR OF k^2 AROUND DISCONTINUITIES

E.I NEAR $\eta = 1$

From equation (2.11), when $\eta = 1$;

$$|f'| = \frac{2}{3} \tag{E.1}$$

Let $\eta = 1 - \delta_1$, where δ_1 is small, then from equation (2.10);

$$f(1-\delta_1) = \frac{2}{27}\,\delta_1(9-12\delta_1 + 4\delta_1^2). \tag{E.2}$$

Hence;

$$f^{\frac{1}{2}} \simeq \sqrt{\frac{2}{3}}\;\;\delta_1^{\frac{1}{2}} \tag{E.3}$$

Substituting for f from equation (E.2) into (2.16) and expanding gives;

$$\left.\begin{aligned} \sin 3\chi &= 3\sqrt{2}\;\delta_1^{\frac{1}{2}}\;(1 - \frac{35}{12}\,\delta_1 + O(\delta_1^2)) \\ \text{and} \\ \cos 3\chi &= 1 - 9\delta_1 + 12\delta_1^2 + O(\delta_1^3) \end{aligned}\right\} \tag{E.4}$$

Since δ_1 is small, χ is small, and so using the expansion;

$$\sin^{-1}x = x + \frac{x^3}{6} + \frac{1}{2}\cdot\frac{3}{4}\cdot\frac{x^5}{5} + O(x^7) \tag{E.5}$$

on (E.4), we obtain the angles;

$$\chi = \sqrt{2}\ \delta_1^{\frac{1}{2}}\ (1 + \frac{1}{12}\ \delta_1 + O(\delta_1^2)) + \frac{2n\pi}{3} \qquad \text{(E.6)}$$

$n = 0,1,2$

Substituting these into the first of equations (2.16) we obtain for the roots α_i (which are the solutions ξ in descending order);

$$\left.\begin{aligned} \alpha_1 &= 1 + \frac{\sqrt{6}}{3}\ \delta_1^{\frac{1}{2}} - \frac{1}{3}\ \delta_1 - \frac{\sqrt{6}}{12}\ \delta_1^{3/2} + O(\delta_1^{5/2}) \\ \alpha_2 &= 1 - \frac{\sqrt{6}}{3}\ \delta_1^{\frac{1}{2}} - \frac{1}{3}\ \delta_1 + \frac{\sqrt{6}}{12}\ \delta_1^{3/2} + O(\delta_1^{5/2}) \\ \alpha_3 &= \frac{2}{3}\ \delta_1 + O(\delta_1^3) \end{aligned}\right\} \qquad \text{(E.7)}$$

Substituting equations (E.7) into (2.14) and expanding, gives, for k^2 near $\eta = 1$;

$$k^2 = 1 - \frac{4\sqrt{6}}{9}\ \delta_1^{3/2} + O(\delta_1^{5/2})\ .$$

E.II NEAR $\eta = -\frac{1}{2}$

Letting $\eta = -\frac{1}{2} + \delta_2$, where δ_2 is small we find, from (2.11);

$$|f'| = \frac{8}{9}\ \delta_2 + O(\delta_2^2) \qquad \text{(E.8)}$$

and from (2.10);

$$f(-\frac{1}{2} + \delta_2) = \frac{4}{27}\ \delta_2^2\ (3 - 2\delta_2) \qquad \text{(E.9)}$$

Hence;

$$f^{\frac{1}{2}} \simeq \frac{2}{3}\ \delta_2 \qquad \text{(E.10)}$$

Substituting for f from (E.9) in (2.16) and expanding gives;

$$\left.\begin{aligned} \sin\chi &= 2\sqrt{3}\ \delta_2\ (1 - \tfrac{1}{3}\delta_2 - \tfrac{14}{9}\delta_2^2 + O(\delta_2^3)) \\ \cos 3\chi &= 1 - 6\delta_2^2 + 4\delta_2^3 \end{aligned}\right\} \qquad \text{(E.11)}$$

We again use the expansion (E.5) to obtain the angles;

$$\chi = \frac{2\sqrt{3}}{3}\ \delta_2(1 - \tfrac{1}{3}\delta_2 + \tfrac{4}{9}\delta_2^2 + O(\delta_2^3) + \frac{2n\pi}{3} \qquad \text{(E.12)}$$

n = 1,2,3.

Substituting these expressions into the first of equations (2.16) we obtain for the roots α_i;

$$\left.\begin{aligned} \alpha_1 &= 1 + \tfrac{2}{3}\delta_2 - \tfrac{4}{9}\delta_2^2 + \tfrac{8}{27}\delta_2^3 + O(\delta_2^4) \\ \alpha_2 &= 1 - \tfrac{2}{3}\delta_2 + O(\delta_2^4) \\ \alpha_3 &= \tfrac{4}{9}\delta_2^2\ (1 - \tfrac{2}{3}\delta_2 + \tfrac{8}{9}\delta_2^2 + O(\delta_2^3) \end{aligned}\right\} \qquad \text{(E.13)}$$

Substituting equations (E.13) into (2.14) and expanding gives, for k^2 near $\eta = -\frac{1}{2}$;

$$k^2 = 1 - \frac{16}{27}\delta_2^3 + O(\delta_2^4) \qquad \text{(E.14)}$$

For $\eta = -\frac{1}{2} - \delta_2$ the sign of δ_2 in (E.13) changes, interchanging α_1 and α_2. Carrying through the same substitusions in (2.14) with the new α's gives the same result as before. Thus (E.14) applies for $\eta = -\frac{1}{2} \pm \delta_2$.

APPENDIX F

APPROXIMATION FOR $K(k^2)$

By definition a complete elliptic integral of the 1st kind $K(k^2)$ is;

$$K(k^2) = \int_0^{\pi/2} \frac{d\phi}{\sqrt{1 - k^2\sin^2\phi}}$$

Near $k^2 = 1$, let $k^2 = 1 - \varepsilon^2$ where ε is a small quantity. Then;

$$K(1-\varepsilon^2) = \int_0^{\pi/2} \frac{d\phi}{\sqrt{\cos^2\phi+\varepsilon^2\sin^2\phi}} \tag{F.1}$$

$$= A + B$$

where;

$$A = \int_0^{\alpha} \frac{d\phi}{\sqrt{\cos^2\phi+\varepsilon^2\sin^2\phi}} \tag{F.1a}$$

and

$$B = \int_{\alpha}^{\pi/2} \frac{d\phi}{\sqrt{\cos^2\phi+\varepsilon^2\sin^2\phi}} \tag{F.1b}$$

If we choose α such that;

$$\varepsilon^2 << \cot^2\alpha \tag{F.2}$$

then over the entire range of integration in equation (F.1a)

$\varepsilon^2 \sin^2\phi << \cos^2\phi$ so that the denominator in the integrand can be expanded in a Taylor series to give;

$$A = 2\int_0^{\alpha} \frac{\cos\phi d\phi}{2\cos^2\phi+\varepsilon^2\sin^2\phi}$$

$$= \int_0^{\sin\alpha} \frac{dx}{1-a^2x^2}$$

by the substitution $x = \sin\phi$, and where $a^2 = 1 - \frac{\varepsilon^2}{2}$.

This integral is of a standard form giving;

$$A = \frac{1}{2a} \ln\left(\frac{1 + a\sin\alpha}{1 - a\sin\alpha}\right). \qquad (F.3)$$

We now define an angle β by;

$$\alpha = \frac{\pi}{2} - \beta.$$

We can make β small and still satisfy the condition (F.2) if we make ε small enough. i.e. we can make β^2 of the first order of smallness if we make ε^2 of the second, and then condition (F.2) becomes;

$$\varepsilon^2 << \beta^2 << 1 \qquad (F.2a)$$

Making these substitutions in equation (F.3) and using condition (F.2a) we find;

$$A = \ln 2 - \ln\beta \qquad (F.4)$$

Letting $\phi = \frac{\pi}{2} - \theta$ the expression (F.1b) for B becomes;

$$B = \int_0^{\beta} \frac{d\theta}{\sqrt{\sin^2\theta+\varepsilon^2\cos^2\theta}} \qquad (F.5)$$

where $\varepsilon^2\cos^2\theta$ is not small compared with $\sin^2\theta$ over this entire range of integration. However, since we have made β small, θ is also small over the whole range, allowing us to expand $\sin^2\theta$ and $\cos^2\theta$, equation (F.5) becoming;

$$B = \int_0^{\beta} \frac{d\theta}{\sqrt{\varepsilon^2+(1-\varepsilon^2)\theta^2}}$$

which is again in a standard form, giving;

$$B = \ell n 2\beta - \ell n \varepsilon. \qquad (F.6)$$

Combining equations (F.4) and (F.6) in (F.1) gives, finally;

$$K(1-\varepsilon^2) = 2\ell n 2 - \ell n \varepsilon$$

if ε^2 is of the second order of smallness as defined by condition (F.2a).

APPENDIX G

ORTHO LINESHAPE BROADENING

We have to perform the convolution;

$$I^T(x) = \frac{1}{a\sqrt{\pi}} \int_{-1}^{1} W(\eta)\exp -\{\frac{(x-\eta)^2}{a^2}\}d\eta \qquad (G.1)$$

where;

$$W(\eta) = w(\eta) + w(-\eta) \qquad (G.2)$$

$w(\eta)$ having discontinuities at $\eta=-\frac{1}{2}$, 1.

Substituting (G.2) into (G.1) leads to;

$$I^T(x) = \int_{-1}^{1} w(\eta)E(x,\eta)d\eta \qquad (G.3)$$

where;

$$E(x,\eta) = \frac{1}{a\sqrt{\pi}} [\exp\{-\frac{(x-\eta)^2}{a^2}\} + \exp\{-\frac{(x+\eta)^2}{a^2}\}] \qquad (G.4)$$

Note that $E(x,-\eta) = E(x,\eta)$.

We split the range of integration in (G.3) into four parts in order to treat the discontinuities analytically, and write;

$$I^T(x) = I_1(x) + I_2(x) + I_3(x) + I_4(x) \qquad (G.5)$$

where;

$$I_1(x) = \int_{-1}^{-\frac{1}{2}-\Delta_1} w(\eta)E(x,\eta)d\eta$$

$$= \int_{\frac{1}{2}+\Delta_1}^{1-\Delta_2} w(-\eta)E(x,\eta)d\eta + \Delta_2 w(-1)E(x,1) \qquad (G.6)$$

$$I_2(x) = \int_{-\frac{1}{2}-\Delta_1}^{-\frac{1}{2}+\Delta_1} w(\eta)E(x,\eta)d\eta$$

$$= E(x,-\tfrac{1}{2}) \int_{-\Delta_1}^{\Delta_1} w(-\tfrac{1}{2}+\eta)d\eta \qquad (G.7)$$

$$I_3(x) = \int_{-\frac{1}{2}+\Delta_1}^{1-\Delta_2} w(\eta)E(x,\eta)d\eta$$

$$= \int_{0}^{\frac{1}{2}-\Delta_1} w(-\eta)E(x,\eta)d\eta + \int_{0}^{1-\Delta_2} w(\eta)E(x,\eta)d\eta \qquad (G.8)$$

$$I_4(x) = \int_{1-\Delta_2}^{1} w(\eta)E(x,\eta)d\eta$$

$$= E(x,1) \int_{0}^{\Delta_2} w(1-\eta)d\eta \qquad (G.9)$$

Δ_1 and Δ_2 being small ($<< 1$).

Combining (G.6) with (G.8) and using (G.2) we obtain;

$$I_1(x)+I_3(x) = \int_{0}^{\frac{1}{2}-\Delta_1} W(\eta)E(x,\eta)d\eta + \int_{\frac{1}{2}+\Delta_1}^{1-\Delta_2} W(\eta)E(X,\eta)d\eta + 2\Delta_1 w(\tfrac{1}{2})E(x,\tfrac{1}{2})$$
$$+\Delta_2 w(-1)E(x,1) \qquad (G.10)$$

Now, from equation (2.10);

$$f(\tfrac{1}{2}) = f(-1) = \frac{4}{27} \qquad (G.11)$$

which means, by equation (2.16);

$$\chi = \frac{\pi}{3}\ ,\ \pi,\ \text{or}\ \frac{5\pi}{3}$$

so that;

$$\left.\begin{aligned} \alpha_1 &= \tfrac{4}{3} \\ \alpha_2 &= \alpha_3 = \tfrac{1}{3} \end{aligned}\right\} \qquad (G.12)$$

This can also be seen by inspection of Figure 2. Hence, from (2.14), $k^2 = 0$, and from standard tables (also from definition of $K(k^2)$ in Appendix F);

$$K(0) = \frac{\pi}{2}\ . \qquad (G.13)$$

Also, from equation (2.11);

$$\left.\begin{aligned} |f'(\tfrac{1}{2})| &= 0 \\ |f'(-1)| &= \tfrac{2}{3} \end{aligned}\right\} \qquad (G.14)$$

Substituting equations (G.11), (G.12), (G.13) and (G.14) into equation (2.13) gives;

$$\left.\begin{aligned} w(\tfrac{1}{2}) &= 0 \\ w(-1) &= \tfrac{3}{4} \end{aligned}\right\} \qquad (G.15)$$

Substituting the approximations (2.23) into (G.7) and (G.) and integrating, leads to;

$$I_2(x) = \frac{2}{\pi} E(x,-\tfrac{1}{2})\Delta_1(1+\ell n3-\ell n\Delta_1) \qquad (G.16)$$

and

$$I_4(x) = \frac{\sqrt{6}}{4\pi} E(x,1)\Delta_2^{\frac{1}{2}}(2+\ell n6 - \ell n\Delta_2) \qquad (G.17)$$

(G.16) and (G.17) in combination with (G.10) and (G.15) constitute the broadened ortho-lineshape, $I^T(x)$, in (G.5)

APPENDIX H

CALCULATION OF SECOND MOMENT

H.I ORTHO-CONTRIBUTION.

The intra-ionic second moment of the ortho-spectrum, M_2' (ortho), is given by;

$$M_2'(\text{ortho}) = \frac{I^o}{A^o} \tag{H.1}$$

where;

$$I^o = \int_0^1 \eta^2 W(\eta) d\eta \tag{H.2}$$

and,

$$A^o = \int_0^1 W(\eta) d\eta \tag{H.3}$$

use being made of the symmetry of $W(\eta)$ about the origin and the fact that $W(\eta) = 0$ for $\eta > 1$.

As in Appendix G, we divide up the range of integration in order to treat the discontinuities of $W(\eta)$ analytically, and write;

$$A^o = A_1 + A_2 + A_3 + A_4 \tag{H.4}$$

where

$$A_1 = \int_0^{\frac{1}{2}-\Delta_1} W(\eta) d\eta \tag{H.5}$$

$$A_2 = \int_{\frac{1}{2}-\Delta_1}^{\frac{1}{2}+\Delta_1} W(\eta)d\eta$$

$$= \int_{-\Delta_1}^{\Delta_1} W(\tfrac{1}{2} + \eta)d\eta \qquad (H.6)$$

$$A_3 = \int_{\frac{1}{2}+\Delta_1}^{1-\Delta_2} W(\eta)d\eta \qquad (H.7)$$

$$A_4 = \int_{1-\Delta_2}^{1} W(\eta)d\eta$$

$$= \int_{0}^{\Delta_2} W(1-\eta)d\eta \qquad (H.8)$$

where Δ_1 and Δ_2 are small ($<< 1$) .

A_1 and A_3 can be computed numerically, their ranges of integration containing no discontinuities.

Now;

$$W(\eta) = w(\eta) + w(-\eta). \qquad (H.9)$$

Substituting this and the approximation (2.23) into (H.6) yields;

$$A_2 = 2\Delta_1 w(\tfrac{1}{2}) + \frac{2}{\pi}\Delta_1 (1+\ell n3 - \ell n\Delta_1)$$

$$= \frac{2}{\pi}\Delta_1 (1 + \ell n3 - \ell n\Delta_1) \qquad (H.10)$$

by equation (G.15).

Similarly, the same substitutions in (H.8) yield:

$$A_4 = \Delta_2 w(-1) + \frac{\sqrt{6}}{4\pi}\,\Delta_2^{\frac{1}{2}}\,(2+\ell n6-\ell n\Delta_2)$$

$$= \frac{3}{4}\,\Delta_2 + \frac{\sqrt{6}}{4\pi}\,\Delta_2^{\frac{1}{2}}\,(2+\ell n6-\ell n\Delta_2) \qquad \text{(H.11)}$$

by (G.15).

Similarly;

$$I^{o} = I_1 + I_2 + I_3 + I_4 \qquad \text{(H.12)}$$

where

$$I_1 = \int_{o}^{\frac{1}{2}-\Delta_1} \eta^2 W(\eta)\,d\eta \qquad \text{(H.13}$$

$$I_2 = \int_{\frac{1}{2}-\Delta_1}^{\frac{1}{2}+\Delta_1} \eta^2 W(\eta)\,d\eta \qquad \text{(H.14)}$$

$$= \frac{1}{4}\,A_2$$

$$I_3 = \int_{\frac{1}{2}+\Delta_1}^{1-\Delta_2} \eta^2 W(\eta)\,d\eta \qquad \text{(H.15)}$$

$$I_4 = \int_{1-\Delta_2}^{1} \eta^2 W(\eta)\,d\eta \qquad \text{(H.16)}$$

$$= A_4$$

I_1 and I_3 can again be computed numerically. Substitution of (H.4) and (H.12) from the above into (H.1) thus

gives M_2' (ortho) for the ortho-contribution;

$$M_2' \text{ (ortho)} = \frac{I_1+A_2/4+I_3+A_4}{A_1+A_2+A_3+A_4} .$$

H.II COMBINED ORTHO-META SECOND MOMENT

The second moment of the combined ortho-meta spectrum, M_2', is;

$$M_2' = \frac{I^M+I^O}{A^M+A^O} \tag{H.17}$$

where I^O and A^O are the ortho integrals defined by (H.2) and (H.3) and I^M and A^M are the corresponding meta integrals.

Dividing top and bottom of (H.17) by A^O we obtain;

$$M_2' = \frac{RM_2'(\text{meta})+M_2'(\text{ortho})}{R+1} \tag{H.18}$$

where

$$R = \frac{A^M}{A^O}$$

and

$$M_2'(\text{meta}) = \frac{I^M}{A^M}$$

M_2'(ortho) is defined by (H.1).

Since the meta spectrum is a delta function, M_2'(meta) = 0. Also, since the weighting of meta:ortho is 5:3, R = 5/3. Hence (H.18) becomes;

$$M_2' = \frac{3}{8} M_2'(\text{ortho}).$$

REFERENCES

Abel, 1850; Ann. der Chemie (und Pharmacie); 76, 251.

Abragam, A., 1961; The Principles of Nuclear Magnetism, Oxford University Press.

Adler, 1899; Z. angew. Chem. 12, 201.

Allen, P. S., 1968; J. Chem. Phys., 48, 3031.

Bersohn, R., and Gutowsky, H.S., 1954; J. Chem. Phys., 22, 651.

Berthelot, 1892; C.R., 114, 876.

Berzélius, 1828; Lehrbuch der Chemie, 3, 282.

Berzélius, 1831; Acad. Handl. Stockholm 1.

Blinc, R., and Levstek, I., 1960; J. Phys. Chem. Solids, 12, 295.

Bosetti, 1889; Arch. Pharm., [3], 27, 120.

Bowman, F., 1961; Introduction to Elliptic Functions, with Applications, Dover Publications.

Bright Wilson Jr., E., 1935; J. Chem. Phys., 3, 276.

Brunt, N. A., 1946; Thesis, Leiden.

Crenshaw and Ritter, 1932; Z. physik. Chem. 16B, 143.

Datta,1913; J. Am. Chem. Soc., 35, 1187.

Druce, 1918; Chem. News, 117, 193.

Engel, G., 1935; Zeits. f. Kryst., 90, 341.

Fock, 1893; Z. Kryst., 22, 29.

Fock and Kluss, 1889; Berlichte der Deutschen Chemischen Gesellschatt, 22, 3099.

Gossner and Mussgnug, 1930; Z. Kryst., 72, 476.

Gossner, 1904; Z. Kryst., 38, 144.

Gutowsky, H. S., Pake, G.E., and Bersohn, R., 1954; J. Chem. Phys., 22, 643.

Hamermesh, M., 1962; Group Theory and its Applications to Physical Problems, Addison-Wesley.

Havighurst, Mack Jr., and Blake, 1925; J. Am. Chem. Soc., 47, 29.

Jaffray, 1952; J. Phys. Radium, 13, 430.

Kraus and Toonder, 1933; Proc. Nat. Acad. Washington, 19, 292.

Kuwabara, S., 1959; J. Phys. Soc. Japan 14, 1205.

Kydon, D.W., Petch, H.E., and Pintar, M., 1969; J. Chem. Phys., 51, 487.

Kydon, D.W., Pintar, M., and Petch, H.E., 1967; J. Chem. Phys., 47, 1185.

Levy, H., and Peterson, S.W., 1952; Phys. Rev. 86, 766.

Levy, H., and Peterson, S.W., 1953; J. Am. Chem. Soc. 75, 1536.

Muspratt, 1849; Ann. Chim. Pharm., 70, 275.

Mukherjee, P. L., 1944; Indian J. Phys. 18, 148.

Nagakura, S., 1957; Acta Cryst., 10, 601.

Neumann, 1921; Z. angew. Chem., 34, 441.

Norblad, 1875; Bull. Soc. Chim., 23, 64.

Ogg and Hopwood, 1919; Phil. Mag., 32, 518.

Okaya, Y., Vedam, K. and Pepinsky, R., 1958; Acta Cryst. 11, 307.

O'Reilly, D.E., Peterson, E.M. and Tsang, T., 1967; Phys. Rev., 160, 333.

O'Reilly, D.E., and Tsang, T., 1967; J. Chem. Phys., 46, 1291.

Reitz, J.R., and Milford, F.J., 1960; Foundations of Electro-Magnetic Theory, Addison Wesley, Chapter 8.

Richards, R.E., and Schaefer, T., 1961; Trans. Faraday Soc., 57, 210.

Riggin, M.T., 1970; Thesis, University of Waterloo.

Rimbach and Fleck, 1915; Z. anorg. Chem., 94, 139.

Schlemper, E.O., and Hamilton, W.C., 1966; J. Chem. Phys., 44, 4498.

Slichter, C. P., 1963; Principles of Magnetic Resonance, Harper and Row.

Structure Reports, 1960a; 24, 418.

Structure Reports, 1960b; 24, 442.

Tomita, K., 1953; Phys. Rev., 89, 429.

Tutton, 1906; J. Chem. Soc. London, 89, 1059.

Von Humboldt, 1804; Ann. du Muséum d'Hist. Nat. de Paris.

Watt, G. W., Jenkins, W.A., and McCuiston, J.M., 1950; J. Am. Chem. Soc., 72, 2260.

Wilhelmi, K.-A., 1951; Acta Chem. Scand. 5, 1003.

Woessner, D. E., and Snowden, Jr., B.S., 1967a; J. Chem. Phys., 47, 378.

Woessner, D.E., and Snowden, Jr., B.S., 1967b; J. Phys. Chem., 71, 952.

Wyckoff, R.W.G., 1923; Am. J. Sci., 4, 469.

Wyckoff, R.W.G., 1951a, Crystal Structures, Interscience Publishers, N.Y., Vol. III, Chapter (XI, b6).

Wyckoff, R.W.G., 1951b; Crystal Structures, Interscience Publishers, N.Y., Vol. I, Table III, 7.

Zachariasen, 1927; Z.physik Chem., 127, 218.